

# Polimery w Medycynie

## Polymers in Medicine

BIANNUAL ISSN: 0370-0747 e-ISSN: 2451-2699

[www.polimery.umw.edu.pl](http://www.polimery.umw.edu.pl)

2021, Vol. 51, No. 1 (January–June)

Ministry of Science and Higher Education – 20 pts.  
Index Copernicus (ICV) – 115.07 pts.



WROCLAW  
MEDICAL UNIVERSITY

Polimery w Medycynie  
Polymers in Medicine



# Polimery w Medycynie

## Polymers in Medicine

ISSN 0370-0747 (PRINT)

ISSN 2451-2699 (ONLINE)

[www.polimery.umw.edu.pl](http://www.polimery.umw.edu.pl)

**BIANNUAL**  
**2021, Vol. 51, No. 1**  
**(January–June)**

“Polymers in Medicine” is an independent, multidisciplinary forum to exchange scientific and clinical information, which publishes original papers (technical, analytical, experimental, clinical), preliminary reports and reviews regarding the use of polymers (natural and synthetic) and biomaterials in different specialties of medicine (biochemistry, clinical medicine, pharmacology, dentistry, implantology), biotechnology and veterinary science.

### Address of Editorial Office

Marcinkowskiego 2–6  
50-368 Wrocław, Poland  
Tel.: +48 71 784 11 33  
E-mail: [redakcja@umw.edu.pl](mailto:redakcja@umw.edu.pl)

### Publisher

Wrocław Medical University  
Wybrzeże L. Pasteura 1  
50-367 Wrocław, Poland

© Copyright by Wrocław Medical University,  
Wrocław 2021

Online edition is the original version of the journal

### Editor-in-Chief

Prof. Witold Musiał

### Deputy Editor

Dr. Konrad Szustakiewicz, DSc., Eng.

### Statistical Editors

Wojciech Bombała, MSc  
Katarzyna Giniewicz, MSc Eng.  
Anna Kopszak, MSc  
Dr. Krzysztof Kujawa

### Scientific Committee

Prof. Mirosława El-Fray  
Prof. Franciszek Główka  
Prof. Jörg Kreßler  
Dr. Anna Krupa  
Prof. Maciej Małecki  
Prof. Bożena B. Michniak-Kohn

Prof. Wojciech Mityk  
Prof. Masami Okamoto  
Prof. Elżbieta Pamuła  
Prof. Wiesław Sawicki  
Prof. Szczepan Zapotoczny

### Section Editors

Dr. Tomasz Urbaniak  
(synthesis, evaluation, medical use  
of polymers, sensitive to environmental  
factors, applied in controlled and targeted  
drug delivery)

Dr. BEng., Agnieszka Gadomska-Gajadur  
(synthesis and characterization of polymers  
having biomedical potential, composites for  
regenerative medicine)

Dr. Monika Gasztych  
(preparation, assessment and application  
of polymers in pharmaceutical technology  
and medical devices)

### Manuscript editing

Marek Misiak, Jolanta Krzyżak

## Editorial Policy

During the review process, the Editorial Board conforms to the “Uniform Requirements for Manuscripts Submitted to Biomedical Journals: Writing and Editing for Biomedical Publication” approved by the International Committee of Medical Journal Editors (<http://www.icmje.org/>). Experimental studies must include a statement that the experimental protocol and informed consent procedure were in compliance with the Helsinki Convention and were approved by the ethics committee.

For more information visit the following page: <http://www.polimery.umw.edu.pl>

“Enhancing the scientific standards and internationalization level of published scientific journals, and improving the level of information dissemination on scientific research outcomes or development work results” – project financed based on agreement No. 746/P-DUN/2019 from the resources of Ministry of Science and Higher Education allocated to science dissemination activities.



„Podniesienie poziomu naukowego i poziomu umiędzynarodowienia wydawanych czasopism naukowych oraz upowszechniania informacji o wynikach badań naukowych lub prac rozwojowych” – zadanie finansowane w ramach umowy 746/P-DUN/2019 ze środków Ministra Nauki i Szkolnictwa Wyższego przeznaczonych na działalność upowszechniającą naukę.



Indexed in: OCLC, WorldCat, PBL, EBSCO, MEDLINE, Index Copernicus

This publication has been co-financed by the Ministry of Science and Higher Education

Typographic design: Monika Kołęda, Piotr Gil  
Cover: Monika Kołęda  
DTP: Wrocław Medical University Press  
Printing and binding: ARG1

Circulation: 11 copies

## Contents

5 Preface

### Original papers

- 7 Olubunmi Olayemi, Oladapo Adetunji, Christianah Isimi  
**Physicochemical, structural characterization and pasting properties of pre-gelatinized *Neorautanenia mitis* starch**
- 17 Agnieszka Gadowska-Gajadhur, Paweł Ruśkowski, Aleksandra Kruk, Jolanta Mierzejewska  
**Kinetics of neomycin release from polylactide spheres and its antimicrobial activity**
- 25 Agnieszka Krause, Katarzyna Kucharska, Witold Musiał  
**Influence of non-ionic, ionic and lipophilic polymers on the pH and conductivity of model ointments, creams and gels**

### Reviews

- 33 Julita Kulbacka, Anna Choromańska, Zofia Łapińska, Jolanta Saczko  
**Natural polymers in photodynamic therapy and diagnosis**
- 43 Paweł Piszko, Bartłomiej Kryszak, Aleksandra Piszko, Konrad Szustakiewicz  
**Brief review on poly(glycerol sebacate) as an emerging polyester in biomedical application: Structure, properties and modifications**



## PREFACE

Dear Readers, Authors, Reviewers,  
Members of the Scientific Committee and Section Editors,

When I took over the role of editor-in-chief of “Polymers in Medicine”, I was overflowing with new ideas and shared many notions with other members of the Editorial Board. Yet, the moment when I realized that I really am the leader, the person in charge, came a few days later, when I was visited in my office by one of my editors. He burst into the room sporting a bicycle helmet and a lycra jacket, took off his backpack and produced a file folder with several documents awaiting my signature. ‘Sir’, he said, ‘Please sign these on the spot, I have to visit several other people and places today.’ Then I thought: “And so it begins”.



The journal “Polymers in Medicine” has been published since 1971. In the last fifty years, the development of natural and synthetic polymers has gained momentum and their application in various fields of medicine, pharmaceuticals, biotechnology, and veterinary science became widespread. We want to be a part of this sweeping wave, to make with every published article a contribution, even if modest, to the progress in medical sciences – hence such progress ultimately leads to helping other people regain their health or stay healthy. Medications that can be easily manufactured and better absorbed by the organism, various implants, prostheses and other medical intervention into human body, not to mention more and more sophisticated medical equipment – all such implementations of polymers can become available also in developing countries, thanks to constant advancement in scientific research on these materials.

Such a long publication span, although not comparable to the most renowned scientific journals from UK and USA, obliges the whole editorial staff – and especially the editor-in-chief – to maintain high standards in their work. To broaden the international impact of our journal, it will accept manuscripts only in English, with the aim of being fully accessible to the international scientific community. The articles written by Polish researchers will continue to be accompanied by abstracts in Polish to enable a broader dissemination of our content, also within the Polish-language scientific journals and databases.

We started this busy year with the great support of the Rectors’ authorities of Wroclaw Medical University, our new members of the Scientific Committee and new Section Editors – please accept my sincere thank you for the efforts of joining the Editorial Board. However, we really count on the support of those without whom no journal can exist: Authors and Reviewers, coming from the farthest scientific institutions of the world. We are all an international community, in which the most important value is the development of science to help patients – the mission which will guide the term of the Editorial Board in 2021–2024.

Editor-in-Chief  
Prof. Witold Musiał





# Physicochemical, structural characterization and pasting properties of pre-gelatinized *Neorautanenia mitis* starch

Olubunmi Olayemi<sup>1,A–F</sup>, Oladapo Adetunji<sup>2,B–E</sup>, Christianah Isimi<sup>1,B,D–F</sup>

<sup>1</sup> Department of Pharmaceutical Technology and Raw Materials Development, National Institute for Pharmaceutical Research and Development, Abuja, Nigeria

<sup>2</sup> Department of Pharmaceutics and Industrial Pharmacy, University of Ibadan, Nigeria

A – research concept and design; B – collection and/or assembly of data; C – data analysis and interpretation;

D – writing the article; E – critical revision of the article; F – final approval of the article

Polymers in Medicine, ISSN 0370-0747 (print), ISSN 2451-2699 (online)

Polim Med. 2021;51(1):7–16

## Address for correspondence

Olubunmi Olayemi  
E-mail: olubunmibiala@yahoo.co.uk

## Funding sources

None declared

## Conflict of interest

None declared

Received on April 23, 2021

Reviewed on May 7, 2021

Accepted on June 15, 2021

Published online on June 26, 2021

## Abstract

**Background.** Pre-gelatinization is one of the most common physical methods of starch modification, which involves heating to bring about significant changes in the nature of starch, such as high swelling, loss of crystallinity, solubility in cold water, and improved pasting.

**Objectives.** To evaluate the structural and physicochemical properties of starch from *Neorautanenia mitis* tubers, and determine the effect of pre-gelatinization on the functional properties of this starch.

**Materials and methods.** Properties of the pre-gelatinized starch (NMPS), such as flow, swelling power, hydration capacity, pH, morphology, Fourier-infrared spectroscopy (FTIR), differential scanning calorimetry, and pasting characteristics, were compared with those of the native starch (NMNS).

**Results.** Pre-gelatinized starch had good flow with the angle of repose at 33.69°. Carr's index was 10.90% and 7.50%, and the Hausner ratio was 1.12 and 1.05 for NMNS and NMPS, respectively. Both starches had neutral to near-neutral pH (7.00 and 6.04, respectively). The hydration capacity of NMPS (59.00%) was about 2 times higher than that of NMNS (25.80%), while the swelling power of NMPS between 40°C and 60°C was higher than that of NMNS, and maximum swelling for both starches was observed at 80°C. Morphology showed that NMNS granules were discrete, smooth and spherical, while those of NMPS were aggregated, with rough surfaces. The FTIR spectra of both starches showed identical absorption peaks but the enthalpy of gelatinization differed for both starches. The pasting properties also varied significantly among the starch samples. Native starch had better peak viscosity, breakdown viscosity and pasting temperature, while NMPS presented better trough viscosity, final viscosity, setback viscosity, and pasting time.

**Conclusions.** The results showed that pre-gelatinized starch from *N. mitis* tubers possesses high swelling and hydration abilities and significant pasting properties, and may be used as a disintegrant in solid dosage formulations and in products requiring low viscosities and bond strength.

**Key words:** physicochemical properties, starch, structural, *Neorautanenia mitis*, pre-gelatinization

## Cite as

Olayemi O, Adetunji O, Isimi C. Physicochemical, structural characterization and pasting properties of pre-gelatinized *Neorautanenia mitis* starch. *Polim Med.* 2021;51(1):7–16. doi:10.17219/pim/138964

## DOI

10.17219/pim/138964

## Copyright

© 2021 by Wrocław Medical University

This is an article distributed under the terms of the Creative Commons Attribution 3.0 Unported (CC BY 3.0) (<https://creativecommons.org/licenses/by/3.0/>)

## Background

Starch is, after cellulose, the most abundant natural carbohydrate found in plants. It can be found in different plant parts, including the seeds, roots, stems, leaves, and fruits, as a ready source of energy. Being commonly found in plants, it is relatively abundant, cheap, safe, degradable, and easily modifiable. As such, starch is a material widely used in food, cosmetics and pharmaceutical industries. However, starch in its native form has limited application in industrial processes because of some of its undesirable inherent properties, such as poor processability, poor solubility in common organic solvents, retrogradation, low shear stress resistance, and susceptibility to thermal decomposition.<sup>1</sup> Modification processes, such as enzymatic hydrolysis, chemical modifications and physical modifications, have been employed to develop new functional properties and to improve the inherent properties of starch.<sup>2</sup>

Physical methods of starch modification, like heat gelatinization, are commonly utilized because they do not require the use of chemicals and thus, are deemed safe for human consumption.<sup>3</sup> Pre-gelatinization is one of the most popular physical methods of starch modification and it involves heating a starch suspension at a temperature below its gelatinization temperature.<sup>4</sup> The process of pre-gelatinization causes an irreversible disruption of the starch granules by reorganizing the hydrogen bonding within them. This process is responsible for several changes in starch properties including high swelling, loss of crystallinity, solubility in cold water, and improved pasting and flow.<sup>5</sup> These properties make pre-gelatinized starch suitable for many processes in the pharmaceutical and food industries.<sup>6</sup>

Starches from various plant sources have their own unique properties that are utilized to meet specific needs. Starch from *Neorautanenia mitis* is examined in this study. *Neorautanenia mitis* (A. Rich) Verdcourt of the *Fabaceae* family is a leguminous subshrubby plant with a tuberous rootstock. It is usually found growing in grasslands, bushy lands and open woodlands and rocky soils of the central, southern and western regions of Africa.<sup>7</sup> Traditionally, this plant was used as a fish poison and an insecticide, and to treat skin infections, syphilis and psychiatric conditions. Experimental studies have also shown that it possesses acaricidal, antimicrobial and antinociceptive properties.<sup>8,9</sup>

Despite the therapeutic potentials of this plant, the starch that abounds in its tubers has not been documented to have nutritional value, nor has it been exploited for use as an excipient in the food, cosmetics or pharmaceutical industries. However, Olayemi et al. has examined the potential of starch from the tuberous roots of *N. mitis* to be used in tablet formulations.<sup>10</sup>

## Objectives

In view of the fact that the traditional sources of starch are overexploited, tubers of *N. mitis* could be used as a new source of starch and starch derivatives. Therefore, the aim of this study is to prepare pre-gelatinized starch from tubers of *N. mitis*, and evaluate the structural, physicochemical and pasting properties of the modified starch, with a view to provide new starch sources with potential functional properties.

## Materials and methods

The materials used included *N. mitis* tubers purchased from Suleja Community Market, Suleja, Nigeria. The *N. mitis* starch was prepared in the NIPRD Laboratory (Abuja, Nigeria). All other reagents used were of analytical grade.

### Extraction of starch

Starch was extracted using a previously described method.<sup>10</sup> Tubers of *N. mitis* were peeled, washed in water and diced. Then, they were soaked in a solution of sodium metabisulphite solution (0.75% w/v) for 2 h and ground using a blender. The blended mixture was sieved using a muslin cloth and the suspension was centrifuged at 1500 rpm for 15 min in a centrifuge (Heraeus Sepatech Labofuge Ae, Münster, Germany). The supernatant was discarded and the sediment (starch) was air-dried at room temperature for 24 h, and then pulverized in a mortar, packaged appropriately and stored in a desiccator.

### Pre-gelatinization of *N. mitis* native starch (NMNS)

A previously described method for pre-gelatinization was adopted.<sup>11</sup> A starch slurry (20% w/v) was prepared in water and heated at 55°C in a water bath (Karl Kobb, Dreieich, Germany) with constant stirring for 15 min. The resulting paste was dried in an oven (Biobase Biotechnology Co. Ltd., Shandong, China) at 60°C for 48 h and sieved using a 250- $\mu$ m sieve mesh. The pre-gelatinized starch (NMPS) was stored in an airtight container and placed in a desiccator until further use.

### Evaluation of NMNS and NMPS

#### Morphology

Starch samples (NMNS and NMPS) were mounted on metal stubs, coated with gold and analyzed using a scanning electron microscope (SEM; ASPEX 3020, PSEM 2; Field Electron and Ion, FEI Corp, Hillsboro, USA). Images of the starch surfaces were obtained at  $\times 1000$  magnification at a current of 7 mA for 90 s.

## Fourier-transform infrared (FTIR) spectra studies

The starches (NMNS and NMPS) were triturated with potassium bromide powder and were made into pellets (1 ton/cm<sup>2</sup>). Infrared (IR) spectra were obtained between scanning ranges of 4000 cm<sup>-1</sup> and 400 cm<sup>-1</sup> from a Magna-IR 560 spectrometer (Perkin Elmer, Waltham, USA).

## Gelatinization temperature

The gelatinization temperature was determined using a differential scanning calorimeter (DSC; Model DSC 204 F1; Netzsch, Selb, Germany). Starch samples were placed in the aluminum pans of the equipment and scanned at between 60°C and 300°C at a heating rate of 10°C/min under constant nitrogen flow.

## pH determination

Slurries (5% w/v) of the starch samples were prepared in distilled water and the pH was measured at room temperature (28°C) using a pH meter (Metler Toledo, Greifensee, Switzerland). Triplicate determinations were made and the average value was recorded.

## Swelling power

Starch slurries (1% w/v) were prepared with distilled water and heated in a water bath at 40°C for 30 min. The dispersions were centrifuged at 1500 rpm for 30 min, the supernatant was discarded, the weight of the starch paste was determined, and the swelling power (SP) was computed using the equation below:

$$SP (\%) = \frac{\text{weight of starch paste}}{\text{initial weight of dry starch}} \times 100$$

This procedure was repeated at 50°C, 60°C, 70°C, 80°C, and 90°C for both starch samples.

## Hydration capacity

The method of Kornblum and Stoopak<sup>12</sup> was adopted to determine the starch hydration capacity (HC). Starch dispersions (1% w/v) were prepared with distilled water, poured into pre-weighed, stoppered centrifuge tubes and shaken intermittently for 10 min. The tubes were allowed to stand for another 10 min at room temperature and then centrifuged at 1500 rpm for 5 min. The supernatant was discarded, and the weight of the sediment (hydrated starch) was determined and used to compute the HC as shown below:

$$HC = \frac{\text{initial weight of dry starch}}{\text{weight of hydrated starch}} \times 100$$

## Flow properties

### Angle of repose

The angle of repose was determined using the funnel method. Twenty grams of starch sample were allowed to flow through the orifice of a funnel clamped at a fixed height from a flat surface. The height (h) and radius (r) of the heap formed were measured and used to compute the angle of repose (A) as shown below:

$$A = \tan^{-1} \frac{h}{r}$$

### Bulk and tapped densities

The volume occupied by the starch samples (50 g) in a graduated measuring cylinder was noted as the bulk volume and used to compute the bulk density [g/mL]. In the same way, the volume occupied by the samples after tapping the measuring cylinder 100 times was noted and used to compute the tapped density [g/mL]. Triplicate determinations were made for each parameter and the average value was computed accordingly.

### Carr's compressibility index (CI) and Hausner ratio (HR)

These were computed with data obtained from the bulk and tapped densities using the equations below:

$$CI = \frac{\text{tapped density} - \text{bulk density}}{\text{tapped density}} \times 100$$

$$HR = \frac{\text{tapped density}}{\text{bulk density}} \times 100$$

### True density

The liquid displacement method was adopted and liquid paraffin was used as the displacement fluid. Three determinations were made and the true density (Trd) was computed as shown below, where W<sub>p</sub> is the weight of starch powder, x is the weight of the bottle and fluid, y is the weight of the bottle, fluid and starch powder, and SG is the specific gravity of liquid paraffin (0.865 g/mL).

$$\text{Trd} = \frac{W_p}{[(x + W_p) - y] \times SG} \times 100$$

## Determination of pasting properties

The pasting properties of the starches (NMNS and NMPS) were determined using a Rapid Visco-Analyzer

(RVA; Perten Instruments, Macquarie Park, Australia). The method used previously by Shevkani et al.<sup>13</sup> was adopted, but with slight modifications. Starch–water suspensions based on a dry starch basis of 25 g were used in monitoring the viscograms of the starches. The different batches of suspensions containing NMNS and NMPS were tested under similar temperature and time conditions.

## Results and Discussion

The physicochemical properties of NMNS and NMPS are displayed in Table 1. The angle of repose is a reflection of the flow ability of a material and values  $<30^\circ$  indicate excellent flow, those between  $31^\circ$  and  $35^\circ$  show good flow, while values between  $36^\circ$  and  $40^\circ$  and  $>40^\circ$  signify that the material exhibits fair and poor flow, respectively.<sup>14</sup> This indirect measurement of the flow properties of the starches show that NMNS and NMPS had angles of repose of  $38.60^\circ$  and  $33.69^\circ$ , respectively (Table 1), and indicate that pre-gelatinization improved flow of the starch powder.

The ability of both starches to deform under pressure was computed using CI. Materials with a CI  $\leq 10\%$  are considered to have excellent flow, those between 11% and 15% – good flow, between 16% and 20% – fair, and those  $>25\%$  – poor flow. On the other hand, the measure of material cohesiveness, which depicts the degree of densification, was determined with the HR. Values  $\leq 1.11$  show that the material is cohesive, and it is less cohesive when HR values are between 1.12 and 1.20.<sup>15</sup> The CI of NMNS was found to be 10.97% and that of NMPS was 7.50%, while the HR was 1.12 and 1.05, respectively. These results indicate that both starches exhibit good flow. However, the process of pre-gelatinization improved the flow characteristics of NMPS appreciably. The Trd of NMPS (1.39) was higher than that of NMNS (0.89), suggesting an increased ability of NMNS to promote even packing when confined into processing spaces such as compaction or tableting dies.<sup>16</sup> The ability of materials to flow

is dependent on the particle size, shape and distribution of the particles in the material. Disruption of the starch granules and consequent agglomeration due to gelatinization (Fig. 1) produces voids within and between the particles. This reduces the friction between particles and allows for better flow, which invariably influences the packing behavior of the starches. Adequate/good flow is highly recommended in high-speed tableting/capsule filling machines as this ensures that the die cavities are uniformly filled, giving rise to tablets/capsules of uniform weight and uniform content.

The pH of the starches was 7.00 and 6.04 for NMNS and NMPS, respectively (Table 1), and falls with the specification of between 4.5 and 7.0 for starch solutions.<sup>17</sup> The near-neutral pH of both starches implies that problems with irritability in the gastrointestinal tract might not arise from the use of these starches, and therefore, they would be desirable for use in oral formulations.<sup>18</sup> The lower pH of NMPS observed in this study, which may be attributed to the modification process, is in agreement with a previous report by Azubuie et al.<sup>11</sup> that examined pre-gelatinized *Borassus aethiopom* starch.

The HC signifies the total amount of water that is retained by starch gel under defined conditions like pressure or heat.<sup>19</sup> Pre-gelatinized starch was observed to have the ability to retain twice the weight of water retained by NMNS (Table 1), and the HC of NMNS was 25.80% while that of NMPS was 59.00%. The increase observed in NMPS can be attributed to the loss of crystalline association in the granules, leading to more available binding sites for water.<sup>20</sup> The process of pre-gelatinization reduces the molecular weight of starch granules resulting in the ability to attract more water molecules and swell as compared to un-gelatinized starches.<sup>21</sup> Materials with high HCs such as NMPS have been documented to be useful as disintegrants because of their increased ability to absorb water and swell, which is part of the mechanism of action of starch as a disintegrant.<sup>22</sup>

Swelling is an important characteristic that reveals the ability of starch granules to absorb water. Investigating the swelling behavior of starch within different temperature ranges is important as it evaluates the performance of a starch under industrial conditions. Table 2 shows that swelling power of both starches increased with an in-

Table 1. Physicochemical properties of NMNS and NMPS (n = 3, mean  $\pm$ SD)

Parameter	NMNS	NMPS
Angle of repose [°]	38.60	33.69
Bulk density [g/mL]	0.61 $\pm$ 0.02	0.63 $\pm$ 0.02
Tapped density [g/mL]	0.69 $\pm$ 0.01	0.66 $\pm$ 0.01
Hausner ratio	1.12 $\pm$ 0.04	1.05 $\pm$ 0.04
Carr's index [%]	10.97 $\pm$ 2.91	7.50 $\pm$ 0.00
True density [g/mL]	0.89 $\pm$ 0.07	1.39 $\pm$ 0.03
Hydration capacity [%]	25.80 $\pm$ 0.04	59.00 $\pm$ 0.23
pH	7.00 $\pm$ 0.11	6.04 $\pm$ 0.50

SD – standard deviation; NMNS – native starch; NMPS – pre-gelatinized starch.

Table 2. Swelling power [%] of starches at different temperatures

Temperature [°C]	NMNS	NMPS
40	27.10	55.20
50	27.90	62.10
60	56.00	70.70
70	144.80	112.20
80	148.20	112.50
90	75.50	87.10

NMNS – native starch; NMPS – pre-gelatinized starch.

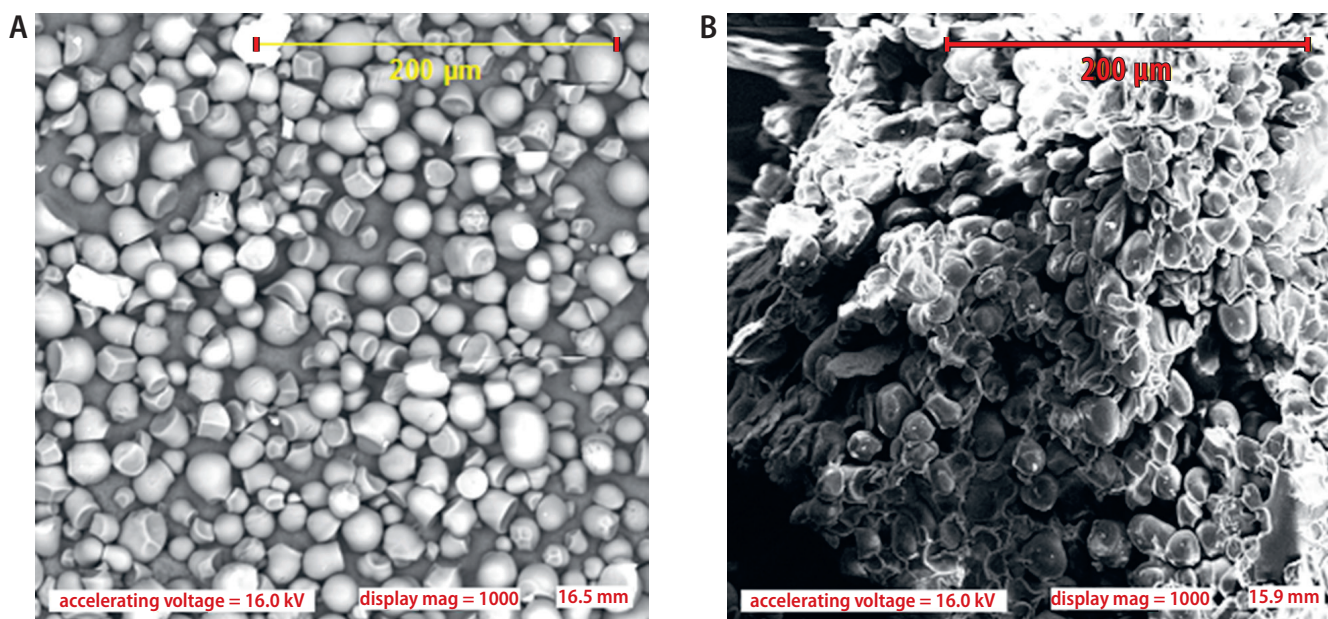


Fig. 1. SEM images of native *N. mitis* starch (NMNS) (A) and pre-gelatinized *N. mitis* starch (NMPS) (B)

crease in temperature up to 80°C, with more pronounced swelling occurring at higher temperatures (70°C and 80°C) than within lower temperature ranges (between 40°C and 60°C). Increased swelling at higher temperatures has been ascribed to a weakening of the intrinsic binding forces in the amorphous regions of the starch granules at varying temperatures.<sup>23</sup> Swelling was also found to be higher between 40°C and 60°C in NMPS than in NMNS. This effect can be ascribed to the destruction of the regular structure of the NMPS during pre-gelatinization, which conferred on it the ability to imbibe water increased over the temperatures. Swelling was observed to decrease considerably at 90°C to 75.50% and 87.10% for NMPS and NMNS, respectively, and can be attributed to total loss of granule structure and rupture of the granules.<sup>24</sup> This suggests that the maximum swelling temperature for both starches is 80°C, and can serve as a guide in determining where and how these starches (NMNS and NMPS) can be used.

Microscopic observation of the starches using SEM revealed that NMNS is discrete, smooth, non-porous, and almost spherical in shape (Fig. 1A), while the shape of NMPS is non-discrete, gel-like, rough, and irregular (Fig. 1B). Granules of pre-gelatinized starch (Fig. 1B) were also observed to be aggregated, which is due to granular disintegration and the subsequent release of soluble components during the thermal process of gelatinization. The particle sizes measured with SEM were 16.5 mm and 5.9 mm for NMNS and NMPS, respectively. Heating starch has been postulated to affect swelling and rupture of starch granules, which invariably affects the size of the resulting starch product.<sup>25</sup> Furthermore, the heating process may have caused the loss of the amylopectin crystalline region, with the consequent rearrangement of bonds within the granules leading to breakdown, distortion and loss of granule integrity. These observations

are in line with similar studies showing the effects of pre-gelatinization on starch morphology.<sup>26,27</sup>

The FTIR spectra of NMNS and NMPS scanned in the 4000–400 cm<sup>-1</sup> range are displayed in Fig. 2 and 3, while the absorption peaks and corresponding peak heights for NMNS and NMPS are presented in Tables 3 and 4, respectively.

Broad bands observed in both spectra at about 3800 cm<sup>-1</sup> and 3000 cm<sup>-1</sup> correspond to O–H stretching of hydrogen bonded hydroxyl groups, which may be ascribed to the presence of intra- and intermolecular hydrogen bonds in the starch granules.<sup>28</sup> The spectra of NMPS (Fig. 3) shows a stronger, broader O–H stretch at about 3800 cm<sup>-1</sup> with a peak height of 17.29 (Table 4) that is about 3 times higher than that of NMNS (6.88;

Table 3. Absorption peaks and corresponding heights of native starch

Peak at [cm <sup>-1</sup> ]	Peak height
938.40	25.14
1460.80	18.75
1938.40	17.44
2361.60	8.74
3803.20	6.88

Table 4. Absorption peaks and corresponding heights of pre-gelatinized starch

Peak at [cm <sup>-1</sup> ]	Peak height
938.40	32.23
1460.00	26.83
1930.40	25.34
2362.40	8.45
3802.40	17.29

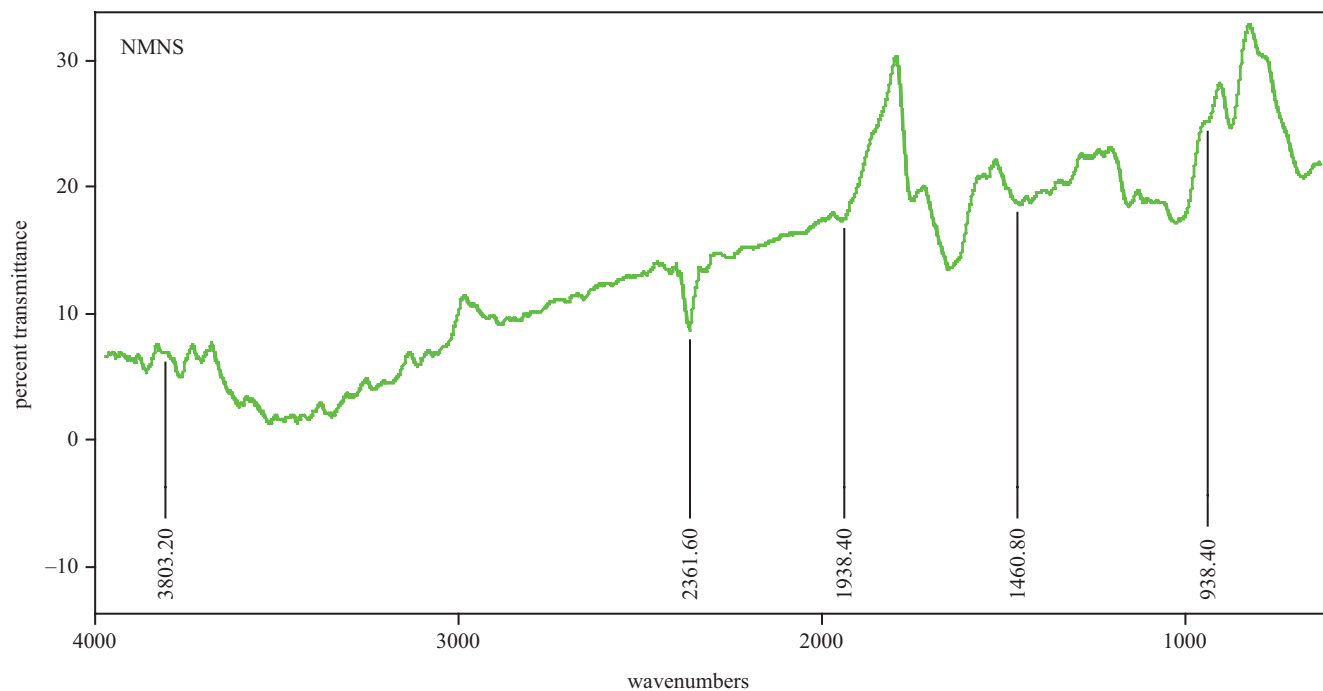


Fig. 2. FTIR spectra of native *N. mitis* starch (NMNS)

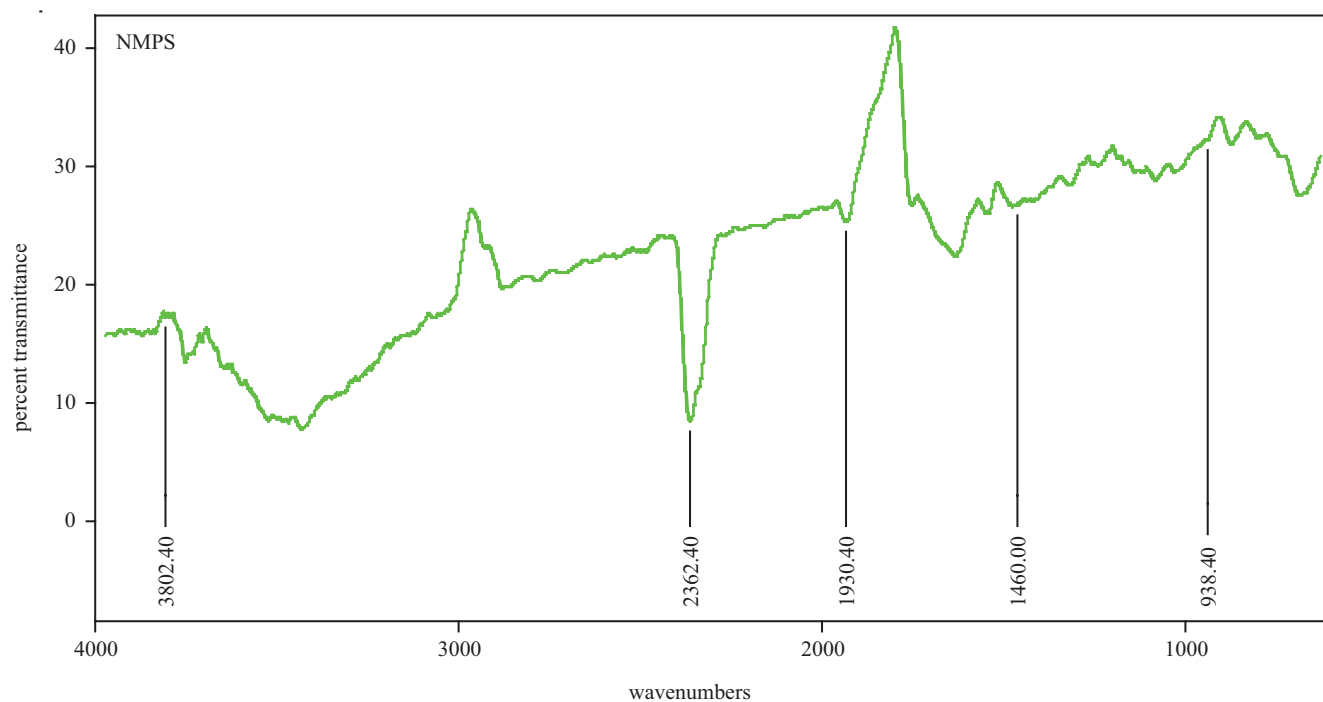


Fig. 3. FTIR spectra of pre-gelatinized *N. mitis* starch (NMPS)

Table 3). This can be attributed to the higher swelling capacity observed for NMPS. Vibrations at  $3000\text{ cm}^{-1}$  and  $2800\text{ cm}^{-1}$  are characteristic of C–H stretches associated with ring hydrogen atoms, and this vibration was observed to be intense in the spectra of NMPS. Previous studies have shown that such changes in modified starches are attributed to changes in the ratio of amylose to amylopectin, with a consequent influence on the physicochemical properties of the starch.<sup>29</sup>

Vibrations at about  $2300\text{ cm}^{-1}$ , which represent C–H stretch for the alkane group of compounds, were found to be similar for both starches (Tables 3,4). Absorption peaks at about  $1930\text{ cm}^{-1}$  (Fig. 2,3) correspond to scissors vibrations of O–H bonds as a result of water of hydration in the starches. However, vibrations in NMPS were observed to be stronger as evidenced by a sharper peak. Vibrations at about  $1460\text{ cm}^{-1}$  are related to C–H bending and both peaks were observed to be more intense

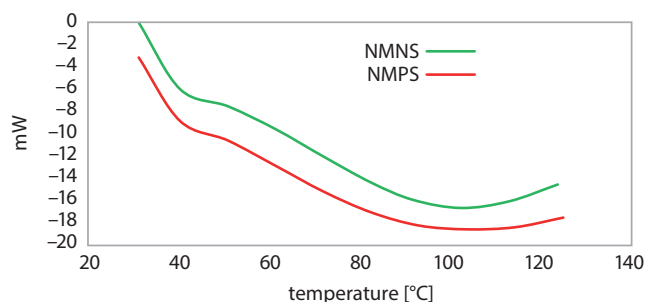


Fig. 4. Differential scanning calorimeter (DSC) thermogram of native *N. mitis* starch (NMNS) and pre-gelatinized *N. mitis* starch (NMPS)

in NMPS than NMNS. Vibrations at about  $930\text{ cm}^{-1}$  are the skeletal absorptions of  $\alpha$ -1,4 glycosidic linkage characteristic of all polysaccharides, consisting of COH and C–O–C glycosidic stretching and bending.<sup>30</sup> These vibrations were observed at the same absorption wave number for both starches and depict similarity in the basic fingerprint of both starches. The last region has been defined as the characteristic fingerprint of materials like starches.<sup>31</sup>

The results from FTIR spectroscopy show that pre-gelatinization did not introduce any new functional groups. However, this process affected the arrangement of the molecules in the starch particles as evidenced by the shifting of some of the bands.

The behavior of NMNS and NMPS when subjected to heat was determined with DSC and the thermograms are displayed in Fig. 4. The thermal properties of the starches such as onset temperature, peak temperature, conclusion temperature, and gelatinization enthalpy, among others, are presented in Table 5.

Although starch granules are insoluble in cold water, heat treatment in the presence of water causes gelatinization, which involves swelling of the granules, melting of the crystallite double helices, leaching of amylose, and consequent disintegration of the granules.<sup>32</sup> This transitional phase of starch granules is a distinguishing property of individual starches that allows for their application in industrial processes.

Enthalpy of gelatinization ( $\Delta H$ ) gives an inclusive measure of the quantity and quality of crystallinity in starch granules, and is an indicator of the loss of molecular order within the granule that occurs with gelatinization.<sup>33</sup>

In other words,  $\Delta H$  is related to the energy required to disrupt starch granules and is a reflection of the heat involved in breaking the bonds between starch granules. The outcome of gelatinization is influenced by shape, amylopectin chain length and crystalline portions of the starch.<sup>34</sup>

Table 5 shows that NMPS has a lower  $\Delta H$  (5.27) compared to NMNS (6.38). This could be attributed to the fact that some double helices in NMPS may have been disrupted during the process of pre-gelatinization. Therefore, lower energy was required to initiate the gelatinization process of the starch granule. Furthermore, weakening of the starch granules during pre-gelatinization could have resulted in early rupture of the amylopectin helices, leading to the observed lower values for onset temperature ( $T_o$ ), conclusion temperature ( $T_c$ ) and peak temperature ( $T_p$ ). Similar results have also been reported regarding some other modified starches.<sup>35,36</sup>

In addition, since  $\Delta H$  reflects melting of the crystalline region of the starch granules, the low values observed for NMPS may also be connected with low crystalline association within starch granules, indicating that less crystalline portions are present.<sup>37,38</sup> The degree of crystallinity of starch is known to be directly related to its granule strength, and demonstrates the extent to which the bond order within the starch molecule is broken and melted during the heating process.<sup>39</sup> High  $\Delta H$  shows that higher energy is required to disrupt the bond order because of the presence of strong bonds between the granules. However, a low  $\Delta H$ , as observed for NMPS, shows that lower energy was required to break the bonds due to the rupture of the starch granules during the process of gelatinization.

The application of heat in an ordered manner and the analysis of the obtained viscograms are the measures that enable determining the pasting properties. When heat is applied to starch, there is a transformation of the granules from an initial ordered state to a randomized, but disordered state, which is a result of the swelling of the granules.<sup>40</sup> Starch granules are usually saturated with water, but as heat is applied, the granules begin to swell and the water that has been imbibed in the granule aids melting of the crystal lattice of the starch, thus creating room for rapid movement of water between the granules and within the granules. Subsequently, more water molecules bind to the starch granules, while the swelling reduces

Table 5. Thermal properties of NMNS and NMPS

Parameter	Peak height for NMNS	Peak height for NMPS
Onset temperature [°C]	31.19	30.58
Peak temperature [°C]	92.40	89.86
Conclusion temperature [°C]	156.89	159.06
Enthalpy of gelatinization [J/(g*K)]	6.38	5.27
$\Delta T$ (gelatinization temperature range) [°C]	125.70	128.48

NMNS – native starch; NMPS – pre-gelatinized starch.

Table 6. Pasting properties of NMNS and NMPS (n = 3, mean  $\pm$ SD)

Starch sample	Peak viscosity [cP]	Trough viscosity [cP]	Breakdown viscosity [cP]	Final viscosity [cP]	Setback viscosity [cP]	Peak time [min]	Pasting temperature [°C]
NMNS	745.33 $\pm$ 0.20	250.08 $\pm$ 0.02	495.25 $\pm$ 0.13	360.75 $\pm$ 0.16	110.67 $\pm$ 0.05	3.80 $\pm$ 0.13	76.8 $\pm$ 0.06
NMPS	585.17 $\pm$ 0.11	407.83 $\pm$ 0.12	177.33 $\pm$ 0.02	689.75 $\pm$ 0.12	281.92 $\pm$ 0.02	4.67 $\pm$ 1.02	75.9 $\pm$ 0.01

SD – standard deviation; NMNS – native starch; NMPS – pre-gelatinized starch.

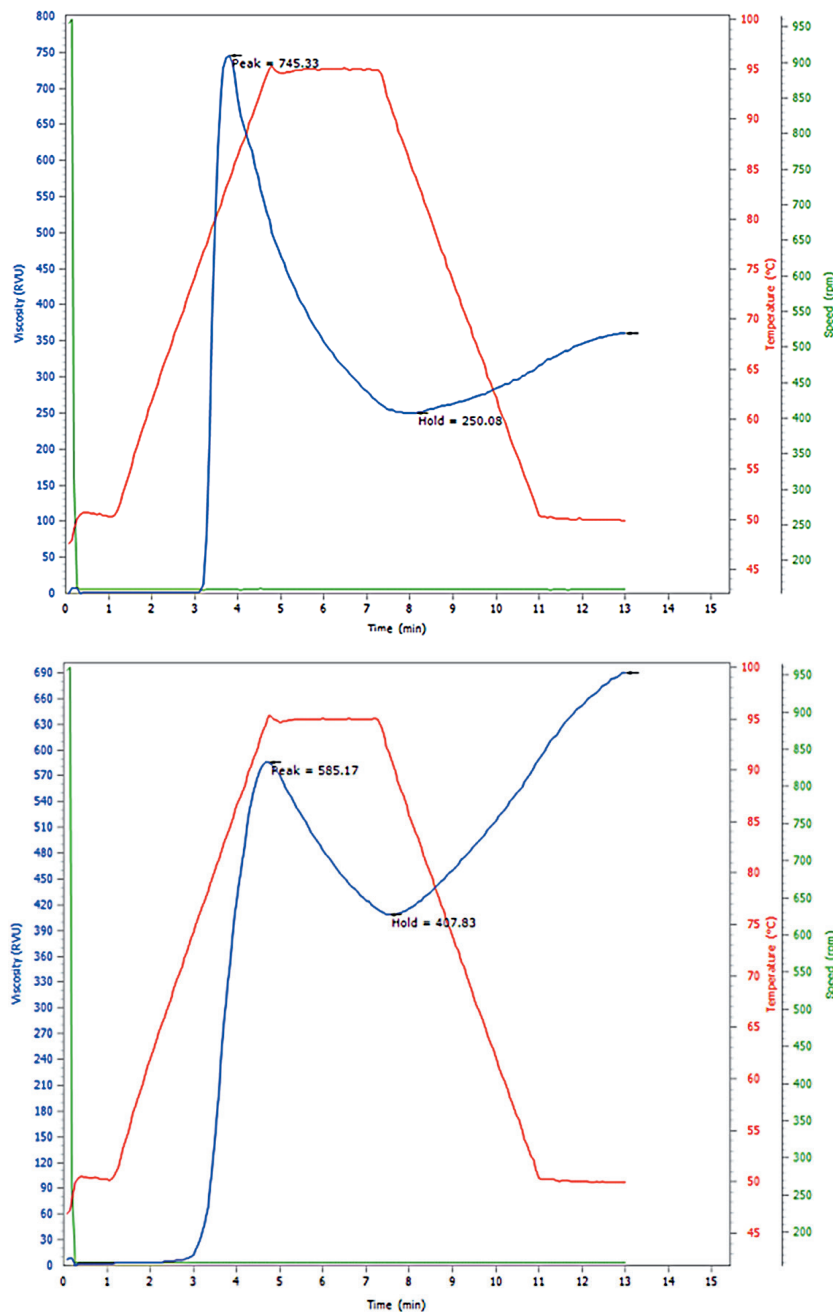


Fig. 5. Pasting profiles of native *N. mitis* starch (NMNS) and pre-gelatinized *N. mitis* starch (NMPS)

the available water, resulting in physical interactions between the granules. These interactions lead to changes in the viscosity of the starch.

The pasting profiles and properties (derived from the viscograms) of NMNS and NMPS are shown in Fig. 5 and Table 6, respectively. The pasting properties varied

significantly among the starch samples. Native starch had better peak viscosity, breakdown viscosity and pasting temperature, while NMPS presented better trough viscosity, final viscosity, setback viscosity, and pasting time.

The high peak viscosity observed for NMNS (745.33 cP) may be due to the nonporous nature of the NMNS gran-



ules, leading to a greater volume of water within the crystal lattice and, consequently, a higher viscosity compared to the NMPS granules. Degradation of starch granules as a result of pre-gelatinization is responsible for reduced viscosity against shear stress,<sup>41</sup> as observed in NMPS. The measure of peak viscosity, which is associated with the rate at which granule swelling equals granule breakdown, is slower for NMNS than for NMPS based on the aggregation of granules, as observed from the morphology using SEM. Granules of NMPS were more compact than those of NMNS and could account for the higher trough viscosity observed for NMPS. Trough viscosity reflects paste viscosity due to the disruption of starch granules upon heating and was observed to be higher in NMPS than NMNS as a result of the compactness of the granules.

Breakdown viscosity is a measure of the degree of disintegration of gelatinized starch granules during heating.<sup>42</sup> The already gelatinized NMPS is thus expected to have a lower breakdown viscosity than NMNS due to the reduction in starch granules available for further disintegration to take place. The final viscosity indicates the stability of starch pastes to heat.<sup>43</sup> The results show that NMPS exhibited a higher final viscosity (689.75 cP) than NMNS (360.75 cP), indicating that pastes from NMPS are more stable to heat than those from NMNS. In addition, final viscosity reflects the resistance of the starch paste to flow. The lower value observed for NMNS suggests its flow ease, which could be a result of more water molecules available within the crystal lattice of NMNS than in NMPS, while NMPS exhibited a higher resistance to shear and flow. Such high final viscosity and low breakdown viscosity properties have been described as desirable for many food and industrial processes.<sup>44</sup>


The setback viscosity is exhibited due to recrystallization of the amylose molecules in the gel<sup>45</sup> and shows the tendency for retrogradation to occur. Although NMPS, which has a higher resistance to flow, would be expected to exhibit low setback viscosity because of the disruption of amylose molecules that took place during the pre-gelatinization process, the setback viscosity of NMPS (281.92 cP) was higher than that of NMNS (110.67 cP). This could suggest the tendency of NMPS to undergo some form of gelling upon cooling, a phenomenon that has also been demonstrated when pre-gelatinized cassava and rice starch were blended together.<sup>46</sup> The temperature at which the viscosity of the starch material begins to increase during the heating process is known as the pasting temperature. According to Salman et al.,<sup>47</sup> high pasting temperature is an indication of a high degree of crystallinity of starch molecules. The crystal lattice in the NMNS was more ordered than in the NMPS, which was disoriented due to pre-gelatinization, thus accounting for NMNS having a slightly higher pasting temperatures. However, the pasting temperatures of NMNS and NMPS were not significantly different. Visco-analysis shows that pre-gelatinization changed the pasting properties of native starch extracted from the tubers of *N. mitis*.


## Conclusions

In this study, we have been able to modify starch from an underutilized crop, *N. mitis* tubers, by pre-gelatinization. Pre-gelatinization improved the flow properties, and increased the absorption capacity and SP, as observed with other pre-gelatinized starches. However, the granule strength was found to decrease. The pre-gelatinized *N. mitis* starch also exhibited peculiar pasting behavior with low viscosities but good thermal stability, as has been reported for other pre-gelatinized starches. The findings of the present study show that pre-gelatinized *N. mitis* starch may be applicable for food, cosmetics and pharmaceutical products where high swelling/hydration, low viscosity and low bond strength are required. However, further research to determine crystallinity and the molecular weight of the native and pre-gelatinized starches may be conducted.

### ORCID iDs

Olubunmi Olayemi  <https://orcid.org/0000-0001-5759-7176>

Oladapo Adetunji  <https://orcid.org/0000-0002-3474-0029>

Christianah Isimi  <https://orcid.org/0000-0002-9066-9984>

### References

- Siregar C, Saleh W. *Pharmaceutical Tablet Dosage Technology. Basics of Practical*. Jakarta, Indonesia: Medical Book Publishers EGC; 2010.
- Chen Q, Yu H, Wang L, et al. Recent progress in chemical modification of starch and its applications. *RSC Adv*. 2015;5(83):67459–67474. doi:10.1039/C5RA10849G
- Kaur B, Ariffin F, Bhat R, Karim AA. Progress in starch modification in the last decade. *Food Hydrocoll*. 2012;26(2):398–404. doi:10.1016/j.foodhyd.2011.02.016
- Rowe RC, Paul JS, Sian CO. *Handbook of Pharmaceutical Excipient*. 5<sup>th</sup> ed. London, UK: The Pharmaceutical Press and Pharmaceutical Pharmacists Association; 2006.
- Anastasiades A, Thanou S, Loulis D, Stapatoris A, Karapantsios TD. Rheological and physical characterization of pregelatinized maize starches. *J Food Eng*. 2002;52:57–66. doi:10.1016/S0260-8774(01)00086-3
- Pramulani ML, Ari W, Hani A. The effect of pregelatinized taro starch (*Colocasia esculenta* (L.) schott) temperature as filler on thiamine hydrochloride tablet. *Open Access Macedonian J Med Sci*. 2019;7(22):3827–3832. doi:10.3889/oamjms.2019.513
- Burkill HM. *The Useful Plants of West Tropical Africa*. Vol. 3 (J–L). Kew, UK: Royal Botanic Garden; 1995:1400–1410.
- Vongtau HO, Abbah J, Mosugu O, et al. Antinociceptive profile of the methanolic extract of *Neorautanenia mitis* root in rats and mice. *J Ethnopharmacol*. 2004;92:317–324. doi:10.1016/j.jep.2004.03.014
- Lasisi AA, Adesomoju A. Neoraudiol: A new isoflavonoid and other antimicrobial constituents from the tuberous root of *Neorautanenia mitis* (A. Rich) verdcourt. *J Saudi Chem Soc*. 2015;19:404–409. doi:10.1016/j.jscs.2012.04.011
- Olayemi OJ, Ekunboyejo A, Bamiro OA, Kunle OO. Evaluation of disintegrant properties of *Neorautanenia mitis* starch. *J Phytomed Ther*. 2016;15(2):53–64.
- Azubuie CP, Ubani-Ukoma U, Madu SJ, Yomi-Faseun O, Yusuf S. Characterization and application of *Borassus aethiopum* (Arecaceae) shoot pre-gelatinized starch as binding agent in paracetamol tablets. *J Rep Pharm Sci*. 2019;8:172–180. doi:10.4103/jrptps.JRPTPS\_29\_18
- Kornblum SS, Stoopak SB. A new tablet disintegrating agent: Cross-linked polyvinylpyrrolidone. *J Pharm Sci*. 1973;62(1):43–49. doi:10.1002/jps.2600620107
- Shevkani K, Singh N, Bajaj R, Kaur A. Wheat starch production, structure, functionality and applications: A review. *Int J Food Sci Technol*. 2017;52(1):38–58. doi:10.1111/ijfs.13266

14. Mohammadi MS, Harnby N. Bulk density modelling as a means of typifying the microstructure and flow characteristics of cohesive powders. *Powder Technol.* 1997;92(1):1–8. doi:10.1016/S0032-5910(96)03254-8
15. Lefnaoui S, Moulai-Mostefa N. Synthesis and evaluation of the structural and physicochemical properties of carboxymethyl pre-gelatinized starch as a pharmaceutical excipient. *Saudi Pharm J.* 2015; 23(6):698–711. doi:10.1016/j.jsps.2015.01.021
16. Eraga SO, Ndukwe JO, Iwuagwu MA. An investigation of the direct compression properties of pre-gelatinized African bitter yam and cassava starches in acetylsalicylic acid tablet formulations. *J App Sci Environ Manag.* 2017;21(5):855–862. doi:10.4314/jasem.v21i5.10
17. British Pharmacopoeia Commission. *British Pharmacopoeia.* London, UK: TSO Publishers; 2017.
18. Hassan LG, Muhammad AB, Aliyu RU, et al. Extraction and characterization of starches from four varieties of *Mangifera indica* seeds. *IOSR J Appl Chem.* 2013;3(6):16–23. doi:10.9790/5736-0361623
19. Lawal OS. Composition, physico-chemical properties and retrogradation, characteristics of native, oxidized, acetylated and acid thinned new cocoyam (*Xanthosoma sagittifolium*) starch. *Food Chem.* 2004; 87(2):205–218. doi:10.1016/j.foodchem.2003.11.013
20. Manmeet-Kaur DPS, Oberoi DS, Sogi BSG. Physicochemical, morphological and pasting properties of acid treated starches from different botanical sources. *J Food Sci Technol.* 2010;48(4):460–465. doi:10.1007/s13197-010-0126-x
21. Adeyanju O, Olademehin OP, Hussaini Y, Nwanta UC, Adejoh AI, Plavec J. Synthesis and characterization of carboxymethyl *Plectranthus esculentus* starch: A potential disintegrant. *J Pharm Appl Chem.* 2016;2(3):189–195. doi:10.18576/jpac/020309
22. Adedokun MO, Itiola OA. Disintegrant activities of natural and pre-gelatinized trifoliolate yams, rice and corn starches in paracetamol tablets. *J Appl Pharm Sci.* 2011;1(10):200–206. [http://japsonline.com/admin/php/uploads/328\\_pdf](http://japsonline.com/admin/php/uploads/328_pdf)
23. Pérez S, Bertoft E. The molecular structures of starch components and their contribution to the architecture of starch granules: A comprehensive review. *Starch/Stärke.* 2010;62:389–420. doi:10.1002/star.201000013
24. Sunarti TC, Richana N, Purwoko FK, Budiyanoto A. *The Characterization of Physicochemical Properties of Flour and Starch of National Varieties Corn and Filing of the Enzyme and Acid. The Research Report.* Bogor, Indonesia: Bogor Agricultural Institute; 2007.
25. Ambigaipalan P, Hoover R, Donner E, et al. Structure of faba bean, black bean and pinto bean starches at different levels of granule organization and their physicochemical properties. *Food Res Int.* 2011;44(9):2962–2974. doi:10.1016/j.foodres.2011.07.006
26. Wijanarka A, Sudargo T, Harmayani E, Marsono Y. Effect of pre-gelatinization on physicochemical and functional properties of gayam (*Inocarpus fagifer* Forst.) flour. *Am J Food Technol.* 2017;12:178–185. doi:10.3923/ajft.2017.178.185
27. Adewumi FD, Lajide L, Adetuyi AO, Ayodele O. Synthesis and characterization of native and pre-gelatinized cassava starches. *Am J Innov Res Appl Sci.* 2019;9(4):418–424.
28. Ferreira-Villadiego J, García-Echeverría J, Vidala MV, et al. Chemical modification and characterization of starch derived from plantain (*Musa paradisiaca*) peel waste, as a source of biodegradable material. *Chem Eng Trans.* 2018;65:763–768. doi:10.3303/CET1865128
29. Olayemi B, Isimi C, Ekere K, Ajeh IJ, Okoh JE, Emeje MO. Green preparation of citric acid crosslinked starch for improvement of physicochemical properties of *Cyperus* starch. *Turkish J Pharm Sci.* 2021; 18(1):34–43. doi:10.4274/tjps.galenos.2019.65624
30. Oniszczyk T, Combrzyński M, Matwijczuk A, et al. Physical assessment, spectroscopic and chemometric analysis of starch-based foils with selected functional additives. *PLoS One.* 2019;14(2):e0212070. doi:10.1371/journal.pone.0212070
31. Ohwoavworhua FO, Osinowo A. Preformulation studies and compaction properties of a new starch-based pharmaceutical aid. *Res J Pharm Biol Chem Sci.* 2010;1:255–270.
32. Šárka E, Dvořáček V. New processing and applications of waxy starch (a review). *J Food Eng.* 2017;206:77–87. doi:10.1016/j.jfoodeng.2017.03.006
33. Cooke D, Gidley MJ. Loss of crystalline and molecular order during starch gelatinization: Origin of the enthalpic transition. *Carbohydr Res.* 1992;227:103–112. doi:10.1016/0008-6215(92)85063-6
34. Singh N, Kaur L. Morphological, thermal, rheological and retrogradation properties of starch fractions varying in granule size. *J Sci Food Agric.* 2004;84:1241–1252. doi:10.1002/jsfa.1746
35. Olayinka OO, Olu-Owolabi BI, Adebowale KO. Effect of chemical modifications on thermal, rheological and morphological properties of yellow sorghum starch. *J Food Sci Technol.* 2015;52(12):8364–8370. doi:10.1007/s13197-015-1891-3
36. Rangelov A, Arnaudov L, Stoyanov S, Spassov T. Gelatinization of industrial starches studied by DSC and TG. *Bulg Chem Commun.* 2017; 49(2):422–429.
37. Bhupender SK, Rajneesh B, Baljeet SY. Physicochemical, functional, thermal and pasting properties of starches isolated from pearl millet cultivars. *Int Food Res J.* 2013;20:1555–1561. [http://www.ifrj.upm.edu.my/20%20\(04\)%202013/6%20IFRJ%2020%20\(04\)%202013%20Bhupender%20\(390\).pdf](http://www.ifrj.upm.edu.my/20%20(04)%202013/6%20IFRJ%2020%20(04)%202013%20Bhupender%20(390).pdf)
38. Lai VMF, Lu S, Lii CY. Molecular characteristics influence retrogradation kinetics of rice amylopectins. *Cereal Chem.* 2000;77(3):272–278. doi:10.1094/CCHEM.2000.77.3.272
39. Shah N, Mewada KR, Meht T. Crosslinking of starch and its effect on viscosity behavior. *Rev Chem Eng.* 2016;32(2):265–270. doi:10.1515/revce-2015-0047
40. Jane JL, Chen YY, Lee, LF, et al. Effects of amylopectin branch chain length and amylose content on the gelatinization and pasting properties of starch. *Cereal Chem.* 1999;76:629–637. doi:10.1094/CCHEM.1999.76.5.629
41. Buchholz BA, Zahn JM, Kenward M, Slater GW, Barron AE. Flow-induced chain scission as a physical route to narrowly distributed, high molar mass polymers. *Polymer.* 2004;45(4):1223–1234. doi:10.1016/j.polymer.2003.11.051
42. Hong PV, Morita N. Physicochemical properties of hydroxypropylated and cross-linked starches from A-type and B-Type wheat starch granules. *Carbohydr Polym.* 2005;59(2):239–246. doi:10.1016/j.carbpol.2004.09.016
43. Daniel S, Wardana AA, Surono IS. Resistant starch content, pasting properties, and morphology of taro (*Colocasia esculenta* L. Schott) flour modified by heat moisture treatment. *J Phys Conf Ser.* 2019; 1363:012007. doi:10.1088/1742-6596/1363/1/012008
44. Yousif EI, Gadallah MGE, Sorour AM. Physico-chemical and rheological properties of modified corn starches and its effect on noodle quality. *Ann Agric Sci.* 2012;57(1):19–27. doi:10.1016/j.aogas.2012.03.008
45. Lovedeep K, Jaspreet S, Owen JM, Harmit S. Physicochemical, rheological and structural properties of fractionated potato starches. *J Food Eng.* 2007;82(3):383–394. doi:10.1016/j.jfoodeng.2007.02.059
46. Tô HT, Karrila SJ, Nga LH, Karrila TT. Effect of blending and pregelatinizing order on properties of pregelatinized starch from rice and cassava. *Food Res.* 2020;4(1):102–112. doi:10.26656/fr.2017.4(1).245
47. Salman H, Blazek J, Lopez-Rubio A, Gilbert EP, Hanley T, Copeland L. Structure–function relationships in A and B granules from wheat starches of similar amylose content. *Carbohydr Polym.* 2009;75: 420–427. doi:10.1016/j.carbpol.2008.08.001

# Kinetics of neomycin release from polylactide spheres and its antimicrobial activity

## Kinetyka uwalniania neomycyny z sfer polilaktydowych i ich aktywność mikrobiologiczna

Agnieszka Gadomska-Gajadur<sup>1,A,B,D</sup>, Paweł Ruśkowski<sup>1,A,C,E,F</sup>, Aleksandra Kruk<sup>3,B,D</sup>, Jolanta Mierzejewska<sup>2,B,C</sup>

<sup>1</sup> Chair of Polymer Chemistry and Technology, Faculty of Chemistry, Warsaw University of Technology, Poland

<sup>2</sup> Chair of Drug and Cosmetics Biotechnology, Faculty of Chemistry, Warsaw University of Technology, Poland

<sup>3</sup> Department of Pharmacognosy and Molecular Basis of Phytotherapy, Faculty of Pharmacy, Medical University of Warsaw, Poland

A – research concept and design; B – collection and/or assembly of data; C – data analysis and interpretation;

D – writing the article; E – critical revision of the article; F – final approval of the article

Polymers in Medicine, ISSN 0370-0747 (print), ISSN 2451-2699 (online)

Polim Med. 2021;51(1):17–24

### Address for correspondence

Paweł Ruśkowski

E-mail: pawel.ruskowski@ch.pw.edu.pl

### Funding sources

Financial support of Warsaw University of Technology, Faculty of Chemistry is gratefully acknowledged.

### Conflict of interest

None declared

Received on May 28, 2021

Reviewed on June 7, 2021

Accepted on June 29, 2021

Published online on July 30, 2021

### Cite as

Gadomska-Gajadur A, Ruśkowski P, Kruk A, Mierzejewska J. Kinetics of neomycin release from polylactide spheres and its antimicrobial activity. *Polim Med.* 2021;51(1):17–24. doi:10.17219/pim/139586

### DOI

10.17219/pim/139586

### Copyright

© 2021 by Wrocław Medical University

This is an article distributed under the terms of the Creative Commons Attribution 3.0 Unported (CC BY 3.0) (<https://creativecommons.org/licenses/by/3.0/>)

## Abstract

**Background.** Neomycin is a natural aminoglycoside antibiotic produced by actinomycete *Streptomyces fradiae*. It exerts bacteriostatic and bactericidal activity against Gram-negative bacteria, certain Gram-positive bacteria and *Mycobacterium tuberculosis*. Neomycin inhibits the biosynthesis of bacterial proteins by impairing their life functions, leading to death of cells.

**Objectives.** To examine the effect of molecular weight of polylactide (PLA), the applied stabilizer as well as mixing speed used in the encapsulation process on the size of obtained spheres. Examination of the kinetics of neomycin release from the obtained PLA spheres and determination of the antimicrobial activity of the neomycin-containing spheres against selected strains of bacteria, yeast and fungi have also been necessary.

**Materials and methods.** Polylactide ( $M_n$  3000–40,000 g/mol) was obtained in-house. Other materials used in the study were as follows: L-lactic acid (PLLA;  $M_n$  66,500 g/mol and 86,000 g/mol), polyvinyl alcohol (PVA) as a stabilizer of emulsion ( $M_w$  30,000 g/mol, 130,000 g/mol; degree of hydrolysis 88%) as well as dichloromethane, p.a. and dimethyl sulfoxide (DMSO), p.a. as solvents. Distilled water was obtained in-house. Neomycin sulfate was used for encapsulation; phosphate (pH 7.2) and acetate (pH 4.5) buffers were used for the examination of the active pharmaceutical ingredient (API) dissolution profile. Antimicrobial activity was tested using commercial cell lines and the following media: Mueller–Hinton agar (MHA), Mueller–Hinton broth (MHB), yeast extract peptone dextrose (YPD), and potato dextrose agar (PDA).

**Results.** Neomycin-containing PLA spheres were obtained using an emulsion method. The average molecular weight of PLA, the average molecular weight of PVA and mixing speed on the size of obtained spheres were investigated. Furthermore, the profile of API dissolution from the spheres and antimicrobial activity of neomycin-containing spheres against certain strains of bacteria, yeast and fungi were determined.

**Conclusions.** We demonstrated that efficient encapsulation of neomycin requires spheres of a <200 mm diameter.

**Key words:** encapsulation, polyesters, drug delivery systems

## Streszczenie

**Wprowadzenie.** Neomycyna jest naturalnym antybiotykiem aminoglikozydowym produkowanym przez promieniowce *Streptomyces fradiae*. Działa bakterio- statycznie i bakterioobójczo na bakterie Gram-ujemne, niektóre bakterie Gram-dodatnie oraz na *Mycobacterium tuberculosis*. Neomycyna hamuje biosyntezę białek bakteryjnych poprzez upośledzenie ich funkcji życiowych, prowadząc do śmierci komórek.

**Cel pracy.** Celem pracy było zbadanie wpływu masy cząsteczkowej polilaktydu (PLA), zastosowanego stabilizatora oraz szybkości mieszania stosowanej w procesie enkapsulacji na wielkość otrzymanych sfer. Niezbędne było również zbadanie kinetyki uwalniania neomycyny z otrzymanych sfer PLA oraz określenie aktywności antymikrobiologicznej sfer zawierających neomycynę wobec wybranych szczepów bakterii, drożdży i grzybów.

**Materiał i metody.** Polilaktyd ( $M_n$  3 000–40 000 g/mol) zsyntetyzowano we własnym zakresie. Inne materiały użyte w badaniach to: kwas mlekowy (PLLA) ( $M_n$  66 500 g/mol i 86 000 g/mol (Nature Works)), poli(alkohol winylowy) (PVA) jako stabilizator emulsji ( $M_w$  30 000 g/mol, 130 000 g/mol oraz stopień hydrolizy 88%, Mowiol) oraz dichlorometan (cz.d.a.), dimetylosulfotlenek (cz.d.a.) jako rozpuszczalniki. Wodę destylowaną uzyskano na miejscu. Do enkapsulacji stosowano siarczan neomycyny (Sigma–Aldrich); Do badania profilu rozpuszczania API zastosowano bufor fosforanowy (pH 7,2) i octanowy (pH 4,5). Aktywność antymikro- biologiczną zbadano przy użyciu komercyjnych linii komórkowych i następujących pożywek: agar Muellera–Hinton, bulion Muellera–Hinton, ekstrakt drożdżowy z peptonem z dekstrozą i ziemniaczany agar z dekstrozą.

**Wyniki.** Polilaktydowe sfery zawierające neomycynę otrzymano metodą emulsyjną. Zbadano wpływ średniego ciężaru cząsteczkowego polilaktydu, średniego ciężaru cząsteczkowego PVA oraz szybkości mieszania na rozmiar otrzymanych sfer. Ponadto wyznaczono profil uwalniania API ze sfer i aktywność antymikrobiologiczną wobec wybranych szczepów bakterii, drożdży i grzybów strzępkowych.

**Wnioski.** Wykazano, że neomycyna efektywnie enkapsuluje w sferach o średnicy <200 nm.

**Słowa kluczowe:** enkapsulacja, poliestry, systemy dostarczania leków

## Background

Controlled-release drug delivery systems (DDS) are a modern form of medicines. Compared to conventional dosage forms, they are characterized by a long-lasting therapeutic effect, improved biodistribution of active pharmaceutical ingredient (API) and minimization of toxic adverse reactions.<sup>1</sup> As a result, they increase the therapeutic index of conventional pharmaceuticals.<sup>2</sup> Among the recently developed DDSs available on the market,<sup>3</sup> polymeric spheres are distinguished by various applications.<sup>4</sup>

Neomycin is a natural aminoglycoside antibiotic produced by the actinomycete *Streptomyces fradiae* (Fig. 1). It has bacteriostatic and bactericidal activity against Gram-negative bacteria, certain Gram-positive bacteria and *Mycobacterium tuberculosis*.<sup>5</sup> Neomycin inhibits the biosynthesis of bacterial proteins by impairing their life functions, leading to cell death. Despite its broad spectrum of activity, neomycin is rarely used due to its harmful effect on the inner ear and kidneys (oto- and nephrotoxicity).

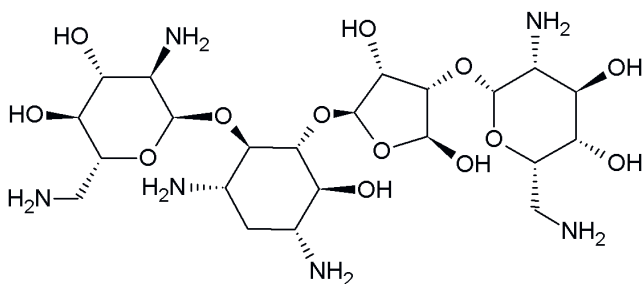


Fig. 1. Neomycin

Therefore, it is applied mainly externally in diseases of the skin, eyes and mucous membranes, or administered parenterally in the treatment of septicemia.<sup>6</sup> For these reasons, efforts have been undertaken to develop novel, more valuable forms of neomycin administration in an attempt to improve its absorption and minimize its toxic adverse effects.<sup>7</sup>

Polymeric spheres bring hope to current limitations related to the delivery of neomycin.<sup>8</sup> The spheres are ball-shaped particles, in which the active substance may be bound to the polymer matrix (prodrugs), suspended therein or adsorbed on their surface.<sup>9</sup> The systems for delivering antibiotics within a polymer matrix ensure a slow release of API to the body,<sup>10</sup> which reduces adverse effects and increases the therapeutic index of API.<sup>11</sup>

Polymer spheres used in DDS have diameters of 10–300 nm. It is believed that small spheres (less than 100 nm in diameter) show better biodistribution within the body and are less prone to premature degradation by phagocytic cells of the immune system.<sup>12</sup> However, it should be noted that due to the size and structural complexity of their molecules, encapsulation of some APIs in polymer matrices requires large spheres (over 100 nm in diameter) and also long-chain polymers.<sup>13</sup> An example of such API is neomycin, which is characterized by a complex structure of 4 aminoglycoside rings.<sup>14</sup>

The polymer widely used in DDS is polylactide (PLA), a biocompatible and biodegradable aliphatic polyester.<sup>15</sup> Within the organism, it undergoes decomposition to non-toxic products (carbon dioxide and water) that are readily eliminated. Polylactide consists of linearly linked moieties

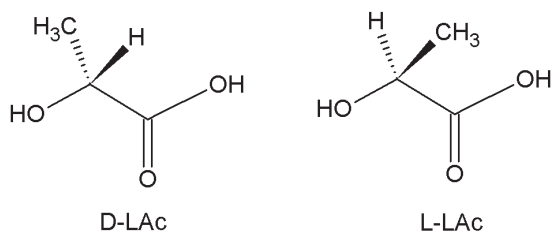


Fig. 2. Enantiomers of lactic acid

of lactic acid (LA).<sup>16</sup> Since LA exists in 2 enantiomeric forms (Fig. 2), it is possible to obtain polymers of various configurations at their chiral centers and, thus, different physical properties.<sup>17</sup> Homochiral PLA that consists solely of molecules of either L-lactic acid (PLLA) or D-lactic acid (PDLA) is characterized by high mechanical strength and long biodegradation time that improves as the carbon chain lengthens. Heterochiral polylactide that contains both enantiomers of LA in its structure is more elastic and undergoes biodegradation more readily.<sup>18</sup> Only the L-isomer of LA is metabolized in the body, while the D-enantiomer may accumulate in tissues leading to acidification of the body.<sup>19</sup> Therefore, PLLA having a low molecular weight and containing several percent of the D-monomer is most relevant for pharmaceutical applications.<sup>20</sup>

The purpose of this study was to examine the effects of the molecular weight of PLA, the applied stabilizer as well as the mixing speed used in the encapsulation process on the size of obtained spheres. Examination of the kinetics of neomycin release from the obtained PLA spheres and determination of the antimicrobial activity of the neomycin-containing spheres against selected strains of bacteria, yeast and fungi have also been necessary.

## Materials and methods

### Material

Poly-L-lactide ( $M_n$  3000–40,000 g/mol) used for preparing the spheres has been obtained in-house. Other materials used in the study were as follows: PLLA ( $M_n$  66,500 g/mol and 86,000 g/mol (Nature Works, Minnetonka, USA)), polyvinyl alcohol (PVA) as a stabilizer of emulsion ( $M_w$  30,000 g/mol and 130,000 g/mol; degree of hydrolysis 88%, Mowiol®; Sigma–Aldrich, St. Louis, USA) as well as dichloromethane, p.a. and dimethyl sulfoxide, p.a. (POCH S.A., Gliwice, Poland) as solvents. Distilled water was obtained in-house. Neomycin sulphate (Sigma–Aldrich) was used for encapsulation; phosphate (pH 7.2) and acetate (pH 4.5) buffers (POCH) were used for the examination of the API dissolution profile. Antimicrobial activity was tested using commercial cell lines and the following media: Mueller–Hinton agar (MHA), Mueller–Hinton broth (MHB), yeast extract peptone dextrose (YPD), and potato dextrose agar (PDA) purchased from Merck Millipore (Burlington, USA)

or BioCorp (Issoire, France). As a control, antibiotic with a well-established antimicrobial activity was used – either Amphotericin B against yeast and filamentous fungi, or Ampicillin sodium salt against bacteria. These were purchased from BioShop (Dourges, France).

### Preparation of neomycin-containing spheres

The neomycin-containing spheres were prepared employing an emulsion method. At first, the following solutions of polymers having various molecular weights were prepared: a 1% wt solution of PLA in dichloromethane and 0.1% wt solution of polyvinyl alcohol (PVA) in distilled water. The PVA solution (100 mL) was placed in a round-bottom flask immersed in a water bath that was standing on a magnetic stirrer (RTC Basic IKA; Sigma–Aldrich) and was provided with a temperature controller (ETS-D5 IKA). The temperature was set at 25°C and the stirring speed at 600 min<sup>-1</sup> or 1200 min<sup>-1</sup>. Next, neomycin (5% wt relative to PLLA) was added to the above solution. After thoroughly mixing the solution and stabilizing experiment conditions, PLLA solution (5 mL) was added dropwise within 15 min through a pressure-equalizing dropping funnel, and the obtained suspension of spheres was stirred for 1 h at 25°C to evaporate the solvent. The flask content was filtered through a 3G sintered glass filter funnel and then analyzed using dynamic light scattering (DLS).

Empty spheres were prepared analogously as the API-containing spheres, except for the active substance addition step.

### Analytical methods

The size ( $d$  – diameter) of the obtained spheres was determined with DLS using Zetasizer Nano Z.S. from Malvern Instruments (Malvern, UK). The measurements were performed in polystyrene cuvettes. The UV-VIS spectra for determining the dissolution profile and optical density of the cultures were recorded using the Synergy H4 microplate reader from BioTek (Winooski, USA).

### Release profile

The profile of API release from the spheres was determined from a calibration curve. The calibration curve of the absorbance of the aqueous solution of neomycin was measured at a concentration of 0.5 mg/mL, 0.25 mg/mL, 0.125 mg/mL, and 0.067 mg/mL. The tests have covered suspensions of neomycin-containing spheres (without any pre-treatment) mixed with the acetate or phosphate buffer (1:1 v/v) and the buffers not containing the spheres. Samples of the solutions were placed in wells of 96-well 200  $\mu$ L Nunc™ plates (Thermo Fisher Scientific, Waltham, USA) and then incubated at 37°C. At appropriate time

intervals, absorbance was measured with spectrophotometry at the wavelength of neomycin maximum absorption  $\lambda = 360$  nm.

## Antimicrobial activity

Antimicrobial activities of neomycin-containing spheres, empty spheres and neomycin were tested against bacteria, yeast and filamentous fungi. Inhibitory activity against bacteria and yeast was determined using 2 methods: tests on a solid medium and in a liquid medium.

The following microorganisms were used for tests: *Staphylococcus aureus* ATCC 6538, *Escherichia coli* ATCC 8739, *Bacillus subtilis* ATCC 6633, *Salmonella typhimurium* ATCC 14028 bacteria, *Candida albicans* ATCC 10231 yeast, *Aspergillus niger* ATCC 16404 mould and *Colletotrichum coccodes* MC 1, *Fusarium oxysporum* M.F. 5, and *Fusarium sambucinum* M.F. 1 filamentous fungi, received from the IHAR-PIB collection of Plant Breeding and Acclimatization Institute (Młochów, Poland).

## Preparation of cultures of bacteria and yeast

A sterile loop full of material from a single colony of bacterium or yeast was used to inoculate 10 mL of liquid MHB or YPD medium in a 100 mL Erlenmeyer flask. Cultures were incubated overnight (about 18 h) at 37°C, shaking at 200 rpm using Benchtop shaker LabCompanion SI-600R (Jeio Tech, Daejeon, South Korea). Next, the overnight cultures were diluted in fresh medium (MHB or YPD) to desired suspension of colony-forming units per mL –  $10^8$  cfu/mL or  $10^5$  cfu/mL, based on the previously prepared growth curves for each microorganism.

## Preparation of the tested solutions

Neomycin, ampicillin and amphotericin were dissolved in sterile dimethyl sulfoxide (DMSO) to obtain concentrations of 20 mg/mL. Suspensions of the spheres containing the active substance and suspensions of empty spheres were added directly to the corresponding medium, without any pre-treatment.

## Tests of antimicrobial activity on a solid medium

Briefly, 100  $\mu$ L of cell suspension of  $10^8$  cfu/mL was distributed evenly on a suitable medium (MHA for bacteria or YPDA for yeast) and allowed to dry. Disks of Whatman paper (5 mm in diameter, 3MM; Sigma–Aldrich) were placed on the seeded agar plates, and 10  $\mu$ L of the samples were prepared as above (neomycin solution, empty spheres, neomycin-containing spheres and control antibiotics, respectively) and the suitable solvents were applied to the medium. The samples were incubated at 37°C for 24 h. After incubation, microbial growth

inhibition zones were measured for the tested samples, pure substances and the solvent, and the results were compared to the zones of microbial growth inhibition obtained for the control antibiotics (for bacteria: ampicillin, for yeast: amphotericin). Sample activity was determined by measuring the diameter of inhibition of the growth zone.

## Tests of activity in a liquid medium

Briefly, 100  $\mu$ L of appropriate medium (MHB for bacteria and YPD for yeast) and 20  $\mu$ L of the tested samples (solution of neomycin, empty spheres and neomycin-containing spheres, respectively) were placed in wells of 96-well plates. Next, 100  $\mu$ L of microorganisms from the suspension of  $10^5$  cfu/mL was added to each well. The plates were placed in an incubator shaker (200 min<sup>-1</sup>) at 37°C for 24 h. After 24 h of incubation, optical density (OD) of the cultures provided with inhibitors was measured using the spectrophotometric method at the wavelength  $\lambda = 600$  nm, and the results were compared to the OD of the controls (without the spheres or free antibiotics). Antimicrobial activity was calculated from the equation (1):

$$\text{activity} = \frac{\text{OD}}{\text{OD}_{\text{control}}} \times 100\% \quad (1)$$

where:

OD – optical density of a culture of microorganisms with the addition of the active substance or spheres and

OD<sub>control</sub> – optical density of a culture of microorganisms without the addition of the active substance.

## Tests of activity against filamentous fungi

Briefly, 1 mL of the tested preparation (solution of neomycin, empty spheres or neomycin-containing spheres, respectively) was added to 100 mL of dissolved PDA medium. The prepared mixtures were poured into Petri dishes and allowed to solidify. Next, mycelial disks (diameter: 6 mm) were cut out of the actively growing fungal mycelium on PDA and transferred onto the Petri dishes containing the tested and reference (without the addition of active substances) preparations, respectively.<sup>21</sup> The Petri dishes were incubated at 25°C for 3–5 days, depending on the fungal growth rate. After incubation, dimensions of the zones of fungal growth in the presence of special preparations were measured. Next, it was compared to those of the reference samples. The activity of the preparations was calculated from the equation (2):

$$\text{activity} = \frac{d_{\text{control}} - d}{d_{\text{control}}} \times 100\% \quad (2)$$

where:

d [mm] – the diameter of the zone of fungal growth in the presence of the tested preparation and

d<sub>control</sub> [mm] – the diameter of the zone of fungal growth without the addition of the active substance.

## Results

### Preparation of neomycin-containing spheres

Effects of molecular weights of PLLA ( $M_n$ ) and PVA ( $M_w$ ) and the mixing rate on the diameter of neomycin-containing spheres were examined (Fig. 3,4).

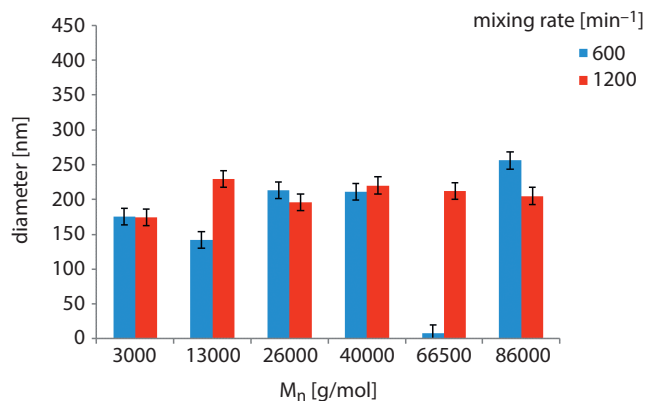


Fig. 3. Diameter of the spheres as a function of the average molecular weight of L-lactic acid (PLLA) and the mixing speed ( $M_w$  polyvinyl alcohol (PVA) 30,000 g/mol)

$M_n$  – number-average molecular weight;  $M_w$  – weight-average molecular weight.

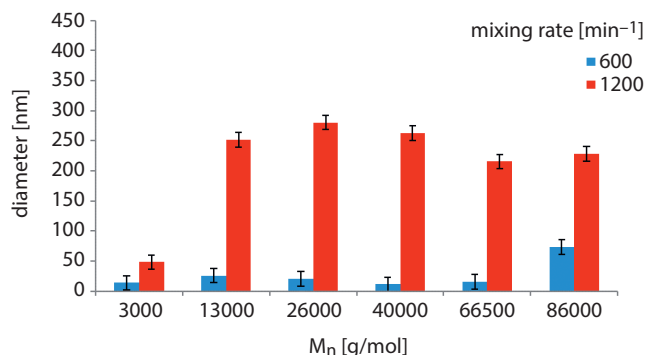


Fig. 4. Diameter of the spheres as a function of the average molecular weight of L-lactic acid (PLLA) and the mixing speed ( $M_w$  polyvinyl alcohol (PVA) 130,000 g/mol)

$M_n$  – number-average molecular weight;  $M_w$  – weight-average molecular weight.

### DLS analysis

The size of the obtained spheres was measured using the DLS method by determining a relationship between light scattering intensity and the number of particles of a certain radius. The relation between the fraction of particle size and the radius of the particles is shown in Fig. 5. In some cases, 2 maxima of particle size distribution could be seen (Fig. 6).

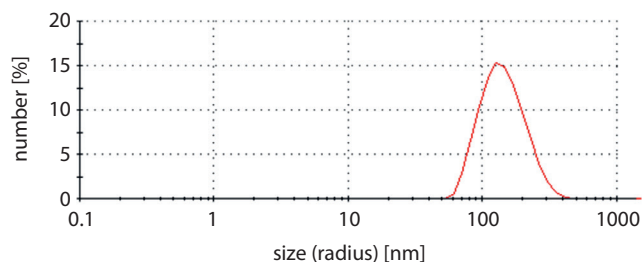


Fig. 5. The relationship between the fraction of spheres at a particular size and the radius of the spheres

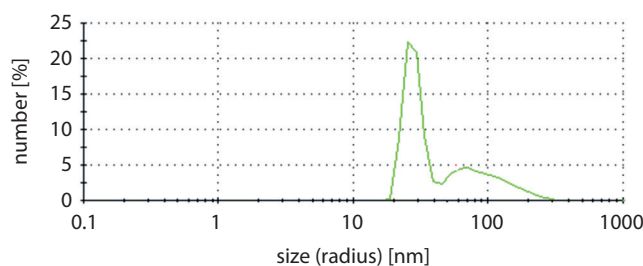


Fig. 6. Two fractions of spheres of different sizes

### API release profile

The profile of API release from the PLA spheres was established by determining a relationship between absorbance (proportional to antibiotic concentration) and incubation time of the samples (Fig. 7). The examined spheres had diameters of 150 nm and 200 nm. The measurements were carried out in acetate buffer (pH 4.5) and in phosphate buffer (pH 7.2) to compare release kinetics in the media of various pH.

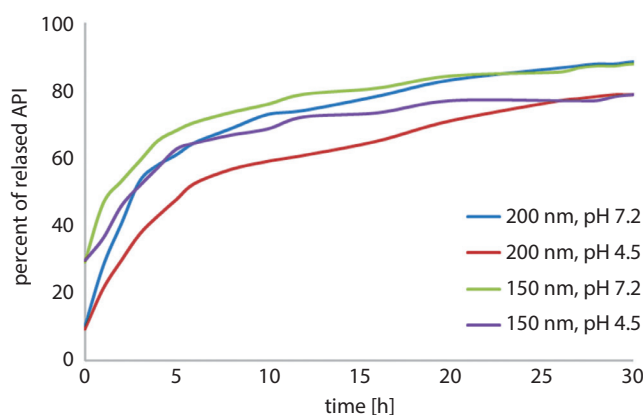


Fig. 7. Profiles of neomycin release from L-lactic acid (PLLA) spheres having diameters of 150 nm and 200 nm in the acetate or phosphate buffers

API – active pharmaceutical ingredient.

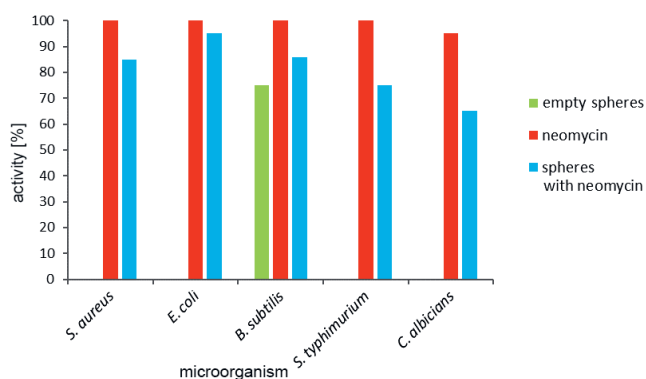
### Antimicrobial activity of the neomycin-containing spheres

#### Tests of activity on a solid medium

Antimicrobial activity of the empty spheres, neomycin and neomycin-containing spheres (diameter ca. 200 nm)

**Table 1.** Antimicrobial activity (diameter of inhibition of growth zone) of neomycin, neomycin-containing spheres, empty spheres and amphotericin and ampicillin against bacteria and yeast on a solid medium

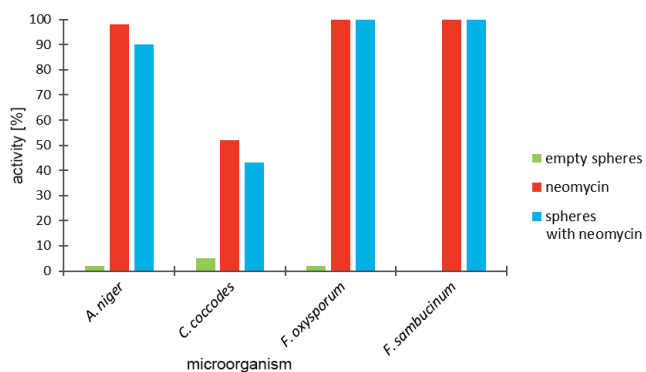
Drug	<i>E. coli</i>	<i>S. aureus</i>	<i>B. subtilis</i>	<i>S. typhimurium</i>	<i>C. albicans</i>
Diameter of inhibition of growth zone [mm]					
Neomycin	30.0	30.0	36.0	30.0	20.9
Spheres with neomycin	29.0	21.0	32.0	28.0	20.1
Empty spheres	0	0	27.1	0	0
Amphotericin	–	–	–	–	13.0
Ampicillin	24.0	26.0	28.0	26.0	–

**Fig. 8.** Antimicrobial activity (percent of inhibition of the growth of a microorganism) of neomycin, neomycin-containing spheres and empty spheres against bacteria and yeast on a liquid medium

against bacteria and yeast has been tested on the solid medium (Table 1). The inhibitory effect of the sample was determined by the size of the inhibition of the growth zone. An inhibitory effect of DMSO (solvent for neomycin) on the tested strains has been excluded.

### Tests of activity in a liquid medium

To examine the accuracy of the tests on a solid medium, the activity of the tested preparations against bacteria and yeast was examined using a liquid medium (Fig. 8). The toxicity of preparation against a given strain was proven by a 50% decrease in OD of the corresponding culture.

**Fig. 9.** Antimicrobial activity (percent of culture growth inhibition) of neomycin, neomycin-containing spheres and empty spheres against filamentous fungi

### Tests of activity against filamentous fungi

The tests have also examined antimicrobial activity against filamentous fungi on a solid medium (Fig. 9). As in previous cases, neomycin-containing spheres having a diameter of ca. 200 nm were used for this purpose, with empty spheres serving as a reference sample. A 50% cell death was adopted as a threshold of toxicity of a tested sample against a given strain.

## Discussion

### Preparation of neomycin-containing spheres

The effect of the number-average molecular weight,  $M_n$ , of PLLA, the weight-average molecular weight,  $M_w$ , of polyvinyl alcohol and stirring speed on the size of obtained spheres were examined (Fig. 3,4). In the case of poly-L-lactide with  $M_n$  3000 g/mol and PVA with  $M_w$  130,000 g/mol, the diameter of the spheres was minimal (approx. 50 nm). On the other hand, larger spheres, 230–300 nm in diameter, were obtained from higher molecular weight polymers ( $M_n$  13,000–86,000 g/mol) (Fig. 4).

We found that the effect of the average molecular weight ( $M_w$ ) of polyvinyl alcohol on the diameter of formed spheres is associated with the applied mixing speed (600  $\text{min}^{-1}$  or 1200  $\text{min}^{-1}$ ). In PVA of  $M_w$  30,000 g/mol, the differences in sphere diameters were minor for each mixing speed (Fig. 3). At the mixing speed of 600  $\text{min}^{-1}$ , the diameter of the obtained spheres was in the range of 140–260 nm (with 1 exception), while at 1200  $\text{min}^{-1}$ , it was in the range of 170–230 nm.

According to the manufacturer's data, the viscosity of PVA solutions increases with elevations in  $M_w$  (at 20°C, the viscosity of a 1% aqueous solution of PVA having  $M_w$  30,000 g/mol is 4 cP, while for PVA having  $M_w$  130,000 it increases to 18 cP). As a rule, the spheres obtained at the mixing speed 600  $\text{min}^{-1}$ , with the use of PVA having  $M_w$  130,000 g/mol, were much smaller (less than 70 nm in diameter) than those obtained at the mixing speed 1200  $\text{min}^{-1}$  (200–300 nm) (Fig. 4). Therefore, to obtain spheres larger than 200 nm, one should appropriately increase the mixing speed.



We also observed that the volume of the spheres obtained from PLLA having  $M_n$  3,000 g/mol was presumably too small to accommodate a neomycin molecule inside it. Hence, PLLA of a higher number average molecular weight was used in further investigations.

## DLS analysis of neomycin-containing spheres

The graph illustrating a relation of the number of same-size spheres (measured with the DLS method) and their radius resembles the Gaussian curve (normal distribution) (Fig. 5). In some cases, curves showing 2 distinct maxima have been recorded (Fig. 6). Two maxima indicate the presence of 2 fractions of spheres varying in diameters. The spheres from the 1<sup>st</sup> fraction had a small diameter, less than 100 nm, whereas those from the 2<sup>nd</sup> fraction had a much larger diameter, over 150 nm. The graph showing only 1 single maximum of the sphere size that corresponds to the diameter of the spheres under 100 nm was related to low stirring speed ( $600 \text{ min}^{-1}$ ) for  $M_w$  of PVA 130,000 g/mol, independently of  $M_n$  of PLLA. In the case of PLLA of  $M_n$  3000 g/mol, the spheres having diameters under 100 nm were obtained using PVA of  $M_w$  130,000 g/mol, both at low ( $600 \text{ min}^{-1}$ ) and high ( $1200 \text{ min}^{-1}$ ) stirring speed. Two maxima of the particle size distribution, corresponding to diameters of the spheres ca. 80 nm and 160 nm (Fig. 6), were obtained for PLLA of  $M_n$  40,000 and 86,000 g/mol, respectively. The observations discussed above have suggested that the spheres smaller than 100 nm most likely do not contain neomycin, whereas the antibiotic is present in the particles having diameters over 150 nm.

## Profile of neomycin release from the spheres

Kinetics of neomycin release from the PLLA spheres was examined in an acidic medium (acetate buffer) and nearly neutral medium (phosphate buffer). Following the hypothesis that neomycin may be contained in spheres having a diameter of at least 150 nm, the examined spheres had diameters of 150 nm and 200 nm. For each size of the spheres, the degradation of PLLA associated with neomycin release was faster and simultaneously more favorable in the phosphate buffer, which is similar to the physiological range. This result has been considered more important because the pH of the phosphate buffer is more closely resembling conditions in the organism. Rates of API dissolution from smaller (150 nm) and larger (200 nm) spheres were similar; however, the amounts of free antibiotic at the starting point were different. The amounts of free neomycin outside the spheres (i.e., in the aqueous solution and on the surface of spheres) were determined by measuring neomycin concentration at the starting point. A low

concentration of neomycin at the starting point proves a high yield of encapsulation and vice versa. From the API dissolution profiles, one could conclude that approx. 70% of the active substance was encapsulated in 150 nm spheres, and approx. 90% in spheres of 200 nm in diameter. An increase of neomycin concentration in the solution during the experiment, compared to the starting point, is a proof of the presence of the antibiotic in the spheres. It has been found that the time required to complete dissolution of the antibiotic from the polymer matrix is relatively long and reaches approx. 30 h.

## Antimicrobial activity of the neomycin-containing spheres

### Tests of activity on a solid medium

Results of antimicrobial activity against bacteria and yeast obtained from tests on a solid medium have confirmed that neomycin inhibits the growth of all tested microorganisms. The neomycin-containing spheres have shown inhibitory activity against the same strains as the active substance, although less distinct. It was shown that poly-L-lactide, and, more precisely, the product of its hydrolysis, i.e., lactic acid and its oligomers (referred to empty spheres), inhibit the growth of *B. subtilis* only (Table 1). It was recognized that the lower activity of neomycin-containing spheres, as compared to the pure substance, represents the occlusion of the antibiotic in the polymer matrix. Due to the necessity of polymer degradation, the release of neomycin from the spheres requires a longer time. This process is advantageous as the slow release of API is the task of polymer spheres as DDS.

### Tests of activity in a liquid medium

Results of the antimicrobial activity tests against bacteria and yeast on a liquid medium were in all cases consistent with those from the tests on a solid medium (Fig. 8). However, the tests in a liquid medium appeared more accurate since the differences of activity between the neomycin-containing spheres and free API were larger. Liquid mediums provided better availability of the examined preparation for the microbial cells, and therefore, they better resemble conditions that naturally prevail in living organisms.

### Tests of activity against filamentous fungi

The tests determined the characteristics of examined preparations against filamentous fungi on a solid medium (Fig. 9). Neomycin inhibits the growth of all kinds of fungi and its lowest activity is observed against *C. coccodes*. Additionally, neomycin-containing spheres did not show toxicity solely against *C. coccodes*; the free antibiotic was

also the least active against this microorganism. It was found that LA and its oligomers originating from hydrolysis of PLLA (empty spheres) do not show activity against any kinds of fungi. As in bacteria and yeast, the neomycin-containing spheres had weaker inhibitory activity than the free antibiotic, which may be attributed to occlusion of the neomycin in the polymer matrix and slow degradation of the polymer. Based on the above observations, it has been concluded that the neomycin-containing spheres have antimicrobial activity against filamentous fungi.

## Conclusions

It was previously understood that the most desirable spheres for DDS should have minimal diameters (<100 nm). On the other hand, due to the size and complexity of the neomycin molecule, its encapsulation requires spheres having diameters over 150 nm. This research shows that efficient encapsulation of neomycin requires PLLA of more considerable molecular weight ( $M_n \geq 13,000$  g/mol). Furthermore, in PLLAs of considerable molecular weight, and hence, high viscosity, encapsulation should be performed with intense stirring ( $1200 \text{ min}^{-1}$ ). Inadequate process conditions could result in empty spheres (without the antibiotic).

Based on the profile of API dissolution from the PLLA spheres, it was demonstrated that the yield of the active substance encapsulation in the 200 nm spheres reaches 90% and in the 150 nm spheres – 70%. The kinetics of antibiotic release was similar for the 150 nm and 200 nm spheres. Considering similar release rates and a larger (90%) yield of neomycin encapsulation in the larger (200 nm) spheres, one could conclude that the larger spheres are more suitable for DDS. We also observed neomycin release to be faster at nearly physiological pH (7.2) than in an acidic medium (pH = 4.5). The total time of neomycin release from the spheres is relatively long (approx. 30 h); hence, it meets the requirements of DDS.

The most important achievement of this study has been the preparation of the neomycin-containing spheres and the demonstration that they have inhibitory activity against bacteria, yeast and filamentous fungi. However, it is weaker than that of the free active substance (controlled release rate).

Up to now, neomycin-containing spheres were not described as a dosage form of this antibiotic. They were considering inhibitory activity against microorganisms and slow dissolution of neomycin. It may be assumed that the application of this DDS would allow for the reduction of adverse effects and could possibly enhance the therapeutic index of the active substance.

## ORCID iDs

Agnieszka Gadomska-Gajadhur

<https://orcid.org/0000-0001-7686-1745>

Paweł Ruśkowski <https://orcid.org/0000-0002-4589-0727>

Aleksandra Kruk <https://orcid.org/0000-0001-5323-7093>

Jolanta Mierzejewska <https://orcid.org/0000-0002-9298-8794>

## References

- Kapetanovic IM. *Drug Discovery and Development: Present and Future*. InTech Open Online. 2011:428–462. doi:10.5772/1179
- Wilczewska AZ, Niemirowicz K, Markiewicz KH, Car H. Nanoparticles as drug delivery systems. *Pharmacol Rep*. 2012;64(5):1020–1037. doi:10.1016/S1734-1140(12)70901-5
- Hoffman A. The origins and evolution of “controlled” drug delivery systems. *J Control Release*. 2008;132(3):153–163. doi:10.1016/j.jconrel.2008.08.012
- Sobczak M, Ołędzka E, Kołodziejski W, Kuźmicz R. Polymers for pharmaceutical applications [in Polish]. *Polimery*. 2007;52(6):411–420.
- Soliman GM, Szychowski J, Hanessian S, Winnik FM. Robust polymeric nanoparticles for the delivery of aminoglycoside antibiotics using carboxymethyl dextran-b-poly (ethyleneglycols) lightly grafted with *n*-dodecyl groups. *Soft Matter*. 2010;6(18):4504–4514. doi:10.1039/C0SM00316F
- Heidary N, Cohen DE. Hypersensitivity reactions to vaccine components. *Dermatitis*. 2005;16(3):115–120. PMID:16242081
- Kruk A, Gadomska-Gajadhur A, Ruśkowski P, Przybysz A, Bijak V, Synoradzki L. Optimization of the preparation of neomycin-containing polylactide spheres by mathematical methods of design of experiments [in Polish]. *Przem Chem*. 2016;95:766–769. doi:10.15199/62.2016.4.10
- Nagavarma BVN, Yadav HKS, Ayaz A, Vasudha LS, Shivakumar HG. Different techniques for preparation of polymeric nanoparticles: A review. *Asian J Pharm Clin Res*. 2012;5(3):16–23.
- Griffiths G, Nyström B, Sable B, Khuller GK. Nanobead-based interventions for the treatment and prevention of tuberculosis. *Nat Rev Microbiol*. 2010;8(11):827–834. doi:10.1038/nrmicro2437
- Rao JP, Geckeler KE. Polymer nanoparticles: Preparation techniques and size-control parameters. *Prog Polym Sci*. 2011;36(7):887–913. doi:10.1016/j.progpolymsci.2011.01.001
- Gimpel K, Luliński P, Maciejewska D. Selected technologies to optimize the delivery of active substances in modern drug formulations [in Polish]. *Biul Wydz Farm WUM*. 2009;3:19–23.
- Varde NK, Pack DW. Microspheres for controlled release drug delivery. *Expert Opin Biol Ther*. 2004;4(1):35–51. doi:10.1517/14712598.4.1.35
- Singh A, Garg JI, Sharma PK. Nanospheres: A novel approach for targeted drug delivery system. *Int J Pharm Sci Rev Res*. 2010;5(3):84–88.
- Szymańska E, Winnicka K. Microspheres: A modern form of controlled-release eye medicine [in Polish]. *Farm Pol*. 2009;65:378–386.
- Nowak B, Pająk J. Biodegradation of poly(lactide) (PLA) [in Polish]. *Arch Gosp Odpad Ochr Środ*. 2010;12:1–10.
- Gadomska A, Warych I, Ruśkowski P, Synoradzki L. Manufacturing of polylactide nanospheres [in Polish]. *Przem Chem*. 2014;93(8):1011–1014. doi:10.12916/przemchem.2014.1311
- Gadomska-Gajadhur A, Mierzejewska J, Ruśkowski P, Synoradzki L. Manufacturing of paracetamol-containing polylactide spheres [in Polish]. *Przem Chem*. 2015;94:1676–1678. doi:10.15199/62.2015.10.3
- Drumright RE, Gruber PR, Henton DE. Polylactic acid technology. *Adv Mat*. 2000;12(23):1841–1846. doi:10.1002/1521-4095(200012)12:23<1841::AID-ADMA1841>3.0.CO;2-E
- Gupta AP, Kumar V. New emerging trends in synthetic biodegradable polymers. Polylactide: A critique. *Eur Polym J*. 2007;43(10):4053–4074. doi:10.1016/j.eurpolymj.2007.06.045
- Datta R, Tsai SP, Bonsignore P, Moon SH, Frank JR. Biotechnological production of lactic acid and its recent applications. *FEMS Microbiol Rev*. 1995;16:221–231.
- Łukowska-Chojnacka E, Mierzejewska J. Enzymatic hydrolysis of esters containing a tetrazole ring. *Chirality*. 2014;26(12):811–816. doi:10.1002/chir.22360

# Influence of non-ionic, ionic and lipophilic polymers on the pH and conductivity of model ointments, creams and gels

## Wpływ polimerów niejonowych, jonowych i lipofilowych na wyniki badań pH i przewodnictwa modelowych maści, kremów i żeli

Agnieszka Krause<sup>A–F</sup>, Katarzyna Kucharska<sup>A–F</sup>, Witold Musiał<sup>A–F</sup>

Department of Physical Chemistry and Biophysics, Wrocław Medical University, Poland

A – research concept and design; B – collection and/or assembly of data; C – data analysis and interpretation; D – writing the article; E – critical revision of the article; F – final approval of the article

Polymers in Medicine, ISSN 0370-0747 (print), ISSN 2451-2699 (online)

*Polim Med.* 2021;51(1):25–32

### Address for correspondence

Witold Musiał  
E-mail: [witold.musial@umw.edu.pl](mailto:witold.musial@umw.edu.pl)

### Funding sources

None declared

### Conflict of interest

None declared

Received on May 31, 2021

Reviewed on June 22, 2021

Accepted on June 30, 2021

Published online on September 10, 2021

### Abstract

**Background.** The pH of the skin surface is usually between 5.4 and 5.9 and functions as a barrier against bacteria and fungi; thus, the composition of the topically applied drug form may be of high importance for proper medication.

**Objectives.** To evaluate the influence of the measurement conditions in aqueous solutions of ointments, creams, and gels, which include polymeric components, on the pH and conductivity results.

**Materials and methods.** The pH and electrolytic conductivity of aqueous dispersions of commercially available ointments, creams and gels were tested and compared to reference vehicles.

**Results.** The results of the dilution method measurements of the pH and electrolytic conductivity of the ointment preparations are highly diverse, ranging from 5.88 to 6.27, whereas the reference pH for *Unguentum simplex* was between 5.40 and 5.43. Furthermore, the measurements of the pH and electrolytic conductivity with the dilution method for creams did not provide repeatable results with a small sample size, and the pH of commercial preparations was in the range between 5.79 and 6.37, compared to the reference pH of 5.23–5.46. However, the dilution method for measurements of the pH and electrolytic conductivity was suitable for hydrogel preparations and the obtained results were repeatable in the range of 6.11–6.90, while the reference preparations were in the range of 5.19–5.62.

**Conclusions.** Evaluation methods of the electrolytic conductivity and pH of the preparations applied on the skin should be further evaluated; however, the pH of the commercial preparation seems to differ from the physiological skin pH, which covers the range of reference preparations.

**Key words:** polymer, pH, electrical conductivity, gel, ointment

### Cite as

Krause A, Kucharska K, Musiał W. Influence of non-ionic, ionic and lipophilic polymers on the pH and conductivity of model ointments, creams and gels. *Polim Med.* 2021;51(1):25–32. doi:10.17219/pim/139613

### DOI

10.17219/pim/139613

### Copyright

© 2021 by Wrocław Medical University  
This is an article distributed under the terms of the Creative Commons Attribution 3.0 Unported (CC BY 3.0) (<https://creativecommons.org/licenses/by/3.0/>)

## Streszczenie

**Wprowadzenie.** Odczyn na powierzchni skóry wynosi zwykle 5.4–5.9. Wartość ta wpływa korzystnie na funkcje barierowe skóry wobec bakterii i grzybów. W konsekwencji skład postaci leku stosowanej miejscowo na skórę może mieć duże znaczenie dla wyników terapii.

**Cel pracy.** Ocena wpływu warunków wykonywania pomiarów w wodnych rozproszeniach maści, kremów i żeli, zawierających składniki polimerowe, na wyniki pH i przewodnictwa.

**Materiał i metody.** Zbadano pH i przewodnictwo elektrolityczne wodnych dyspersji maści, kremów i żeli dostępnych na rynku, oraz porównano te wartości z preparatami odniesienia.

**Wyniki.** Wyniki pomiarów pH i przewodności elektrolitycznej preparatów maści metodą rozcieńczania są bardzo zróżnicowane, w zakresie 5.88–6.27, podczas gdy referencyjne pH dla maści prostej wynosiło 5.40–5.43. Również pomiary pH i przewodności elektrolitycznej metodą rozcieńczania w przypadku kremów nie dają powtarzalnych wyników, kiedy stosuje się niewielką ilość próbek. Odczyn pH preparatów handlowych zawiera się w przedziale 5.79–6.37, w porównaniu do odniesienia 5.23–5.46. Metoda rozcieńczania pomiaru pH i przewodności elektrolitycznej wydaje się być odpowiednia dla preparatów hydrożelowych: uzyskane wyniki dla preparatów handlowych są powtarzalne w zakresie 6.11–6.90, a dla preparatów odniesienia w zakresie 5.19–5.62.

**Wnioski.** Metody oceny przewodności elektrolitycznej i pH preparatów podawanych miejscowo na skórę wymagają dalszej oceny, jednak pH preparatów handlowych wydaje się odbiegać od fizjologicznego pH skóry, które obejmuje zakres preparatów referencyjnych.

**Słowa kluczowe:** polimer, pH, przewodnictwo elektryczne, żel, maść

## Background

The pH of the skin surface is usually between 5.4 and 5.9, and provides a barrier function against bacteria and fungi.<sup>1</sup> Medicinal substances are usually delivered to the skin in the form of an acid or base, rather than a salt, as far as the technological considerations allow. Consequently, the penetration of these drugs through the skin is a function of the dissociation constant (pKa), along with the pH of the preparation and the pH of the superficial layer of the skin. European Pharmacopoeia contains a chapter on physical testing, including a description of the method of pH aqueous solutions and a recommendation for samples to be diluted in distilled water.<sup>2</sup> Typically, fatty formulations before measurement must be emulsified in distilled water. Hydrophilic gels and creams may be diluted before the measurements and the results are recorded after a certain time. The measurements of lipophilic ointments may be carried out in an aqueous extract obtained by extraction in hot water. Various polymers are applied to constitute the drug form, which may be crucial for the pH and conductivity conditions of the preparation. Moreover, lipophilic ointments often contain the long chain alkanes, which are classified usually behind the polymers, whereas creams and ointments are composed using classical macromolecules described as polymers. Many topically applied drugs are developed on the basis of non-ionic or ionic polymers – for example, methylcellulose or polyacrylic acid.

The applied pH tests are diversified. For aqueous solutions of ointments, different authors propose various modes of sample preparation. Popescu et al. mixed

2 g of ointment sample with 30 cm of water and 5 g of paraffin in a baker, heated the mixture in a steam bath for 30 min with occasional stirring, and then assessed the pH only after cooling and filtering the sample to remove paraffin.<sup>3</sup> According to Rajasree et al., 1 g of the ointment was dissolved in 100 mL of distilled water, left for 2 h, and the pH was measured.<sup>4</sup> Kenley et al. diluted the cream sample before measurement with distilled water at a ratio of 1:4.<sup>5</sup> Kumar et al. postulate that the direct measurement of cream in the layer is 0.5 cm.<sup>6</sup> Nesseem recommends the preparation of 1 g of cream in 30 mL of distilled water with a stable pH of 7.<sup>7</sup> Aqueous gels show good performance in topical applications due to the hydrophilic nature of the polymers and high dispersibility in water. Some authors propose direct examination of the pH of the hydrophilic gels in undiluted samples.<sup>8</sup> Nagaich et al. studied the pH of a 1% aqueous gel solution after its dissolution in 100 mL of distilled water and incubation for 2 h in standard conditions.<sup>9</sup> Quiñones and Ghaly dissolved 0.3 g of gel in 100 mL of distilled water, protected the sample from light for 2 h, and then measured the pH.<sup>10</sup> Other investigators have dissolved the gel in distilled water at a proportion of 10% by volume, and the pH measurement was performed in triplicate.<sup>11</sup>

## Objectives

The aim of this study was to evaluate the influence of the measurement conditions in aqueous solutions of ointments, creams and gels, which include polymeric components, on the pH and conductivity results.

## Materials and methods

### Materials

The following ointments were used: 1) *Unguentum simplex* consisting of white petrolatum and anhydrous lanolin in a ratio of 90:10, prepared in-house using certified pharmacopoeial components (US); 2) a protective ointment with vitamin A containing 800 IU/g of retinol palmitate with white petrolatum and Palsgaard 0291 as an emulsifier (UA); 3) the zinc ointment containing zinc oxide on a base of hydrophilic petrolatum (UZ). The assessed creams included: 1) cream base Hascobaza with hydrocarbons, emulsifiers, and typical polar solvents (CH); 2) cream with 0.5% of hydrocortisone acetate with white petrolatum (CA); 3) 1% cream with clotrimazole (CC). The following aqueous gels were assessed: 1) 0.5% methylcellulose gel (GM); 2) gel with 100 mg/g of ibuprofen lysine salt, with macrogol and polyacrylic acid (GI); 3) gel with 8.5 mg/g of sodium heparin, using a base of neutralized acrylic acid polymer (GH).

### Methods

Aqueous dispersions of the ointments were prepared using 5 g of the ointment and the addition of 45 mL of distilled water. The closed flask was then heated in a water bath at 70°C with frequent shaking. After macroscopic homogenization of the components, shaking was continued for another 5 min. Dispersions were then cooled and filtered through a medium porosity filter. Aqueous dispersions of creams and gels were produced with 5 g of formulation supplemented with 45 mL of distilled water, so that the weight to volume ratio of the mixture was 1:10.

The mixture was dispersed to obtain a homogenous suspension or solution. The aqueous solutions prepared this way, with the dilution of 1:10, were subject to potentiometric and conductometric measurements. During the measurements, the samples were diluted with distilled water to the value of 1:20, 1:30, 1:40, and 1:50, and were also studied.

The pH was tested using the pH-meter from Meratronik (type 517; Warszawa, Poland) with a combined electrode SAg P201 and temperature compensator Pt-100. Each sample test was performed 5 times, and 2 samples were evaluated in parallel. A stabilization time of 3 min was applied before every measurement.

The electrolytic conductivity tests were performed using the conductivity device CC-505 from Elmetron (Zabrze, Poland). Each sample measurement was performed 5 times, and 2 samples were performed in parallel. A stabilization time of 2 min was applied, and each test was conducted at room temperature.

## Results

### The pH and conductivity values of ointment-type preparations

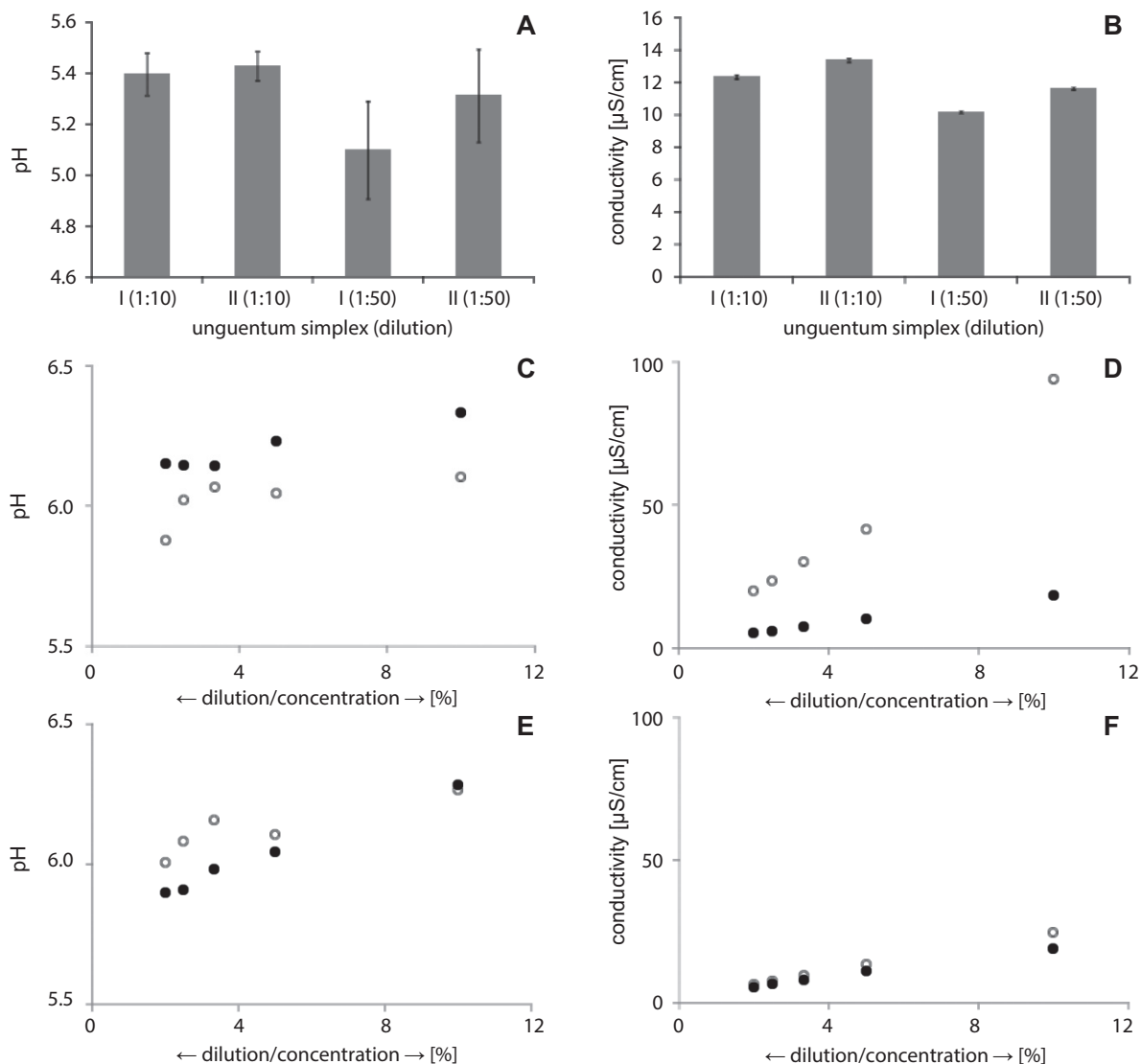
As shown in Fig. 1 in the column graph, the pH of the reference ointment base (US) with a dilution of 1:10 ranged from 5.40 to 5.43, while for the dilution of 1:50 it was between 5.10 and 5.31 (Fig. 1A). The electrolytic conductivity of the US with the dilution of 1:10 was 12.35–13.39  $\mu\text{S}/\text{cm}$ .

Figure 1C presents the pH of the ointment with vitamin A (UA) after dilution with distilled water at a ratio of 1:10 – it ranged between the values of 6.10 and 6.33. When we increased the dilution to 1:20, the pH slightly decreased to the range of 6.04–6.23. As we diluted the samples further (1:30, 1:40 and 1:50), the average pH value ranges were 6.07–6.14, 6.02–6.14 and 5.88–6.15, respectively. Interestingly, the lowest (1:10) and highest (1:50) dilutions showed a wide range of pH values in the investigation of the UA ointment, while the 1:30 dilution showed low variability. The Student's t-test showed statistically significant differences of the pH measurements between the 2 samples performed at a 95% confidence interval (95% CI).

The average value of electrolytic conductivity of UA in the 1:10 dilution presented significant differences in both samples (I and II), ranging from 18.41  $\mu\text{S}/\text{cm}$  to 94.06  $\mu\text{S}/\text{cm}$  (Fig. 1D). At the higher dilution of 1:20, the pH values decreased by almost 50% and ranged from 10.19  $\mu\text{S}/\text{cm}$  to 41.44  $\mu\text{S}/\text{cm}$ . In the 1:30, 1:40 and 1:50 dilutions of the ointment sample, the average conductivities decreased, and were, respectively, 7.28–30.16  $\mu\text{S}/\text{cm}$ , 5.87–23.42  $\mu\text{S}/\text{cm}$  and 5.14–19.85  $\mu\text{S}/\text{cm}$ . The highest result, characterized by the greatest variation, was observed in the lowest dilution of 1:10. The remaining results were more uniform.

The average pH of the UZ at a dilution of 1:10 represented a narrow range of 6.27–6.28 (Fig. 1E). The 1:20 dilution resulted in decreased values (6.04–6.11). This decrease was consistently shown in further dilutions, as the 1:50 dilution reduced the pH values to a range of 5.90–6.01. The decreasing pH values were characterized by a slightly increased variability.

The conductivity value of UZ in the 1<sup>st</sup> dilution with distilled water (1:10) was in the range of 19.00–24.62  $\mu\text{S}/\text{cm}$  (Fig. 1F). With higher dilutions – 1:20 and 1:30 – the values were, respectively, 11.01–13.37  $\mu\text{S}/\text{cm}$  and 8.00–9.55  $\mu\text{S}/\text{cm}$ . In further successive dilutions of UZ at ratios of 1:40 and 1:50, the average electrolytic conductivity values were similar – in the range of 6.49–7.52  $\mu\text{S}/\text{cm}$  and 5.47–6.45  $\mu\text{S}/\text{cm}$ , respectively. The Student's t-test analysis did not show any significant statistical differences between the results of the electrolytic conductivity study using a 95% CI. Similar to the pH study of the UZ, the result that was most different from the rest was obtained with the lowest dilution (1:10). This result, however, was characterized



**Fig. 1.** Parameters of pH (A) and conductivity (B) of the assessed formulation – simple ointment (USP, Ph. Eur.) (US). The Y-bars represent standard deviation (SD);  $n = 5$ . I – 1<sup>st</sup> batch of measurements, II – 2<sup>nd</sup> batch of measurements; parameters of pH (C) and conductivity (D) as a function of concentration of dispersed preparation of the protective ointment with vitamin A containing 800 IU/g of retinol palmitate with white petrolatum and Palsgaard O291 as an emulsifier (UA), parameters of pH (E) and conductivity (F) as a function of concentration of dispersed preparation of the ointment-containing zinc oxide on the base of hydrophilic petrolatum (UZ). The black (●) and white (○) dots represent 1<sup>st</sup> and 2<sup>nd</sup> batch of measurements, respectively

by the largest spread, in comparison to the rest. The other results showed the downward trend, similar to the results identified in the pH values of UZ.

### The pH and the conductivity of oil/water (o/w) cream-type preparations

The pH of the model base of o/w cream CH was 5.23 and 5.46 for dilutions of 1:10 and 1:50, respectively (Fig. 2A), whereas the electrolytic conductivity, as shown in Fig. 2B, was in the range of 44.46–44.66  $\mu\text{S}/\text{cm}$  and 23.62–24.24  $\mu\text{S}/\text{cm}$ , respectively.

After diluting with distilled water at a ratio of 1:10, the average pH values of CC were fairly divergent at 5.79 and 6.29 (Fig. 2C). With respect to the 1:20 sample dilution, values of both series slightly increased, respectively, to 5.86 and 6.37.

In sample I, the average values of the pH obtained slightly increasing values along with the increasing dilution (1:30, 1:40 and 1:50); specifically, they were 5.81, 5.86 and 5.91, respectively. In sample II, we observed minimal reductions in pH following dilution – to 6.37, 6.36 and 6.35, respectively. The spread of the values was also similar, which may prove the lack of homogeneity of the studied cream. Moreover, the obtained results provided information on the repeatability of the study, regardless of the dilution ratio.

The average values of the electrolytic conductivity in both samples were similar at every stage of the study (Fig. 2D). At the 1:10 dilution, the results were in the range of 15.46–16.24  $\mu\text{S}/\text{cm}$ . At dilutions of 1:20, 1:30 and 1:40, the value of the measured parameter was in the range of 12.17–13.49  $\mu\text{S}/\text{cm}$ , 9.42–10.06  $\mu\text{S}/\text{cm}$  and 7.72–8.21  $\mu\text{S}/\text{cm}$ , respectively. The highest diluted

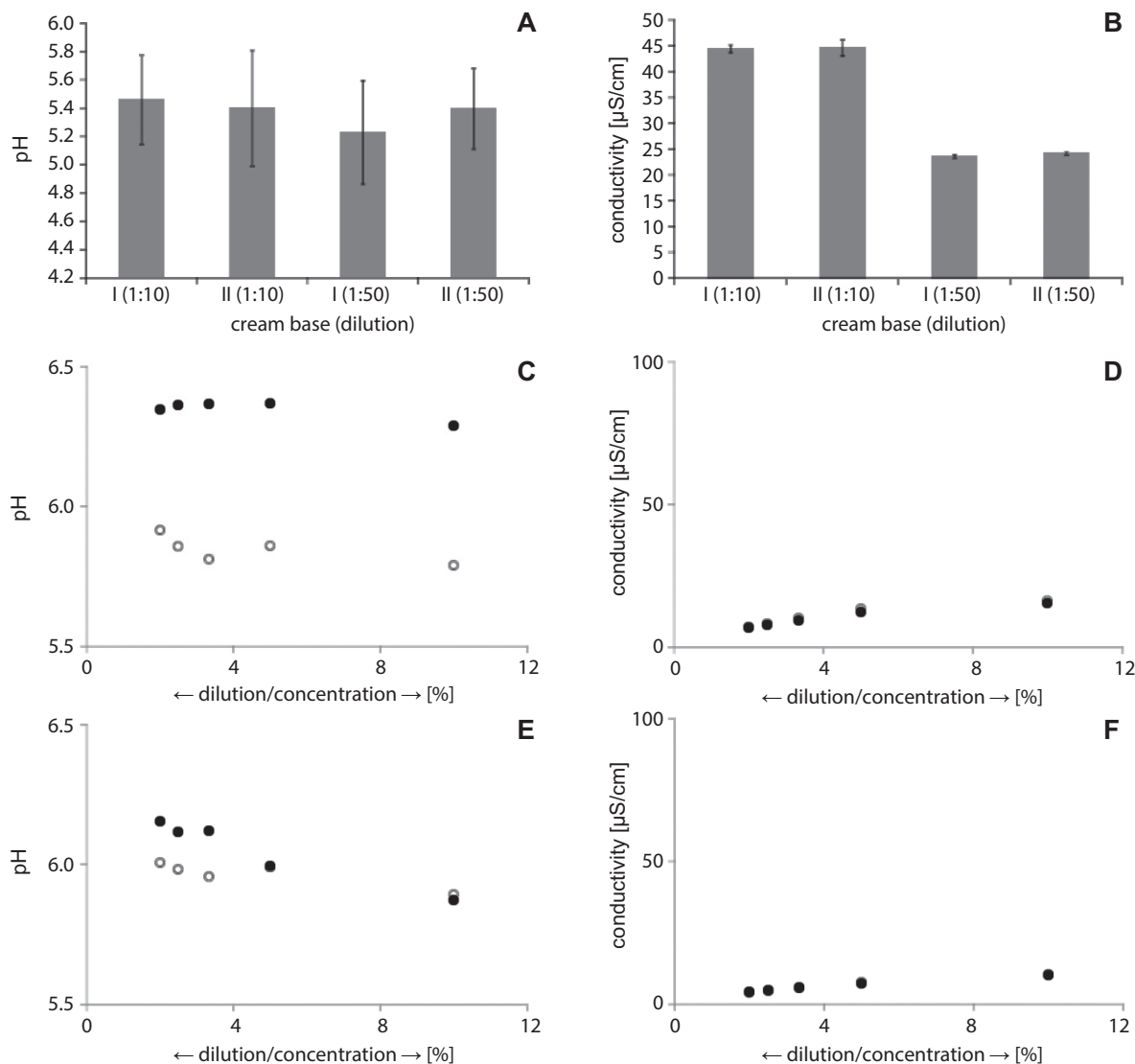


**Fig. 2.** Parameters of pH (A) and conductivity (B) of the assessed formulation – cream base (CH). The Y-bars represent standard deviation (SD);  $n = 5$ . I – 1<sup>st</sup> batch of measurements, II – 2<sup>nd</sup> batch of measurements; parameters of pH (C) and conductivity (D) as a function of concentration of dispersed preparation of 1% cream with clotrimazole (CC), parameters of pH (E) and conductivity (F) as a function of concentration of dispersed preparation of cream with 0.5% of hydrocortisone acetate with white petrolatum (CA). The black (●) and white (○) dots represent the 1<sup>st</sup> and 2<sup>nd</sup> batch of measurements, respectively

sample (1:50) displayed an average electrolytic conductivity value of 6.88–7.04  $\mu\text{S}/\text{cm}$ . These results showed a similar downward trend that was seen above in present research. The broadest range of the obtained results was observed with the 1:10 and 1:20 dilutions, whereas the 1:30, 1:40 and 1:50 dilutions displayed a much narrower range.

The distribution in the test results of the pH of the aqueous solution of cream with hydrocortisone (CA) was similar in both samples. The 1:10 dilution pH values ranged between 5.87 and 5.89. Further dilution (1:20, 1:30, 1:40, and 1:50) of the CA led to values of 5.99, 5.96, 5.98, and 6.01, respectively. In sample II, the 1:30 and 1:40 dilutions exhibited pH values of 6.12, and reached 6.15 in the 1:50 dilution (Fig. 2E). The analysis of the CA pH test results showed that, contrary to data from the studies of other preparations, the lowest pH values occurred in the 1<sup>st</sup> dilution

of 1:10. In the other studied preparations, this value was the highest. These results showed a rising trend that significantly deviated from the results obtained in the 1<sup>st</sup> dilution. The values obtained for the dilutions of 1:30, 1:40 and 1:50 showed a rather large spread in comparison to the results obtained for the 1:10 and 1:20 dilutions.

The results of the conductivity measurements showed slight differences (Fig. 2E). Initially (1:10), the conductivity was 10.03–10.26  $\mu\text{S}/\text{cm}$ , and this decreased to 7.16–7.50  $\mu\text{S}/\text{cm}$  in the 1:20 dilution. Further dilutions of the CA (1:30, 1:40 and 1:50) displayed the following results: 5.62–5.77  $\mu\text{S}/\text{cm}$ , 4.60–4.86  $\mu\text{S}/\text{cm}$  and 4.07–4.16  $\mu\text{S}/\text{cm}$ , respectively (Fig. 2F). Based on these data, we can conclude that conductivity values decreased in response to increasing dilutions with a relatively low amount of variability.

## The pH and conductivity of hydrogel-type preparations

Results of the pH measurements of the dilution of reference preparation (GM) with methylcellulose 1:10 were in the range of 5.61–5.62, whereas after the highest dilution (1:50) the values ranged between 5.19 and 5.24 (Fig. 3A). The electrolytic conductivity of the 1:10 dilution was in the range of 4.99–5.05  $\mu\text{S}/\text{cm}$ , while it was in the range of 2.86–2.90  $\mu\text{S}/\text{cm}$  in the 1:50 dilution (Fig. 3B).

Average pH values of the gel preparation with 100 mg/g of ibuprofen lysine salt, with macrogol and polyacrylic acid (GI), ranged between 6.78 and 6.84 (Fig. 3C). At dilutions of 1:20, 1:30, 1:40, and 1:50, the pH of the tested sample slightly increased and showed a rising trend: 6.85–6.86, 6.86–6.88, 6.88–6.89, and 6.89–6.90, respectively. The smallest value of the studied parameter was obtained

at the 1:10 dilution, and this dilution displayed the largest range as well.

The average results of the five-time measurements of the electrolytic conductivity of GI indicated significantly higher values, in comparison to the previously analyzed data (Fig. 3D). The results for the samples diluted 1:10 were in the range of 1133.80–1240.0  $\mu\text{S}/\text{cm}$ . In further dilutions (1:20, 1:30, 1:40, and 1:50), electrolytic conductivity values decreased (666.40–695.80  $\mu\text{S}/\text{cm}$ , 446.00–476.20  $\mu\text{S}/\text{cm}$ , 348.00–361.80  $\mu\text{S}/\text{cm}$ , and 281.00–283.60  $\mu\text{S}/\text{cm}$ , respectively). A downward trend was observed following dilution, together with a range narrowing. The highest values were observed for the lowest (1:10) dilution.

The pH values for the gel preparation with heparin sodium salt (GH) increased on every step of dilution in both samples. This increase was significant, as each dilution resulted in a change of approx. 0.1 of a pH unit. In appropriate dilutions

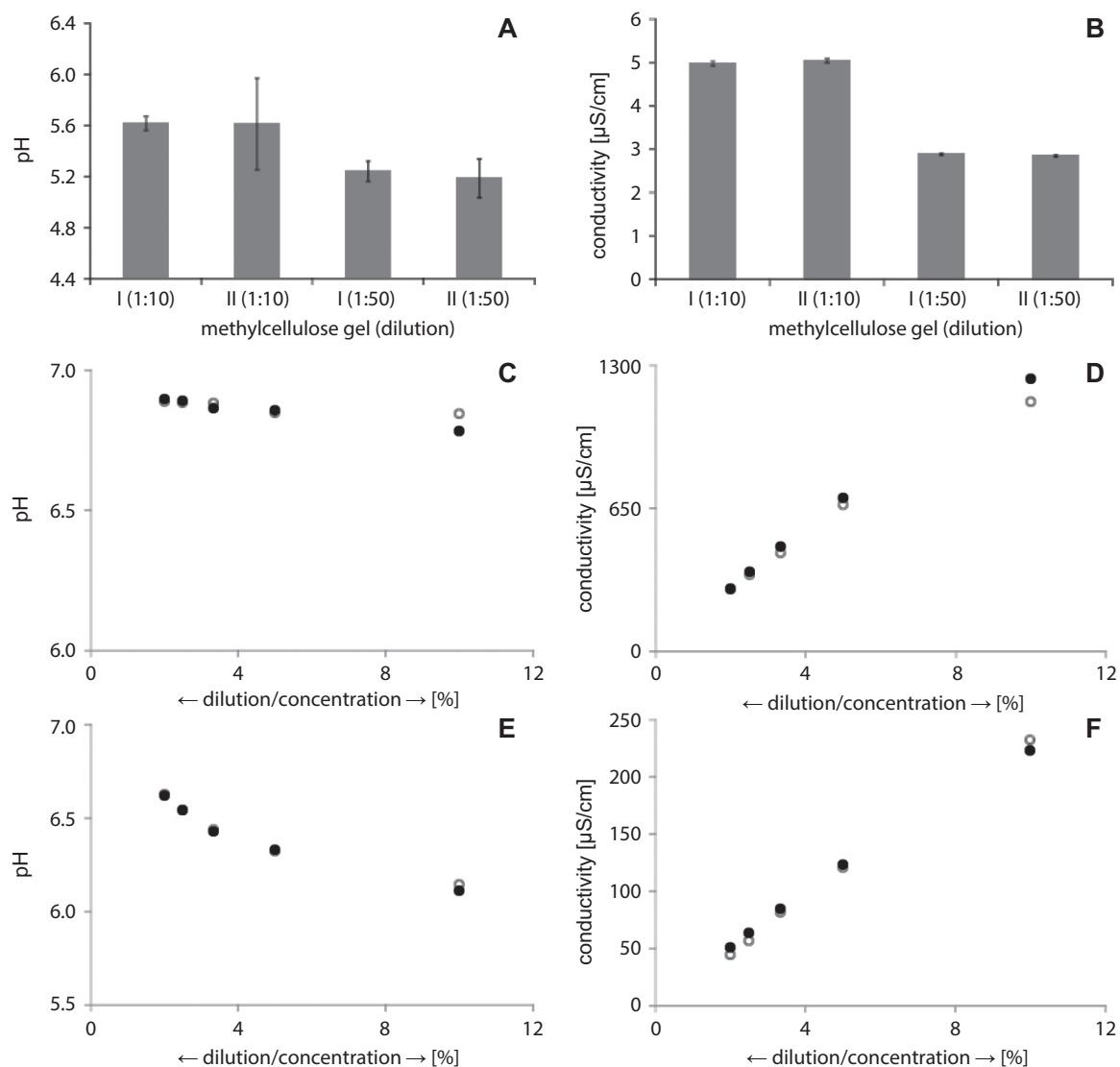


**Fig. 3.** Parameters of pH (A) and conductivity (B) of the assessed formulation – methylcellulose gel (GM). The Y-bars represent standard deviation (SD);  $n = 5$ . I – 1<sup>st</sup> batch of measurements, II – 2<sup>nd</sup> batch of measurements; parameters of pH (C) and conductivity (D) as a function of concentration of dispersed preparation of gel with 100 mg/g of ibuprofen lysine salt, with macrogol and polyacrylic acid (GI), parameters of pH (E) and conductivity (F) as a function of concentration of dispersed preparation of gel with 8.5 mg/g of sodium heparin, on the basis of the neutralized acrylic acid polymer (GH). The black (●) and white (○) dots represent 1<sup>st</sup> and 2<sup>nd</sup> batch of measurements, respectively



– 1:10, 1:20 and 1:30 – the pH values were in the range of 6.11–6.14, 6.32–6.33 and 6.43–6.44, respectively, while in the 1:40 and 1:50 dilutions, the average pH values were at 6.54 and 6.62 (Fig. 3E). The lowest values of pH for the GH samples were observed in the 1:10 dilution, and further dilutions caused a rising trend. Overall, the span of the obtained results was narrow, and the highest values were observed in the distilled water dilution of 1:50.

The electrolytic conductivity data for GH are presented in Fig. 3F. The 1:10 dilution values were in the range of 223.20–232.40  $\mu\text{S}/\text{cm}$ , determined based on five-time measurements. With the increase in dilution to 1:20, the average results of the electrolytic conductivity decreased to the range of 120.60–123.40  $\mu\text{S}/\text{cm}$ . In further dilutions, the average electrolytic conductivity value was in the range of, respectively, 81.40–84.40  $\mu\text{S}/\text{cm}$ , 56.80–63.30  $\mu\text{S}/\text{cm}$  and 44.60–51.00  $\mu\text{S}/\text{cm}$ . The highest electrolytic conductivity value of GH was observed in the lowest dilution of 1:10, and these values decreased with subsequent dilutions. The narrowest span was shown by the values in the 1:20 dilution.

## Discussion

In the study of the ointment, which analyzed separate samples for the same preparation, diversified pH and electrolytic conductivity results were clearly observed. In the preparation of the US, we observed a slight decrease in pH and electrolytic conductivity along with sample dilution. The greatest variability was observed in the UA. The wide changeability concerned both, the pH and the electrolytic conductivity. Due to the large amounts of lipophilic substances, UA hardly underwent dispersion in the aqueous environment. Numerous clumps of lipophilic substance were observed. In the case of UZ, we also noted high diversification of the results between successive samples in the pH measurements. Furthermore, a slightly smaller variability between sample measurements was observed in the study of electrolytic conductivity of UZ. This may result from different aqueous base numbers applied respectively in the UA and in the UZ. They are, respectively, 10 and 250. In the UA, white petrolatum was used with a low aqueous number, which does not favor particle hydrophilicity of the lipophilic substrate. The substrate in UZ, which contains the hydrophilic petrolatum with a high aqueous number, can be easily dispersed in water. No information was found on the influence of the Palsgaard 0291 used in the UA on the change of the aqueous number of petrolatum.

In the studies on the pH and conductivity of creams, we showed a clear difference between particular measurement series, particularly in the case of the ointment studies. In the case of CH, no pH changes were observed with dilution increasing from 1:10 to 1:50. Conductivity tests of this substrate showed that increased dilution significantly reduces its electrolytic conductivity. Particularly, large diversification between the measurement series was noted during

the study of the pH in the case of CC; however, the diversity of results within one sample was small. This may reflect the heterogeneity of the parts of preparation squeezed from the tube, that were collected for testing. In the case of CA, a deviation of the obtained pH values was also present, but not to the same degree as observed in the ointments. The diversity of the results of the tested creams may be the outcome of their lipophilic nature. In studies on the electrolytic conductivity, significant changes were observed in the various dilutions. This may represent the so-called systematic error, which can result from the applied measurement method or other environmental influences. It should be emphasized that in the cream preparations, the diversity of the electrolytic conductivity results between the samples was smaller when compared to the ointment preparations.

In the gel preparation case studies, we noted a smaller diversity in the results. The values of the results were higher compared to those obtained for the ointment creams, and were nevertheless characterized by uniformity. For GM, the pH and electrolytic conductivity measurements displayed a clear decline with dilution. Results of the pH and electrolytic conductivity measurements for GI and GH showed slight differences, which can be categorized as a random error. These do not have a significant impact on the final measurement result, and their cause is unknown – likely a significant effect on the obtained results can be exerted by the composition of gel preparations, whose main component is water, while they contain little active substance and polymer.

Comparing the pH and conductivity changes in response to dilutions in the case of creams, we observed that the pH in particular samples was variable; however, the results of conductivity measurements were repeatable. Thus, further research should include conductivity as an auxiliary measurement allowing the quantitative assessment, comparable with the preparations of the cream type. The diversity of the pH values in the successive cream measurements, in the context of repeatable conductivity measurement results, requires further study. The formation of the balance between the concentration of ions connected with the emulsion system and the concentration of free ions in the solution likely occurs in the emulsion systems. This balance, however, does not reflect the concentrations of aqueous ions responsible for the pH.

## Conclusions


The results of the dilution method measurements of the pH and electrolytic conductivity of the ointment preparations are highly diverse. Furthermore, the measurements of the pH and electrolytic conductivity using the dilution method in the case of creams do not give repeatable results when a small number of samples is used. Conversely, the dilution method for the measurement of the pH and the electrolytic conductivity is suitable for the hydrogel

preparations based on polymeric materials, and the obtained results are repeatable. The methods of evaluation of the electrolytic conductivity and pH of the preparations applied on the skin should be further evaluated. The pH of the commercial preparations appears to be different from the physiological pH of the skin, which covers the range of reference preparations.

### ORCID iDs

Agnieszka Krause  <https://orcid.org/0000-0001-9215-7803>

Katarzyna Kucharska  <https://orcid.org/0000-0001-6591-3917>

Witold Musiał  <https://orcid.org/0000-0001-5695-5998>

### References

- Schmid-Wendtner MH, Korting HC. The pH of the skin surface and its impact on the barrier function. *Skin Pharmacol Physiol*. 2006;19(6): 296–302. doi:10.1159/000094670
- Council of Europe; European Pharmacopoeia Commission; European Directorate for the Quality of Medicines & Healthcare. *European Pharmacopoeia*. 7<sup>th</sup> ed. Strasbourg, France: Council Of Europe & European Directorate for the Quality of Medicines and Healthcare; 2010. Chapter 2.2.3: 2426.
- Popescu V, Soceanu A, Dobrinas S, Stanciu G. Characterization and stability study of some pharmaceutical ointments. *Ovidius Univ Ann Chem*. 2012;23(1):87–91. doi:10.2478/v10310-012-0014-5
- Rajasree PH, Vishwanad V, Cherian M, Eldhose J, Singh R. Formulation and evaluation of antiseptic polyherbal ointment. *Int J Pharm Life Sci*. 2012;3(10):2021–2031. <http://www.ijplsjournal.com/issues%20PDF%20files/oct2012/6.pdf>.
- Kenley RA, Lee MO, Sukumar L, Powell MF. Temperature and pH dependence of fluocinolone acetonide degradation in a topical cream formulation. *Pharm Res*. 1987;4(4):342–347. doi:10.1023/A:1016457522866
- Kumar KK, Sasikanth K, Sabareesh M, Dorababu N. Formulation and evaluation of diacerein cream. *Asian J Pharm Clin Res*. 2011;4(2):93–98. [https://www.researchgate.net/publication/287760991\\_Formulation\\_and\\_evaluation\\_of\\_diacerein\\_cream](https://www.researchgate.net/publication/287760991_Formulation_and_evaluation_of_diacerein_cream)
- Nesseem DI. Formulation and evaluation of itraconazole via liquid crystal for topical delivery system. *J Pharm Biomed Anal*. 2001;26:387–399. doi:10.1016/s0731-7085(01)00414-9
- Basha BN, Prakasam K, Goli D. Formulation and evaluation of Gel containing fluconazole-antifungal agent. *Int J Drug Dev Res*. 2011;3(4): 109–128. <https://www.ijddr.in/drug-development/formulation-and-evaluation-of-gel-containing-fluconazoleantifungal-agent.php?aid=5677>
- Nagaich U, Sharan P, Kumar R, Sharan S, Gulati N, Chaudhary A. Development and characterization of anti-aging topical gel: An approach towards gerontology. *J Adv Pharm Ed Res*. 2013;3(3):260–266. <https://japer.in/storage/models/article/ITBBIBz6mDvz9vB8dJczWjm1RwckZQ5ZUBZLWm2klxXuA92Tt4WSefaYjMd/development-and-characterization-of-anti-aging-topical-gel-an-approach-towards-gerontology.pdf>
- Quiñones D, Ghaly ES. Formulation and characterization of nystatin gel. *PR Health Sci J*. 2008;27(1):61–67. PMID:18450235
- Dhawan S, Medhi B, Chopra S. Formulation and evaluation of diltiazem hydrochloride gels for the treatment of anal fissures. *Sci Pharm*. 2009;77(2):465–482. doi:10.3797/scipharm.0903-10

# Natural polymers in photodynamic therapy and diagnosis

## Naturalne polimery w terapii i diagnostyce fotodynamicznej

Julita Kulbacka<sup>A,B,D,F</sup>, Anna Choromańska<sup>B–D,F</sup>, Zofia Łapińska<sup>B–D,F</sup>, Jolanta Saczko<sup>B–D,F</sup>

Department of Molecular and Cellular Biology, Faculty of Pharmacy, Wrocław Medical University, Poland

A – research concept and design; B – collection and/or assembly of data; C – data analysis and interpretation; D – writing the article; E – critical revision of the article; F – final approval of the article

Polymers in Medicine, ISSN 0370-0747 (print), ISSN 2451-2699 (online)

*Polim Med.* 2021;51(1):33–41

### Address for correspondence

Julita Kulbacka  
E-mail: Julita.Kulbacka@umw.edu.pl

### Funding sources

None declared

### Conflict of interest

None declared

Received on May 21, 2021

Reviewed on June 9, 2021

Accepted on June 29, 2021

Published online on July 30, 2021

### Abstract

Natural polymers have been commonly applied in medicine and pharmacy. Their primary function is to enhance drug delivery, tissue regeneration or wound healing, and diagnostics. Natural polymers appear promising for photodynamic protocols, including photodiagnosis (PDD) and photodynamic therapy (PDT). Currently, the most challenging issue with natural polymers is to appropriately select the most effective material regarding the type of cancer treated. The technological achievements enable functionalization of natural polymers by specific antibodies, or enhancement using fluorescent or quantum dot markers for diagnostic applications. This review will discuss the types and properties of natural polymers and available applications of PDD and PDT which seem to be promising in cancer treatment. Treatment of neoplastic diseases is still a challenge for both physicians and scientists, so the search for alternative methods of treatment and diagnosis based on natural materials is relevant.

**Key words:** photodynamic therapy, anticancer therapy, natural polymers, photodynamic diagnosis

### Streszczenie

Naturalne polimery są powszechnie stosowane w medycynie i farmacji. Ich podstawowym zadaniem jest lepsze dostarczanie leków, regeneracja tkanek i gojenie ran oraz diagnostyka. Naturalne polimery są obiecujące w protokołach fotodynamicznych, w tym fotodiagnostyce (PDD) i terapii fotodynamicznej (PDT). Jednak największym wyzwaniem jest odpowiedni dobór optymalnego i skutecznego materiału pod kątem wybranego typu nowotworu. Osiągnięcia technologiczne umożliwiają funkcjonalizację naturalnych polimerów przez specyficzne przeciwciała lub wzmocnienie za pomocą znaczników fluorescencyjnych lub kropek kwantowych do zastosowań diagnostycznych. W niniejszej pracy przeglądowej omówiono i podsumowano ostatnie dane dotyczące rodzajów i właściwości naturalnych polimerów oraz ich możliwe zastosowania w PDD i PDT, które wydają się obiecujące w leczeniu chorób nowotworowych. Leczenie chorób nowotworowych wciąż jest wyzwaniem zarówno dla lekarzy, jak i naukowców, zatem poszukiwanie alternatywnych metod leczenia i diagnozowania w oparciu o naturalne materiały jest wciąż aktualne.

**Słowa kluczowe:** terapia fotodynamiczna, diagnostyka fotodynamiczna, naturalne polimery, terapia przeciwnowotworowa

### Cite as

Kulbacka J, Choromańska A, Łapińska Z, Saczko J.  
Natural polymers in photodynamic therapy and diagnosis.  
*Polim Med.* 2021;51(1):33–41. doi:10.17219/pim/139587

### DOI

10.17219/pim/139587

### Copyright

© 2021 by Wrocław Medical University  
This is an article distributed under the terms of the  
Creative Commons Attribution 3.0 Unported (CC BY 3.0)  
(<https://creativecommons.org/licenses/by/3.0/>)

## Introduction

Cancer remains a worldwide health problem and is one of the pathologies with the most severe impact on global health. Despite advances in knowledge on recent technological improvements, the mechanisms of recurrence and metastasis, progression, and development of these cancers remain unclear.<sup>1,2</sup> Current treatments such as surgery, chemo- and radiotherapy are not effective and have side effects. Photodynamic therapy (PDT) and diagnosis (PDD) are still promising and alternative treatment options for cancer. Early detection of cancer, particularly at a curable stage, is an essential factor to effectively reduce mortality rates.<sup>3</sup> Unfortunately, conventional imaging technologies, including ultrasonography (US), computed tomography (CT) or magnetic resonance imaging (MRI), provide only anatomical and physiological information.<sup>4</sup> Their limitations include a lack of possibility for distinction of malignancies from benign lesions. Moreover, nonspecific distribution throughout the body, fast metabolism and other side effects affecting individual's comfort need to be taken into consideration. Similar drawbacks are associated with conventional chemotherapy. Issues of drug resistance development and poor bioavailability need to be taken into account as well.<sup>5</sup> Thus, PDT or PDD combined with natural polymers for the enhanced photosensitizing agent delivery may represent an excellent alternative therapy for controlling malignant diseases. This therapy is based on the photosensitizer (PS) molecule application, which is excited by the light in an established wavelength and, after excitation, can react with oxygen. This reaction generates reactive oxidant species (ROS) such as singlet oxygen, hydroxyl radical and hydrogen peroxide superoxide anion radical, leading to an oxidative imbalance in cells. The oxidant species attack many molecules in cells, including nucleic acid proteins, and lipids. The ROS cause severe changes in the physiological mechanism of signaling cascade or gene expression regulation and lead to cell death by apoptosis, necrosis or autophagy. The type of death depends on different conditions (PS, localization of PS, energy applied, and individual tumor resistance).<sup>6–8</sup>

The PDT involves the photosensitized oxidation of biomolecules which may undergo 2 mechanisms (type I and type II). Type I involves the light energy being transferred from excited molecules to biomolecules through electron/hydrogen transfer. It is involved in the damage of specific biomolecules and the initiation of radical chain reactions. In type II, the excitation energy is transferred to molecular oxygen, leading to the formation of highly electrophilic singlet oxygen that directly causes damage to membranes, proteins and DNA. The consequence of PDT critically depends on the intracellular efficiency of the PS. The available PSs can be engaged in both PDT mechanisms with various activities. These activities can be divided into the following groups depending on their solubility: hydrophobic, hydrophilic and amphiphilic.<sup>9</sup> However, in clinical

practice, another classification into short-acting, intermediate-acting and long-acting PSs is utilized.<sup>10</sup> The primary “weapon” of PDT against cancer is its ability to promote protein damage and membrane destruction; therefore, it is crucial to optimize the cytotoxic efficiency of this anticancer strategy. Furthermore, a higher degree of PS accumulation in cancer cells usually causes more cytotoxic effects.<sup>11,12</sup> Free radicals and singlet oxygen formation provoke a secondary effect of lipid peroxidation, resulting in leakage out of the membrane.<sup>6</sup> The PS is one of the 3 decisive elements of PDT, the other 2 being from light and oxygen.<sup>13</sup> Because of their photochemical properties and uptake efficiency, only a few PSs have official approval for clinical application – mainly, porfimer sodium (Photofrin), mTHPC (Foscan), talaporfin sodium (NPe6, Laserphyrin), SnEt2 (Purlytin), veteprofin (Visudyne), and motexafin lutetium (LuTex).<sup>14,15</sup> Numerous investigations have focused on a better characterization and development of PS with higher wavelengths, allowing for deeper penetration, a phenomenon known as the 2<sup>nd</sup> generation of PSs. The 3<sup>rd</sup> generation of PSs is the most effective in targeting cancer cells. These PSs are directed by antibodies or loaded in nanocarriers.<sup>16</sup> The PDT can be involved in 3 crucial mechanisms of cancer tissue destruction. In the 1<sup>st</sup> one, cancer cells are killed directly by the damaging action of ROS induced by PS excitations, leading to cell death through necrosis or apoptosis.<sup>8</sup> Photodynamic therapy can also lead to indirect tumor destruction through damage of tumor vasculature, which obstructs the supply of oxygen, nutrients and vitamins, as well as to the activation of the immune system that stimulates inflammation and an immune response against tumor cells.<sup>9,17,18</sup>

The PDT may also be improved through connection with other anticancer therapies such as chemo- or radiotherapy and electropermeabilization of cancer cell membranes.<sup>19–21</sup> Currently, PDT has been used to treat various cancers, such as skin, lung, bladder, breast, brain, ovarian, etc., in preclinical models and clinical investigations. Photodynamic reaction may also find use as a method of early cancer diagnosis, and as such is named photodynamic diagnosis (PDD). The PDD includes exciting and detecting tissue fluorescence from an earlier administered photosensitizing drug and illustrating diagnostic conclusions from the signals achieved. Finally, other non-cancer illnesses can also be treated by PDT, such as dermatological, mouth and cardiovascular diseases.<sup>22–24</sup>

## Types of polymeric materials

Natural polymers, called biopolymers, are structures created in the life cycle of plants, fungi, bacteria, or animals. Most of the biopolymers found in nature are produced by a highly energy-efficient process termed molecular self-assembly. Overall, the driving forces of this process display structural compatibility through non-covalent,

weak interactions and chemical complementarity.<sup>25,26</sup> Biopolymers are assigned into the following groups: polypeptides, polysaccharides and polynucleotides. In particular, polysaccharide-based polymers exhibit high stability, biodegradability, biocompatibility, and a lack of toxicity.<sup>27</sup> Different biopolymers such as pullulan, dextran, alginate, chitin, chitosan, albumin, hyaluronic acid (HA), gelatin, and guar gum are used for the creation of nanocarriers for drug delivery, especially in cancer drugs.<sup>28</sup> It has been shown that some biopolymers have an anti-tumor effect themselves.<sup>27</sup> For example, chitosan can induce membrane disruption in tumor cells and induce apoptosis. Biopolymers are also applied as a foundation to which drugs can be attached and delivered to targeted cells, which can result in less drug loss and lower toxicity for the whole organism.<sup>27</sup> Moreover, proteins are used for drug delivery systems. For instance, collagen is used in ophthalmology as a component of the drugs delivery system – gelatin is easily cross-linkable and forms valuable hydrogels, and these are used to create matrices in tissue engineering.<sup>25</sup> Likewise, albumin is used as a matrix in endovascular drug delivery systems.<sup>29</sup>

## Collagen

In human tissues, the structural and biochemical support of cells is given by the external cellular matrix (ECM). The structure of the ECM is formed by a three-dimensional (3D) collagen scaffold to which adhesive glycoproteins and proteoglycans are attached.<sup>30</sup> Collagen is an essential ECM component and one of the most beneficial scaffolding materials in tissue engineering. Apart from the fact that it is very well tolerated and biodegradable, its presence promotes the attachment and proliferation of the host cells. It also has good mechanical properties.<sup>27</sup> Collagen proteins are made of triple helices which oligomerize into fibrils by self-assembly. Currently, 29 types of collagen have been identified, and differ based on the 3 chains that make up their triple helix.<sup>25</sup> The most common type of collagen is collagen I, which can be found in tendons, skin and bones. Type II collagen dominates in intervertebral discs, cartilage and cornea.<sup>31</sup>

The sources of collagen type I for in vitro studies are bovine skin, bovine Achilles tendons and rat tails, while collagen type II is mainly obtained from articular cartilage.<sup>25</sup> An alternative to obtaining collagen is its laboratory production using genetic engineering techniques developed by the Fibrogen company.<sup>32</sup> Collagen obtained in this way is characterized by a defined composition and lower immunogenicity. The hierarchical organization of the collagen scaffold ensures excellent mechanical properties and supports cell adhesion. Its limitation is sensitivity to elevated temperature and gamma radiation. Despite the above limitations, collagen structures have found wide application in skin regeneration therapies. Collagen hydrogels that bind fibroblasts are a respectable substitute for

the skin. By using different cross-linking collagen assemblies, it is possible to influence the tensile strength and biodegradability of the entire structure. Furthermore, these collagen hydrogels containing fibroblast cells are used to heal chronic wounds. Growth factors secreted by fibroblasts positively affect wound regeneration, while the collagen structure itself protects it against contamination.<sup>25</sup> An example of a commercial collagen hydrogel dressing is Apligraf®.<sup>33</sup> Freeze-drying collagen solutions produce collagen sponges with pore diameters ranging from 50 µm to 200 µm. Such structures can be enriched with other ECM structures like fibronectin or glycosaminoglycans.<sup>34</sup> This modification improves the rate of cell adhesion and promotes their proliferation. These products are perfect for the treatment of extensive burn wounds. Other uses of collagen are nerve regeneration, tendon regeneration, bone regeneration, and intervertebral disc regeneration.<sup>25</sup>

## Elastin

Elastin is another significant and important component of the ECM. It is a hydrophobic, fibrillar, structural protein found in connective tissue, and the main component of tendons, ligaments, lung tissue, and walls of larger blood vessels. Remarkably, tissues abundant in elastin are capable of regaining their original size and shape following stretching or compression.<sup>25</sup> The elastin maturation process is called elastogenesis. Ripe elastin is a highly solid biopolymer, and its half-life is approx. 40 years.<sup>35</sup> Its biomedical application concerns skin repair processes and the reconstruction of blood vessels.<sup>36</sup> Elastin is often combined with collagen to create an environment with adequate mechanical strength, and to promote cell adhesion and proliferation.<sup>25</sup> A technique for producing recombinant elastin has also been developed in a way that, depending on the temperature, can assume a disordered, fully hydrated or organized and cross-linked structure. These modified elastins are used in eye regeneration, bone regeneration or vascular grafting.<sup>37</sup>

## Silk

Although the human body does not naturally produce silk, structures based on it are used in tissue engineering to regenerate liver tissues, bones, blood vessels, cartilage, ligaments, and cornea. The structure of silk shows exceptional mechanical properties, surpassing even synthetic materials.<sup>38</sup> Natural silk fibers mainly consist of fibroin fibers stuck together with sericin. Fibroin is a protein from the scleroprotein group; its chains are mostly composed of glycine (about 40%), alanine, serine, and tyrosine. Sericin (silk glue), in turn, is a protein that binds fibroin fibers together. It contains serine, glycine and aspartic acid residues. Silk is produced by various arthropods. Furthermore, the leading natural producer of this biopolymer is the mulberry silkworm *Bombyx mori*.<sup>39</sup> Also noteworthy is the fact

that in order to use silkworm-derived silk as a biomaterial, removal of sericin must be performed to ensure biocompatibility. Nevertheless, this negatively affects the biomaterial features.<sup>40</sup> With the use of genetic engineering techniques, it is possible to create silk-based chimeric proteins with desirable properties on a large scale and with low variability of the obtained biopolymer.<sup>41</sup> Various forms of silk-based biopolymers are currently produced, including hydrogels, fibers, foams, and meshes. Silk is also combined with other materials, such as elastin or peptides with antimicrobial properties, to increase its usefulness. Silk-based materials have also been shown to promote cell attachment, proliferation and differentiation of fibroblasts, osteoblasts, osteoclasts, and mesenchymal stem cells.<sup>39</sup>

## Marine biopolymers

Marine organisms are a powerful source of highly functional polymer structures that create 3D scaffolds with high mechanical strength.<sup>25</sup> These structures are increasingly used as scaffolds in tissue engineering. The main building materials of marine biopolymers are carbonate and calcium phosphate, but they also contain an admixture of an organic component in the form of proteins. Three types of collagen exist in sea sponges, along with human growth factor analogs. The main marine producers of biopolymers used in bone tissue engineering are corals, sea sponges, cuttlefish, and starfish.<sup>42</sup> Finally, trace elements such as strontium, fluorine and magnesium present in the inorganic part of these structures are of key importance for the induction of bone mineralization.<sup>43</sup>

Marine organisms are also a rich reservoir of biopolymers used in the engineering of soft shells. These include HA, alginate and chitosan. Hyaluronic acid is a high molecular weight water-soluble polysaccharide and it is mainly derived from the ECM of cartilaginous fish. It is a linear polymer composed of alternating 1-4-D-glucuronic and 1-3-N-acetyl-D-glucosamine residues.<sup>44</sup> Hyaluronic acid exhibits viscoelastic properties, and because of this, is used to regenerate synovial fluid, treat rheumatoid arthritis and wounds, and to create skin substitutes.<sup>25</sup> Modifications of HA are also used to reduce its solubility and slow its quick biodegradation. These modifications include esterification and combination with collagen, gelatin or chitosan.<sup>45</sup>

Alginate is a polysaccharide that builds the cell walls of brown algae. It consists of unbranched mannuronic and guluronic acid chains connected by glycosidic bonds.<sup>46</sup> The main useful property of alginate is its gelling ability, which is why it is used to form wound dressings. Gelling of alginate helps absorb wound exudate and promote healing.<sup>47</sup>

Chitosan is a product of the deacetylation of chitin, a polymer that builds crustaceans. The structure of chitosan consists mainly of D-glucosamine (70–90%) and N-acetyl-D-glucosamine (10–30%) chains that are linked

by glycosidic bonds. Due to its antibacterial, moisturizing and hemostatic properties, chitosan is widely used in wound products.<sup>48</sup>

## Nanocarriers based on biopolymers

Biopolymers are used to create systems for the effective and safe delivery of drugs to specific tissues. Using nanoencapsulation, it is possible to modulate the physicochemical and pharmacological properties of the transferred substances,<sup>49</sup> increase the stability and bioavailability of drugs, while simultaneously reducing their side effects.<sup>50</sup> The gelling and bioadhesive properties of biopolymers are used to form hydrogels to deliver anti-cancer compounds. The phenomenon of the sol-gel process, which is temperature-dependent, is exploited when administering the drug in a liquid form with the subsequent formation of a 3D matrix at the body temperature (ca. 37°C). The adhesive properties promote the appropriate residence time of the drug in the matrix, which allows for avoiding the side effects of conventional systemic administration of therapeutics. Paclitaxel nanoformulation (PTX) with endogenous serum albumin is currently the first-line treatment in metastatic breast cancer, pancreatic cancer and advanced non-small cell lung cancer.<sup>49</sup> This high-pressure homogenization procedure favors the reversible non-covalent albumin-PTX bonds and the formation of 130-nm nanoparticles (NPs). The drug accumulates more efficiently in solid tumors in this form due to the interaction between albumin particles and gp60 glycoprotein.<sup>51</sup> Previously, Yoshioka et al. developed a hydrogel based on sodium alginate with an admixture of hydroxyapatite for the controlled release of the cytostatic.<sup>52</sup> These hydrogel structures retain a high degree of structural integrity and release the bound drug at an appropriate rate.<sup>49</sup> Furthermore, Ruel-Gariépy et al. have developed a chitosan-based hydrogel loaded with cytostatic, which was administered to the sites after tumor resection to inhibit its regrowth. The starting material was the patented formula of chitosan and  $\beta$ -glycerophosphate that undergoes a sol-gel transformation after reaching body temperature.<sup>53</sup> This chitosan-based hydrogel is a promising strategy to avoid the drawbacks of systemic chemotherapy, providing relatively high local drug concentrations. Moreover, chitosan itself has a pro-apoptotic effect, inhibits the glycolytic pathway and modulates the activity of macrophages, leukocytes, and interleukin (IL)-1 and IL-2.<sup>53</sup>

Watanabe et al. have developed a HA nanoparticle-loaded PTX that was embedded in a hydrogel based on collagen. Researchers observed that highly transducing breast cancer cells were very susceptible to the above hydrogel, which was explained by the release of cytostatic from nanostructures under the influence of metalloproteinases (MMPs) released by cancer.<sup>54</sup>

Biodegradability and non-toxicity are the essential features of innovative drug delivery systems. The use of gelling and adhesive properties of various polysaccharides and proteins to obtain a formulation using a local bioactive compound is a reasonable strategy to maximize the therapeutic effectiveness of different molecules.<sup>49</sup>

## Natural polymer-based delivery of photosensitizers

Although numerous platforms exist for enhanced drug distribution, natural polymers seem to be promising in PS delivery. The main aim for PSs encapsulation is to improve the stability of hydrophobic PSs, protect the cargo and facilitate drug activity by longer release.<sup>9,55,56</sup> The other crucial issue is the enhanced permeability and retention (EPR) effect, where tumor vasculature is efficiently used in nanomedicine. However, in solid and low vascularized tumors, PSs delivery is still challenging.<sup>57,58</sup> This problem can be solved with natural and biodegradable polymers, which are easily eliminated from the body. In the photodynamic procedures, polymeric nanocarriers were prepared from natural polymers, such as albumin, HA or chitosan.<sup>59</sup> Wacker et al. used human serum albumin (HSA) as a drug carrier system for 5,10,15,20-tetrakis (m-hydroxyphenyl) porphyrine (mTHPP) and 5,10,15,20-tertrakis (m-hydroxyphenyl) chlorin (mTHPC). They examined the efficacy of these nanosystems against human leukemia cells. The previously performed study revealed that PSs were efficiently delivered and induced an increased singlet oxygen generation in photodynamic protocols.<sup>60</sup> In another study, bovine serum albumin (BSA) nanospheres were developed for the treatment of human esophageal carcinoma (Eca-109). These nanospheres synchronously encapsulated Au<sub>2</sub>Se/Au core-shell nanostructures and significantly increased PS efficiency in cancer phototherapy.<sup>61</sup> Portilho et al. also used BSA for nanosphere preparation and encapsulation of zinc-phthalocyanine tetrasulfonate (ZnPcS<sub>4</sub>-AN). Nanospheres were tested on in vivo model (Swiss albino mice) with breast cancer. That study indicated that nanosphere administration may inhibit tumor growth and necrotic cell death, with no side effects.<sup>62</sup>

The other type of polymers used in PDT is chitosan-based material. Chitosan is a biocompatible polysaccharide carrier that is an excellent material for producing highly biocompatible chlorin e6-loaded chitosan NPs. Ding et al. verified NPs in vitro and observed that PDT efficiency of Ce6-loaded CNPs considerably improved, in contrast to free Ce6, based on MTT and flow cytometry (FCM) assays.<sup>63</sup> Kardumyan et al. chose a different approach; they used the presence of chitosan in a model reaction of tryptophan photo-oxidation. In their study, various porphyrins were used: disodium salt of 3,8-di (1-methoxyethyl) deuteroporphyrin IX, and sodium salts of chlorin e6, 5,10,15,20-tetraphenylporphyrin, and fluorinated

tetraphenyl porphyrin-5,10,15,20-tetrakis (pentafluorophenyl) porphyrin. Physicochemical studies indicated that PSs in the presence of chitosan exhibited higher photocatalytic activity. In the case of PSs solubilized additionally in Pluronic F127, higher efficiency of singlet oxygen generation was observed.<sup>64</sup>

Chitosan NPs were also implemented for the early diagnosis of cancer. It was reported that MRI contrast agents loaded in chitosan nanosystems can be of use in cancer imaging.<sup>65</sup> Further studies by Wang et al. documented the application of chitosan particles in photothermal therapy (PTT). Authors developed chitosan polymers with gold nanorods for stabilization, and these nanosystems demonstrated improved stability and biocompatibility in human colon HT-29 cancer cells.<sup>66</sup> In other research, arachidyl chitosan (chitosan oligosaccharide-arachidic acid; CSOAA)-based self-assembled nanoprobe were used for cancer MRI imaging. Here, NPs were labeled with Cy5.5 and tested on head and neck cancer cell lines (Hep-2 and FaDu). In comparison to the commercially applied contrast agents, these chitosan-based probes revealed better effects.<sup>67</sup> Li et al. showed that micelles based on the chitosan might be effective in PDT as well. Authors used Photosan as a photosensitive cargo for the in vitro therapy on human pancreatic cancer cells (Panc-1). The researchers discovered that Photosan-DA-Chitosan micelles demonstrated a strong photocytotoxic effect in their specific cell model, and provoked an increased release of ROS.<sup>68</sup>

Hyaluronic acid can also be used for nanoparticle creation. It is known that HA-based nanosystems are quickly captured by reticuloendothelial system (RES),<sup>59</sup> which is a part of the immune system and includes phagocytic cells such as monocytes and macrophages.<sup>69</sup> Currently, surface modification of HA with poly(ethylene glycol) (PEG) is the most encouraging method to lower RES uptake.<sup>59,69</sup> Moreover, hyaluronan may affect tumorigenesis by converting an alternative energy source to glucose for malignant cells.<sup>70</sup> Wang et al. used HA-based polymeric micelles for targeted delivery of protoporphyrin IX (PpIX) for photodynamic therapy toward human lung cancer cells (A549).<sup>71</sup> In Table 1 below, a collection of the combinations of natural polymers and PSs used on in vitro and in vivo models is shown.

## Conjugated nanoparticles

Nanoparticles, natural and synthetic, conjugated with targeting ligands of the representative cancer cells (e.g., antibodies, peptides, organic molecules) or anticancer drugs, which can be encapsulated by the NPs or attached directly, significantly enhancing the localization specificity and cytotoxic drug delivery, while minimizing toxicity.<sup>5,72,73</sup> Furthermore, NPs can target other structures (e.g., vessels) and components of the cancer environment.<sup>74</sup> They also enable detection of pathological changes at the molecular and cellular level in cellular processes

**Table 1.** Natural polymers in photodynamic therapy (PDT) procedures in vitro and in vivo

Type of nanocarrier	Photosensitizer	Model in vitro/in vivo
Chitosan nanoparticles <sup>62</sup>	chlorin e6	human lung adenocarcinoma (A549) and human liver cell (L02)
HSA as a drug carrier system <sup>59</sup>	for 5,10,15,20-tetrakis (m-hydroxyphenyl) porphyrine (mTHPP) and 5,10,15,20-tertrakis (m-hydroxyphenyl) chlorin (mTHPC)	human leukemia cells (Jurkat)
BSA-nanospheres <sup>61</sup>	zinc-phthalocyanine tetrasulfonate (ZnPcS <sub>4</sub> -AN)	Swiss albino mice with breast cancer
BSA – nanospheres with Au <sub>2</sub> Se/Au core-shell <sup>60</sup>	zinc phthalocyanine (ZnPc)	human esophageal carcinoma (Eca-109)
Arachidyl chitosan (chitosan oligosaccharide-arachidic acid; CSOAA)-based self-assembled nanoprobes <sup>66</sup>	Cy5.5	head and neck cancer cell lines (Hep-2 and FaDu cells)
Amphiphilic chitosan derivative (photosan-DA-Chit) micelles <sup>67</sup>	photosan	human pancreatic cancer cells (Panc-1 cells)
Hyaluronic acid-b-poly (d,l-lactide-co-glycolide) copolymer (HA-b-PLGA micelles) <sup>70</sup>	protoporphyrin IX (PpIX)	human lung cancer (A549 cells)

HSA – human serum albumin; BSA – bovine serum albumin.

of the living cell without disturbing them; e.g., genetic mutations, protein overexpression or dysregulation, and cancer cells proliferation and metabolism. Moreover, Chen et al. emphasized the revolutionizing importance of theragnostic NPs for the future of treatment management.<sup>16</sup> This multifunctional system is based on 1 NP simultaneously linked with diagnostic agents and therapeutic compounds. The solution enables the use of targeted therapy while monitoring its progress. According to these advantages, the use of ligand-conjugated NPs in molecular imaging or as a drug delivery system indicates that the method may represent a promising solution in cancer therapy and diagnosis.

Basing the production of these NPs on natural polymers ensures high biocompatibility, biodegradability, non-toxicity, and lack of immunogenicity.<sup>5</sup> Additionally, the presence of specific protein binding sites and functional groups on their surface can improve target transport or tissue engineering protocols for efficient binding with therapeutic compounds or characteristic ligands.<sup>75,76</sup>

Among the NPs widely used in biomedical imaging, there are silver (AgNPs) and gold NPs (AuNPs), quantum dots conjugated NPs, and iron oxide NPs (ION). Recently, natural cellulosic polymers have found use in the formulation of silver NPs (AgNPs).<sup>77,78</sup> A few methods of AgNPs synthesis exist, including biological, chemical and physical. Unfortunately, each of them is limited by several factors, such as solvent contamination, toxic reducing agents or particle aggregation. Abdellatif et al. investigated methylcellulose (MC), hydroxypropyl methylcellulose (HPMC) and ethylcellulose (EC).<sup>77</sup> The obtained results showed that cellulosic polymers might act as an efficient reducing agent for AgNPs production. The AgNPs based on natural polymers exhibited no aggregation and the MC, HPMC and EC negative charge enhanced NP stability. Recently, Zhou et al. reviewed the use of natural polymers, such as chitosan, lignin, cellulose, and sugarcane bagasse pulp

in the production of carbon dots (CDs).<sup>79</sup> They appeared as high-potential green replacements for conventional high-potential quantum dots (QDs) due to improved biocompatibility and great photoluminescence (PL).

The available literature sources report an extensive analysis of ligand-conjugated NPs based on natural polymers, and present promising candidates to improve cancer therapy with reduced toxicity. Among them we can distinguish: chitosan-based NPs loaded with doxorubicin (DOX)<sup>78,80</sup> and curcumin<sup>81</sup>; alginate-based NPs loaded with docetaxel (DXL),<sup>82</sup> paclitaxel (PXL)<sup>83</sup> or DOX<sup>84</sup>; and dextran-based NPs loaded with DOX.<sup>85,86</sup> Moreover, NPs used to increase stability or improve delivery and uptake of microRNAs and siRNAs by tumor cells are currently in the spotlight.<sup>87–89</sup>

## Conclusions

In conclusion, this review serves as a summary of the application of natural polymers in nanocarriers for drug delivery. Natural materials used in nanosystems are favorable because of biodegradability, limited side effects and improved bioavailability. In PDT, the usability of nanosystems based on natural polymers can solve one of the problems which involves restrictions in application of various PSs because of their low water solubility. The latest nanotechnology research demonstrates the high potency in surface functionalization, which aims to selectively detect and destroy cancerous tissues. Thus, natural polymers in anticancer therapies appear to be suitable and promising for clinical applications.

### ORCID iDs

Julita Kulbacka  <https://orcid.org/0000-0001-8272-5440>  
 Anna Choromańska  <https://orcid.org/0000-0001-9997-7783>  
 Zofia Łapińska  <https://orcid.org/0000-0001-5070-2746>  
 Jolanta Saczko  <https://orcid.org/0000-0001-5273-5293>



## References

- Minn AJ, Gupta GP, Siegel PM, et al. Genes that mediate breast cancer metastasis to lung. *Nature*. 2005;436(7050):518–524. doi:10.1038/nature03799
- Weigelt B, Peterse J, van 't Veer L. Breast cancer metastasis: Markers and models. *Nat Rev Cancer*. 2005;5(8):591–602. doi:10.1038/NRC1670
- Chen X, Zhou H, Li X, et al. Plectin-1 targeted dual-modality nanoparticles for pancreatic cancer imaging. *EBioMedicine*. 2018;30:129–137. doi:10.1016/j.ebiom.2018.03.008
- Ma YY, Jin KT, Wang SB, et al. Molecular imaging of cancer with nanoparticle-based theranostic probes. *Contrast Media Mol Imaging*. 2017;2017:1026270. doi:10.1155/2017/1026270
- Wong KH, Lu A, Chen X, Yang Z. Natural ingredient-based polymeric nanoparticles for cancer treatment. *Molecules*. 2020;25(16):3620. doi:10.3390/molecules25163620
- Bacellar IOL, Tsubone TM, Pavani C, Baptista MS. Photodynamic efficiency: From molecular photochemistry to cell death. *Int J Mol Sci*. 2015;16(9):20523–20559. doi:10.3390/ijms160920523
- Tsubone TM, Martins WK, Pavani C, Junqueira HC, Itri R, Baptista MS. Enhanced efficiency of cell death by lysosome-specific photodamage. *Sci Rep*. 2017;7(1):1–19. doi:10.1038/s41598-017-06788-7
- Galluzzi L, Vitale I, Aaronson SA, et al. Molecular mechanisms of cell death: Recommendations of the Nomenclature Committee on Cell Death 2018. *Cell Death Differ*. 2018;25(3):486–541. doi:10.1038/s41418-017-0012-4
- Kwiatkowski S, Knap B, Przystupski D, et al. Photodynamic therapy: Mechanisms, photosensitizers and combinations. *Biomed Pharmacother*. 2018;106:1098–1107. doi:10.1016/j.biopha.2018.07.049
- Niculescu AG, Grumezescu AM. Photodynamic therapy: An up-to-date review. *Appl Sci*. 2021;11(8):3626. doi:10.3390/app11083626
- Jensen TJ, Vicente MGH, Luguya R, Norton J, Fronczek FR, Smith KM. Effect of overall charge and charge distribution on cellular uptake, distribution and phototoxicity of cationic porphyrins in HEP2 cells. *J Photochem Photobiol B Biol*. 2010;100(2):100–111. doi:10.1016/j.jphotobiol.2010.05.007
- Pavani C, Iamamoto Y, Baptista MS. Mechanism and efficiency of cell death of type II photosensitizers: Effect of zinc chelation. *Photochem Photobiol*. 2012;88:774–781. doi:10.1111/j.1751-1097.2012.01102.x
- Feng X, Shi Y, Xie L, et al. Synthesis, characterization, and biological evaluation of a porphyrin-based photosensitizer and its isomer for effective photodynamic therapy against breast cancer. *J Med Chem*. 2018;61(16):7189–7201. doi:10.1021/acs.jmedchem.8b00547
- Anand S, Ortel BJ, Pereira SP, Hasan T, Maytin EV. Biomodulatory approaches to photodynamic therapy for solid tumors. *Cancer Lett*. 2012;326(1):8–16. doi:10.1016/j.canlet.2012.07.026
- Banerjee SM, MacRobert AJ, Mosse CA, Periera B, Bown SG, Keshtgar MRS. Photodynamic therapy: Inception to application in breast cancer. *Breast*. 2017;31:105–113. doi:10.1016/j.breast.2016.09.016
- Chen F, Ehlerding EB, Cai W. Theranostic nanoparticles. *J Nucl Med*. 2014;55(12):1919–1922. doi:10.2967/jnumed.114.146019
- Spring BQ, Rizvi I, Xu N, Hasan T. The role of photodynamic therapy in overcoming cancer drug resistance. *Photochem Photobiol Sci*. 2015;14(8):1476–1491. doi:10.1039/c4pp00495g
- van Straten D, Mashayekhi V, de Bruijn HS, Oliveira S, Robinson DJ. Oncologic photodynamic therapy: Basic principles, current clinical status and future directions. *Cancers (Basel)*. 2017;9(2):19. doi:10.3390/cancers9020019
- Wezgowiec J, Kulbacka J, Saczko J, Rossowska J, Chodaczek G, Kotulska M. Biological effects in photodynamic treatment combined with electroporation in wild and drug resistant breast cancer cells. *Bioelectrochemistry*. 2018;123:9–18. doi:10.1016/j.bioelechem.2018.04.008
- Zimmermann A, Walt H, Haller U, Baas P, Klein SD. Effects of chlorin-mediated photodynamic therapy combined with fluoropyrimidines in vitro and in a patient. *Cancer Chemother Pharmacol*. 2003;51(2):147–154. doi:10.1007/s00280-002-0549-9
- Crescenzi E, Varriale L, Iovino M, Chiaviello A, Veneziani BM, Palumbo G. Photodynamic therapy with indocyanine green complements and enhances low-dose cisplatin cytotoxicity in MCF-7 breast cancer cells. *Mol Cancer Ther*. 2004;3(5):537–544. PMID:15141011
- Babilas P, Karrer S, Sidoroff A, Landthaler M, Szeimies RM. Photodynamic therapy in dermatology: An update. *Photodermatol Photoimmunol Photomed*. 2005;21(3):142–149. doi:10.1111/j.1600-0781.2005.00147.x
- Kossodo S, LaMuraglia GM. Clinical potential of photodynamic therapy in cardiovascular disorders. *Am J Cardiovasc Drugs*. 2001;1(1):15–21. doi:10.2165/00129784-200101010-00002
- Prazmo EJ, Kwaśny M, Łapiński M, Mielczarek A. Photodynamic therapy as a promising method used in the treatment of oral diseases. *Adv Clin Exp Med*. 2016;25(4):799–807. doi:10.17219/acem/32488
- Bassas-Galia M, Follonier S, Pusnik M, Zinn M. Natural polymers: A source of inspiration. In: Perale G, Hilborn J. *Bioresorbable Polymers for Biomedical Applications: From Fundamentals to Translational Medicine*. Sawston, UK: Woodhead Publishing; 2017:31–64. doi:10.1016/B978-0-08-100262-9.00002-1
- Zhao X, Zhang S. Fabrication of molecular materials using peptide construction motifs. *Trends Biotechnol*. 2004;22(9):470–476. doi:10.1016/j.tibtech.2004.07.011
- Khan MJ, Svedberg A, Singh AA, Ansari MS, Karim Z. Use of nanostructured polymer in the delivery of drugs for cancer therapy. In: Swain SK, Jawaid M. *Nanostructured Polymer Composites for Biomedical Applications*. Amsterdam, the Netherlands: Elsevier; 2019:261–276. doi:10.1016/b978-0-12-816771-7.00013-2
- Coviello T, Matricardi P, Marianecci C, Alhaique F. Polysaccharide hydrogels for modified release formulations. *J Control Release*. 2007;119(1):5–24. doi:10.1016/j.jconrel.2007.01.004
- Merodio M, Irache JM, Valamanesh F, Mirshahi M. Ocular disposition and tolerance of ganciclovir-loaded albumin nanoparticles after intravitreal injection in rats. *Biomaterials*. 2002;23(7):1587–1594. doi:10.1016/S0142-9612(01)00284-8
- Bosman FT, Stamenkovic I. Functional structure and composition of the extracellular matrix. *J Pathol*. 2003;200(4):423–428. doi:10.1002/path.1437
- Parenteau-Bareil R, Gauvin R, Berthod F. Collagen-based biomaterials for tissue engineering applications. *Materials (Basel)*. 2010;3(3):1863–1887. doi:10.3390/ma3031863
- Yang C, Hillas PJ, Báez JA, et al. The application of recombinant human collagen in tissue engineering. *BioDrugs*. 2004;18(2):103–119. doi:10.2165/00063030-200418020-00004
- Karr J. Utilization of living bilayered cell therapy (Apligraf) for heel ulcers. *Adv Skin Wound Care*. 2008;21(6):270–274. doi:10.1097/01.asw.0000323504.68401.d6
- Doillon CJ, Silver FH. Collagen-based wound dressing: Effects of hyaluronic acid and firponectin on wound healing. *Biomaterials*. 1986;7(1):3–8. doi:10.1016/0142-9612(86)90080-3
- Stitzel J, Liu J, Lee SJ, et al. Controlled fabrication of a biological vascular substitute. *Biomaterials*. 2006;27(7):1088–1094. doi:10.1016/j.biomaterials.2005.07.048
- Wang E, Lee SH, Lee SW. Elastin-like polypeptide based hydroxyapatite bionanocomposites. *Biomacromolecules*. 2011;12(3):672–680. doi:10.1021/bm101322m
- Gotoh Y, Ishizuka Y, Matsuura T, Niimi S. Spheroid formation and expression of liver-specific functions of human hepatocellular carcinoma-derived FLC-4 cells cultured in lactose/silk fibroin conjugate sponges. *Biomacromolecules*. 2011;12(5):1532–1539. doi:10.1021/bm101495c
- Altman GH, Diaz F, Jakuba C, et al. Silk-based biomaterials. *Biomaterials*. 2003;24(3):401–416. doi:10.1016/S0142-9612(02)00353-8
- Liu H, Ge Z, Wang Y, Toh SL, Sutthikhum V, Goh JCH. Modification of sericin-free silk fibers for ligament tissue engineering application. *J Biomed Mater Res B Appl Biomater*. 2007;82(1):129–138. doi:10.1002/jbm.b.30714
- Green DW, Padula MP, Santos J, Chou J, Milthorpe B, Ben-Nissan B. A therapeutic potential for marine skeletal proteins in bone regeneration. *Mar Drugs*. 2013;11(4):1203–1220. doi:10.3390/md11041203
- Vago R, Plotquin D, Bunin A, Sinelnikov I, Atar D, Itzhak D. Hard tissue remodeling using biofabricated coralline biomaterials. *J Biochem Biophys Methods*. 2002;50(2–3):253–259. doi:10.1016/S0165-022X(01)00235-4
- Bonnelye E, Chabadel A, Saltel F, Jurdic P. Dual effect of strontium ranelate: Stimulation of osteoblast differentiation and inhibition of osteoclast formation and resorption in vitro. *Bone*. 2008;42(1):129–138. doi:10.1016/j.bone.2007.08.043

43. Liu H, Mao J, Yao K, Yang G, Cui L, Cao Y. A study on a chitosan-gelatin-hyaluronic acid scaffold as artificial skin in vitro and its tissue engineering applications. *J Biomater Sci Polym Ed.* 2004;15(1):25–40. doi:10.1163/156856204322752219
44. Rinaudo M. Main properties and current applications of some polysaccharides as biomaterials. *Polym Int.* 2008;57(3):397–430. doi:10.1002/pi.2378
45. Wiegand C, Hipler UC. Polymer-based biomaterials as dressings for chronic stagnating wounds. In: *Macromolecular Symposia*. Vol. 294. Hoboken, USA: John Wiley & Sons, Ltd; 2010:1–13. doi:10.1002/masy.200900028
46. Ravi Kumar MNV. A review of chitin and chitosan applications. *React Funct Polym.* 2000;46(1):1–27. doi:10.1016/S1381-5148(00)00038-9
47. Dai T, Tanaka M, Huang YY, Hamblin MR. Chitosan preparations for wounds and burns: Antimicrobial and wound-healing effects. *Expert Rev Anti Infect Ther.* 2011;9(7):857–879. doi:10.1586/eri.11.59
48. Chenthamara D, Subramaniam S, Ramakrishnan SG, et al. Therapeutic efficacy of nanoparticles and routes of administration. *Biomater Res.* 2019;23(1):1–29. doi:10.1186/s40824-019-0166-x
49. Voci S, Gagliardi A, Molinaro R, Fresta M, Cosco D. Recent advances of taxol-loaded biocompatible nanocarriers embedded in natural polymer-based hydrogels. *Gels.* 2021;7(2):33. doi:10.3390/gels7020033
50. Gagliardi A, Giuliano E, Venkateswararao E, et al. Biodegradable polymeric nanoparticles for drug delivery to solid tumors. *Front Pharmacol.* 2021;12:17. doi:10.3389/fphar.2021.601626
51. Parodi A, Miao J, Soond SM, Rudzińska M, Zamyatnin AA. Albumin nanovectors in cancer therapy and imaging. *Biomolecules.* 2019;9(6):218. doi:10.3390/biom9060218
52. Yoshioka T, Ikoma T, Monkawa A, et al. Preparation of hydroxyapatite-alginate gels as a carrier for controlled release of paclitaxel. *Key Eng Mater.* 2007;330–332:1053–1056. doi:10.4028/www.scientific.net/kem.330-332.1053
53. Ruel-Gariépy E, Shive M, Bichara A, et al. A thermosensitive chitosan-based hydrogel for the local delivery of paclitaxel. *Eur J Pharm Biopharm.* 2004;57(1):53–63. doi:10.1016/S0939-6411(03)00095-X
54. Watanabe K, Nishio Y, Makiura R, Nakahira A, Kojima C. Paclitaxel-loaded hydroxyapatite/collagen hybrid gels as drug delivery systems for metastatic cancer cells. *Int J Pharm.* 2013;446(1–2):81–86. doi:10.1016/j.ijpharm.2013.02.002
55. Zhang Y, Wang B, Zhao R, Zhang Q, Kong X. Multifunctional nanoparticles as photosensitizer delivery carriers for enhanced photodynamic cancer therapy. *Mater Sci Eng C.* 2020;115:111099. doi:10.1016/j.msec.2020.111099
56. Huang YY, Sharma SK, Dai T, et al. Can nanotechnology potentiate photodynamic therapy? *Nanotechnol Rev.* 2012;1(2):111–146. doi:10.1515/ntrev-2011-0005
57. Maeda H, Tsukigawa K, Fang J. A retrospective 30 years after discovery of the enhanced permeability and retention effect of solid tumors: Next-generation chemotherapeutics and photodynamic therapy. Problems, solutions and prospects. *Microcirculation.* 2016; 23(3):173–182. doi:10.1111/micc.12228
58. Gao W, Wang Z, Lv L, et al. Photodynamic therapy induced enhancement of tumor vasculature permeability using an upconversion nanoconstruct for improved intratumoral nanoparticle delivery in deep tissues. *Theranostics.* 2016;6(8):1131–1144. doi:10.7150/thno.15262
59. Debele TA, Peng S, Tsai HC. Drug carrier for photodynamic cancer therapy. *Int J Mol Sci.* 2015;16(9):22094–22136. doi:10.3390/ijms160922094
60. Wacker M, Chen K, Preuss A, Possemeyer K, Roeder B, Langer K. Photosensitizer loaded HSA nanoparticles. I: Preparation and photophysical properties. *Int J Pharm.* 2010;393(1–2):254–263. doi:10.1016/j.ijpharm.2010.04.022
61. Yu C, Wo F, Shao Y, Dai X, Chu M. Bovine serum albumin nanospheres synchronously encapsulating gold selenium/gold nanoparticles and photosensitizer for high-efficiency cancer phototherapy. *Appl Biochem Biotechnol.* 2013;169(5):1566–1578. doi:10.1007/s12010-012-0078-x
62. Portilho FA, De Oliveira Cavalcanti CE, Miranda-Vilela AL, et al. Antitumor activity of photodynamic therapy performed with nanospheres containing zinc-phthalocyanine. *J Nanobiotechnology.* 2013;11:41. doi:10.1186/1477-3155-11-41
63. Ding YF, Li S, Liang L, et al. Highly biocompatible chlorin e6-loaded chitosan nanoparticles for improved photodynamic cancer therapy. *ACS Appl Mater Interfaces.* 2018;10(12):9980–9987. doi:10.1021/acsami.8b01522
64. Kardumyan VV, AksenoVA NA, Timofeeva VA, et al. Effect of chitosan on the activity of water-soluble and hydrophobic porphyrin photosensitizers solubilized by amphiphilic polymers. *Polymers (Basel).* 2021;13(7):1007. doi:10.3390/polym13071007
65. Key J, Park K. Multicomponent, tumor-homing chitosan nanoparticles for cancer imaging and therapy. *Int J Mol Sci.* 2017;18(3):594. doi:10.3390/ijms18030594
66. Wang CH, Chang CW, Peng CA. Gold nanorod stabilized by thiolated chitosan as photothermal absorber for cancer cell treatment. *J Nanoparticle Res.* 2011;13(7):2749–2758. doi:10.1007/s11051-010-0162-5
67. Termsarasab U, Cho HJ, Moon HT, Park JH, Yoon IS, Kim DD. Self-assembled magnetic resonance imaging nanoprobe based on arachidyl chitosan for cancer diagnosis. *Colloids Surfaces B Biointerfaces.* 2013;109:280–286. doi:10.1016/j.colsurfb.2013.03.058
68. Li H, Yu Z, Wang S, et al. Photosensitizer-encapsulated amphiphilic chitosan derivative micelles: Photoactivity and enhancement of phototoxicity against human pancreatic cancer cells. *J Photochem Photobiol B Biol.* 2015;142:212–219. doi:10.1016/j.jphotobiol.2014.10.020
69. Misra S, Heldin P, Hascall VC, et al. Hyaluronan-CD44 interactions as potential targets for cancer therapy. *FEBS J.* 2011;278(9):1429–1443. doi:10.1111/j.1742-4658.2011.08071.x
70. Smedsrød B, Seljelid R. Fate of intravenously injected aminated  $\beta(1 \rightarrow 3)$  polyglucose derivatized with 125I-tyraminyl cellobiose. *Immunopharmacology.* 1991;21(3):149–158. doi:10.1016/0162-3109(91)90020-Y
71. Wang X, Wang J, Li J, Huang H, Sun X, Lv Y. Development and evaluation of hyaluronic acid-based polymeric micelles for targeted delivery of photosensitizer for photodynamic therapy in vitro. *J Drug Deliv Sci Technol.* 2018;48:414–421. doi:10.1016/j.jddst.2018.10.018
72. Błaszczak-Świątkiewicz K, Olszewska P, Mikiciuk-Olasik E. Zastosowanie nanocząsteczek w leczeniu i diagnostyce nowotworów. *Nowotwory.* 2013;63(4):320–330. doi:10.5603/NJO.2013.0020
73. Shivani S, Ravindranath S. Nanoparticle in pharmaceutical drug delivery system: A review. *J Drug Deliv Ther.* 2019;9(3):543–548.
74. Shin SJ, Beech JR, Kelly KA. Targeted nanoparticles in imaging: Paving the way for personalized medicine in the battle against cancer. *Integr Biol (Camb).* 2013;5(1):29–42. doi:10.1039/c2ib20047c
75. Ulbrich K, Holá K, Šubr V, Bakandritsos A, Tuček J, Zbořil R. Targeted drug delivery with polymers and magnetic nanoparticles: Covalent and noncovalent approaches, release control, and clinical studies. *Chem Rev.* 2016;116(9):5338–5431. doi:10.1021/acs.chemrev.5b00589
76. Ige OO, Umoru LE, Aribi S. Natural products: A minefield of biomaterials. *ISRN Mater Sci.* 2012;2012:1–20. doi:10.5402/2012/983062
77. Abdellatif AAH, Alturki HNH, Tawfeek HM. Different cellulosic polymers for synthesizing silver nanoparticles with antioxidant and antibacterial activities. *Sci Rep.* 2021;11(1):84. doi:10.1038/s41598-020-79834-6
78. Niu S, Williams GR, Wu J, et al. A chitosan-based cascade-responsive drug delivery system for triple-negative breast cancer therapy. *J Nanobiotechnology.* 2019;17(1):95. doi:10.1186/s12951-019-0529-4
79. Zhou Y, Sharma SK, Peng Z, Leblanc RM. Polymers in carbon dots: A review. *Polymers (Basel).* 2017;9(2):67. doi:10.3390/polym9020067
80. Tian Q, Zhang CN, Wang XH, et al. Glycyrhethinic acid-modified chitosan/poly(ethylene glycol) nanoparticles for liver-targeted delivery. *Biomaterials.* 2010;31(17):4748–4756. doi:10.1016/j.biomaterials.2010.02.042
81. Esfandiarpour-Boroujeni S, Bagheri-Khouljenani S, Mirzadeh H, Amanpour S. Fabrication and study of curcumin loaded nanoparticles based on folate-chitosan for breast cancer therapy application. *Carbohydr Polym.* 2017;168:14–21. doi:10.1016/j.carbpol.2017.03.031
82. Chiu HI, Ayub AD, Mat Yusuf SNA, Yahaya N, Abbd Kadir E, Lim V. Docetaxel-loaded disulfide cross-linked nanoparticles derived from thiolated sodium alginate for colon cancer drug delivery. *Pharmaceutics.* 2020;12(1):38. doi:10.3390/pharmaceutics12010038
83. Ayub AD, Chiu HI, Mat Yusuf SNA, Abd Kadir E, Ngalm SH, Lim V. Biocompatible disulfide cross-linked sodium alginate derivative nanoparticles for oral colon-targeted drug delivery. *Artif Cells Nanomed Biotechnol.* 2019;47(1):353–369. doi:10.1080/21691401.2018.1557672
84. Gao C, Tang F, Zhang J, Lee SMY, Wang R. Glutathione-responsive nanoparticles based on a sodium alginate derivative for selective release of doxorubicin in tumor cells. *J Mater Chem B.* 2017;5(12):2337–2346. doi:10.1039/c6tb03032g
85. Tang Y, Li Y, Xu R, et al. Self-assembly of folic acid dextran conjugates for cancer chemotherapy. *Nanoscale.* 2018;10(36):17265–17274. doi:10.1039/c8nr04657c

86. Thambi T, You DG, Han HS, et al. Bioreducible carboxymethyl dextran nanoparticles for tumor-targeted drug delivery. *Adv Healthc Mater.* 2014;3(11):1829–1838. doi:10.1002/adhm.201300691
87. Foerster F, Bamberger D, Schupp J, et al. Dextran-based therapeutic nanoparticles for hepatic drug delivery. *Nanomedicine (Lond).* 2016;11(20):2663–2677. doi:10.2217/nnm-2016-0156
88. Nascimento AV, Singh A, Bousbaa H, Ferreira D, Sarmento B, Amiji MM. *Mad2* checkpoint gene silencing using epidermal growth factor receptor-targeted chitosan nanoparticles in non-small cell lung cancer model. *Mol Pharm.* 2014;11(10):3515–3527. doi:10.1021/mp5002894
89. Zhang L, Iyer AK, Yang X, et al. Polymeric nanoparticle-based delivery of microRNA-199a-3p inhibits proliferation and growth of osteosarcoma cells. *Int J Nanomedicine.* 2015;10(1):2913–2924. doi:10.2147/IJN.S79143



# Brief review on poly(glycerol sebacate) as an emerging polyester in biomedical application: Structure, properties and modifications

## Przegląd literatury dotyczący poli(sebacynianu glicerolu) jako nowego poliestru do zastosowań biomedycznych: struktura, właściwości i modyfikacje

Paweł Piszko<sup>1,A–F</sup>, Bartłomiej Kryszak<sup>1,A–F</sup>, Aleksandra Piszko<sup>2,B–D,F</sup>, Konrad Szustakiewicz<sup>1,A–F</sup>

<sup>1</sup> Department of Polymer Engineering and Technology, Faculty of Chemistry, Wrocław University of Science and Technology, Poland

<sup>2</sup> Department of Pediatric Dentistry and Preclinical Dentistry, Wrocław Medical University, Poland

A – research concept and design; B – collection and/or assembly of data; C – data analysis and interpretation; D – writing the article; E – critical revision of the article; F – final approval of the article

Polymers in Medicine, ISSN 0370-0747 (print), ISSN 2451-2699 (online)

*Polim Med.* 2021;51(1):43–50

### Address for correspondence

Bartłomiej Kryszak  
E-mail: bartlomiej.kryszak@pwr.edu.pl

### Funding sources

None declared

### Conflict of interest

None declared

Received on June 5, 2021

Reviewed on June 16, 2021

Accepted on June 29, 2021

Published online on July 29, 2021

### Abstract

Poly(glycerol sebacate) (PGS) is an aliphatic polyester which attracted significant scientific attention in recent years due to its vast potential in biomedical applications with regard to tissue engineering. It has been presented in the literature in the form of 2D films, porous scaffolds or nonwovens, to name just a few. Moreover, various applications have been proposed as a component of composite materials or polymer blends. Its physicochemical properties can be significantly adjusted by means of synthesis and post-synthetic modifications, including cross-linking or chemical modification, such as copolymerization. Many scientists have discussed PGS as a new-generation polymer for biomedical applications. Its regenerative potential has been confirmed, in particular, in tissue engineering of soft tissues (including nerve, cartilage and cardiac tissues). Therefore, we must anticipate a growing importance of PGS in contemporary biomedical applications. This brief review aims to familiarize the readers with this relatively new polymeric material for tissue engineering applications.

**Key words:** tissue engineering, biomaterial, PGS, biomedical application, poly(glycerol sebacate)

### Cite as

Piszko P, Kryszak B, Piszko A, Szustakiewicz K.  
Brief review on poly(glycerol sebacate) as an emerging polyester in biomedical application: Structure, properties and modifications. *Polim Med.* 2021;51(1):43–50.  
doi:10.17219/pim/139585

### DOI

10.17219/pim/139585

### Copyright

© 2021 by Wrocław Medical University  
This is an article distributed under the terms of the Creative Commons Attribution 3.0 Unported (CC BY 3.0) (<https://creativecommons.org/licenses/by/3.0/>)

## Streszczenie

Poli(sebacynian glicerolu) (PGS) jest poliestrem alifatycznym, który w ostatnich latach skupił na sobie zainteresowanie wielu zespołów badawczych głównie ze względu na potencjał w zastosowaniach biomedycznych, w tym w inżynierii tkankowej. W literaturze jest opisywany, między innymi, w postaci dwuwymiarowych filmów, porowatych scaffoldów oraz włókien. Ponadto, w niektórych przypadkach, naukowcy proponują wykorzystanie PGSu jako składnika kompozytów bądź mieszanin polimerowych. Właściwości fizykochemiczne poli(sebacynianu glicerolu) mogą być optymalizowane zarówno za pośrednictwem metody oraz parametrów syntezy, jak i poprzez modyfikacje post-syntetyczne takie jak sieciowanie, modyfikacja chemiczna lub kopolimeryzacja. Badacze przedstawiają PGS jako polimer nowej generacji do zastosowań biomedycznych. Jego potencjał regeneracyjny został potwierdzony w inżynierii tkanek miękkich (w tym tkanek nerwowych, chrzęstnych i sercowych). Jest więc kwestią czasu jego szerokie wykorzystanie we współczesnych rozwiązaniach z pogranicza biomedycyny. Ten artykuł przeglądowy stawia sobie za cel przybliżenie zastosowania poli(sebacynianu glicerolu) w inżynierii tkankowej.

**Słowa kluczowe:** inżynieria tkankowa, biomateriały, PGS, zastosowania biomedyczne, poli(sebacynian glicerolu)

## Introduction

There are multiple biocompatible polyesters developed for biomedical applications including poly(L-lactide), polycaprolactone or polyglycolide.<sup>1</sup> Among the aforementioned polymers, we can indicate a new emerging one: Poly(glycerol sebacate) (PGS). Poly(glycerol sebacate) is an excellent candidate for biomedical applications thanks to its physicochemical properties including its elastomeric capabilities,<sup>2</sup> cross-linking potential,<sup>3</sup> biodegradability<sup>4</sup> and biocompatibility<sup>5</sup> displayed in several in vitro and in vivo studies. Substantive research has been carried out on the field of PGS applications in various areas, especially biomedicine. The gradual increase in the annual number of papers regarding PGS is presented in Fig. 1.

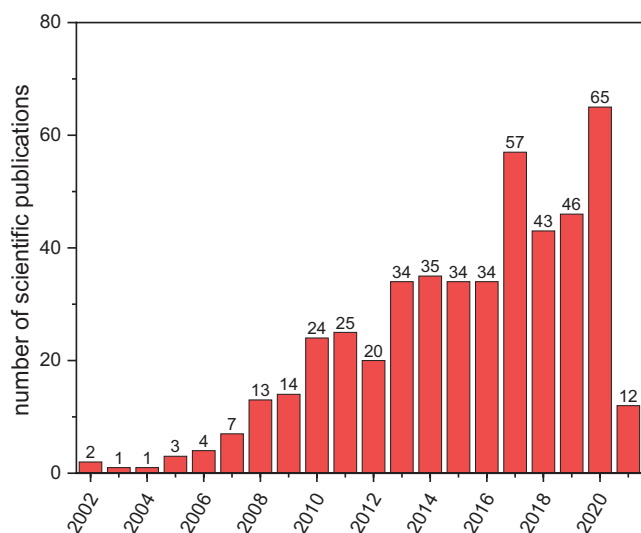


Fig. 1. Number of scientific publications regarding poly(glycerol sebacate) in years 2002–2021. Source: Web of Science database. Data gathered on May 19, 2021

## PGS: structure, synthesis, properties, and forming techniques

The PGS was first reported in terms of biomedical application by Wang et al.<sup>6</sup> However, the described polymer was investigated in the aliphatic copolymers synthetic

study by Nagata et al. in 1999.<sup>7</sup> The PGS is an elastomeric, biodegradable polyester material, most commonly derived from dicarboxylic sebacic acid and glycerol through polycondensation.

### Prepolymer synthesis

Commonly, PGS is obtained as a prepolymer (pPGS) which is subject to further structural modification, curing, blending, and forming. Each synthetic method results in different polymer structure. We can outline the most popular approaches in pPGS synthesis:

- reduced-pressure polycondensation,
- enzymatic synthesis and
- microwave-assisted polymerization.

Introduced in 2002,<sup>6</sup> reduced-pressure polycondensation is undeniably the most trending synthetic pathway of obtaining pPGS.<sup>2,4,5,8–15</sup> It consists of synthesis at elevated temperatures for a certain period of time in the inert gas atmosphere, combined with the subsequent reduction in pressure, most commonly to around 40 mTorr.

However, polycondensation in atmospheric pressure has been reported as well.<sup>7,16,17</sup> The major difference in utilizing pressure is the propagation of inter-molecular bonding (i.e., cross-linking). Decreased pressure in combination with increased temperature in the 2<sup>nd</sup> stage of polymer synthesis results in the aforementioned cross-linked structure. Sometimes this stage may be delayed due to the process limitation (e.g., during porous scaffold formation cross-linking is postponed to the moment when scaffold is partially formed<sup>18</sup>).

Also noteworthy, reduced-pressure polycondensation is also mostly used as a technique for the synthesis of PGS copolymers (i.e., poly(glycerol-sebacate)-co-polyethylene glycol<sup>19</sup> or poly(glycerol-sebacate)-co-polycaprolactone<sup>20</sup>).

In the enzymatic synthesis, the most commonly encountered catalyst is *Candida antarctica* lipase B (CALB), which is utilized to obtain PGS.<sup>21,22</sup> Perin and Felisberti reported a correlation between CALB selectivity and acyl migration phenomenon, which causes branching during the PGS polycondensation.<sup>22</sup> The enzymatic synthesis is performed at slightly elevated temperature and has proven to produce polymer with increased linearity.<sup>21</sup>

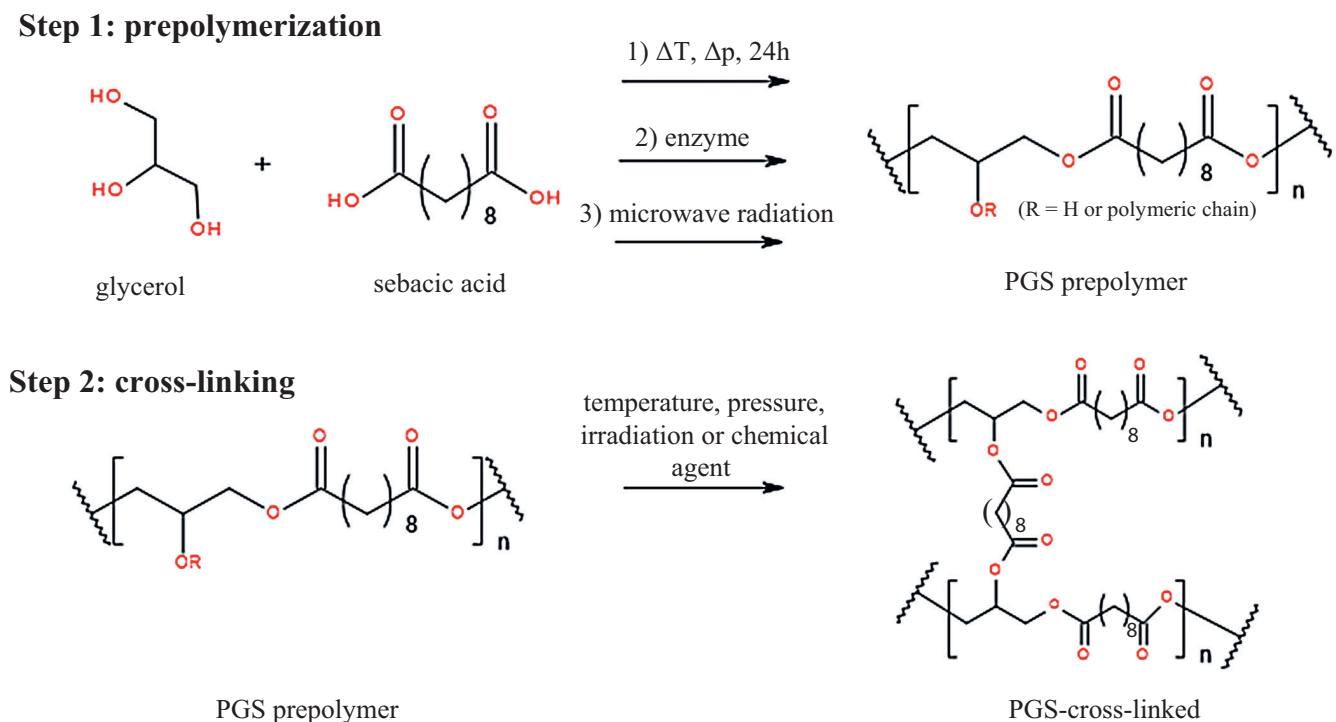


Fig. 2. Synthesis options for poly(glycerol sebacate) (PGS)

Microwave radiation has also proven to shorten the prepolymer synthesis time before the cross-linking stage occurs.<sup>23</sup> Moreover, it helps to obtain homogeneous polymer mixture or dispersion (e.g., when forming composites).<sup>3</sup> The most commonly encountered approach consists of interval microwave irradiation (e.g., 1 min 650 W with 10 s interval<sup>24</sup>). In terms of backbone architecture, microwave synthesis can lead to more branched structures in comparison to conventional melt polycondensation.<sup>25</sup>

The described synthetic approaches are presented graphically as a synthetic pathway in Fig. 2.

### Cross-linking and branching of the polymer chain

A thorough PGS branching characterization method by means of <sup>1</sup>H NMR spectrum was introduced by Perin and Felisberti.<sup>22</sup> This method allows for an easy and effective structural characterization of prepolymer before subsequent cross-linking or modification. In-depth structural analysis conducted by means of <sup>1</sup>H NMR allows for an in-depth definition of the pPGS structure. Namely, one can outline the presence and abundance of specific glyceridic units in the polymeric chain and therefore, analyze the topology of the molecular chain.<sup>22,26</sup> This method can be utilized to determine the linearity of the obtained PGS by confirming the presence of 2 individual linear units. As described in the previous section, various synthetic approaches result in different branching degree, degree of esterification or simply degree of polymerization.

One can distinguish cross-linking techniques depending on the utilized agent. The most popular pathway to form intermolecular bonding is thermal cross-linking. It can be performed for a shorter period of time at higher temperature (taking into consideration degradability of PGS) or longer (even several days) in a lower range of temperatures (120–150°C).<sup>27,28</sup> The cross-linking temperature and time considerably influence the degree of cross-linking and thus, the mechanical properties of the polymer.

Chemical cross-linking of pPGS can take effect by compounds such as methylene diphenyl diisocyanate (MDI) or hexamethylene diisocyanate (HDI). They can be introduced to pPGS prior to the curing process in order to increase the cross-linking degree, tensile stress and Young's modulus.<sup>13,17</sup>

There is a broad array of structural modifications which introduce photocurable groups to the prepolymer (e.g., methacrylate groups<sup>12</sup>). Modified polymeric backbone can be further subjected to irradiation resulting in photocured structures. Therefore, we consider an irradiation as another agent capable of cross-linking poly(glycerol sebacate).<sup>12,14,26,29</sup>

### PGS polymer properties

Until now, PGS has been seen as a material that resembles soft tissues.<sup>17,30</sup> Thanks to the endogenous character of sebacic acid and glycerine,<sup>5,6,25</sup> PGS and PGS-based composites are recognized as biocompatible.<sup>14,31</sup> The PGS is obtained as transparent or slightly yellow polyester (depending on the presence of oxygen during the reaction).

The structural analysis of the PGS performed using Fourier-transform infrared spectroscopy (FTIR) confirms the presence of all important bonds and functional groups, including polar hydroxyl, terminal carboxyl groups, ester bonding, and aliphatic backbone.<sup>27</sup>

In terms of physicochemical characteristics, PGS is considered an elastomeric material. Tests on tensile strength performed on PGS strips divulged an elastomeric character of the polymer by the presence of the characteristic stress-strain curve.<sup>6</sup> According to literature reports, PGS exhibits Young's modulus in the range of 0.12–0.5 MPa, a tensile strength of 0.27–0.50 N/m<sup>2</sup>, and an elongation at break of 180–274%.<sup>6,23,32</sup> Moreover, the polymer is considered hydrophilic with a water contact angle around 70–80°. <sup>20,33</sup> At body temperature (~37°C: the temperature of potential biomedical applications) it is fully amorphous.<sup>6,23</sup>

In addition, the prepolymer (pPGS) is soluble in many readily available organic solvents, such as 1,3-dioxolane, tetrahydrofuran, ethanol, isopropanol, and N,N-dimethylformamide, dioxane. This makes it easy to process using a variety of techniques.<sup>6</sup>

## Processing techniques of PGS and PGS-based materials

Poly(glycerol sebacate) has proven to be readily processable using various techniques. The simplest of them is to give it the suitable shape using in-mold polymerization combined with cross-linking.<sup>6,27</sup> However, in addition to the target shape, several other factors must be considered when designing the material for potential tissue engineering applications. These include porosity, mechanical properties and biocompatibility. When discussing PGS processing, one should also note that the prepolymer form is mostly processed (in non-cross-linked form). Cross-linking is one of the last steps that stabilizes the properties of the product. Some of the most commonly used techniques for poly(glycerol sebacate) processing are described below.

### Solvent casting

The solvent casting method is the most commonly used method of producing materials based on PGS. It consists of the following steps: 1) dissolving the polymer in a solvent (in the case of PGS – dissolving the non-cross-linked prepolymer); 2) pouring the solution into a prepared mold or vessel (e.g., Petri dish); and 3) evaporating the solvent, and cross-linking of the product.

In the case of PGS and PGS-based materials, the most commonly used solvents are dimethylformamide (DMF),<sup>13,34,35</sup> tetrahydrofuran (THF)<sup>2,5,17</sup> and dimethyl carbonate (DMC).<sup>36</sup> The solvent casting method is often supported by the particulate leaching technique. The aim of this treatment is to obtain larger pores optimal for cell growth and development. For this purpose, solid particles

are introduced into the polymer solution and washed out of the material after the cross-linking step. Lee et al. used 25–32- $\mu\text{m}$  grounded salts as porogens, which after the production of the final element were washed out in water bath.<sup>14</sup>

The PGS-based materials made by solvent casting are very often subjected to a freeze-drying process in order to remove solvent residues from the structure.<sup>9,37,38</sup> The solvent casting method has also been used to modify PGS by introducing a filler into the system.<sup>2,35</sup> For example, Gaharwar et al. introduced 1% wt of carboxyl functionalized multi-walled CNTs into the solution of PGS (in THF). These authors proved that, thanks to interaction between the filler and polymer matrix, the obtained material is characterized by much better mechanical parameters and resistance to degradation than unmodified PGS.<sup>2</sup>

### Thermally induced phase separation method

The thermally induced phase separation (TIPS) method is based on the induction of phase separation in the liquid-liquid or liquid-solid system.<sup>39</sup> The standard PGS manufacturing process using this method can be divided into 4 stages: 1) dissolving the prepolymer in a solvent (e.g., dioxane<sup>40</sup>); 2) freezing the system; 3) freeze drying – sublimation under reduced pressure of the polymer-lean phase (solvent); and 4) cross-linking. The product obtained using the TIPS method, after curing, takes the form of an elastic foam. An example is shown in Fig. 3.

The TIPS method is used, i.a., to produce chemically cross-linked PGSU.<sup>40,41</sup> Hexamethylene diisocyanate (HDI) is used as a cross-linking agent. It reacts with the hydroxyl groups of PGS to form a chemically cross-linked poly(glycerol sebacate urethane) (PGSU).

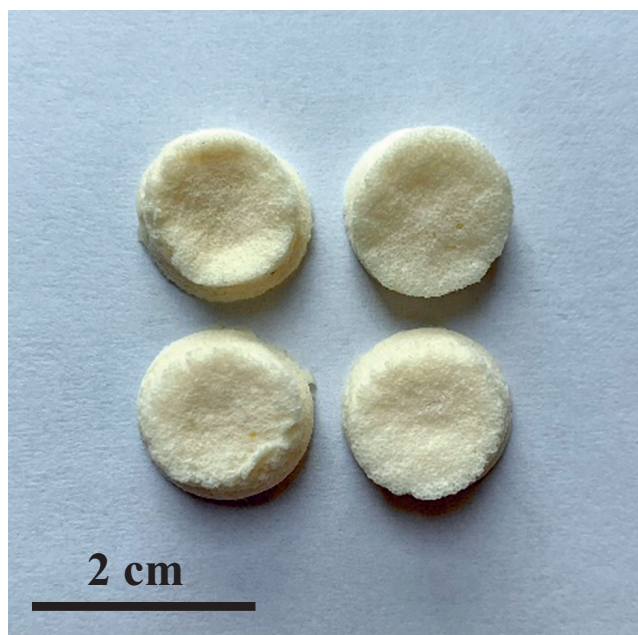


Fig. 3. PGS porous scaffolds with inorganic filler obtained using TIPS method (source: own research)



## Particulate leaching

The particulate leaching technique is most often used in parallel with other methods of PGS-based material fabrication. The use of solid porogens with specific geometry and particle size allows for the strict control of porosity of the biomaterial. This is important primarily for proper cell development. The size of the pores is also a very important factor in determining the ability to infiltrate cells deep into the scaffold.

Two approaches are mainly used in the production of PGS-based materials using the particulate leaching technique. The 1<sup>st</sup> of them is described in more detail above. It is based on the solvent casting method.<sup>9,37,42</sup> It consists of the following steps: 1) filling the mold with solid porogen particles; 2) flooding the porogen bed with PGS and solvent solution; 3) evaporating the solvent and cross-linking the product; and 4) washing out the porogen. The 2<sup>nd</sup> frequently used approach is to mix the prepolymer directly with the porogen particles without the use of a solvent.<sup>31,43</sup> The rest of the procedure is similar.

The most commonly used porogens are sodium chloride particles (NaCl).<sup>9,36,42</sup> Depending on the size of the target pores, the salt is ground and filtered prior to the process. Pashneh-Tala et al. have previously used sucrose as a porogen.<sup>11</sup> The advantage of both compounds is their good solubility in water, and thus, the possibility of non-invasive removal of solid particles from the system using just distilled or deionized water (H<sub>2</sub>O) baths.<sup>36,42</sup> In addition to water, ethanol is used to wash the final product in order to remove unwanted post-process residues (e.g., residues of a cross-linking agent or oligomer fractions).<sup>44</sup>

## Electrospinning

Electrospinning can be defined as a spinning fiber forming process based on an electrohydrodynamic phenomenon that uses electrostatic force to draw continuous fibers in the form of a liquid jet, from a polymer solution or melt.<sup>45</sup> Typically, the product made using this method is in the form of a nonwoven mat of randomly ordered fibers.

When discussing the processing of PGS by electrospinning, it should be noted that the form of the prepolymer is processed. As with other methods, cross-linking is carried out only in the final stage of material production.

Scientific reports show that it is practically impossible to process PGS itself using the electrospinning technique. The main reason for this is its low molecular weight, resulting in the absence of entanglements.<sup>46,47</sup> This problem can be solved in several ways. One example is the electrospinning of PGS with a carrier polymer (e.g., PVA<sup>48</sup>), which is removed from the system after the process (by leaching). Another interesting approach is the electrospinning of PGS as a biocomponent in a blend with another polymer (i.e., poly(lactic acid) (PLA)<sup>46,47</sup> polycaprolactone (PCL)<sup>49</sup> or poly(methyl methacrylate) (PMMA)<sup>50</sup>).

An important aspect is the selection of an appropriate solvent for the preparation of the polymer solution. Fakhrli et al. produced PGS/PCL fibers using various solvents (i.e., acetic acid, acetone, N,N-dimethylformamide, formic acid).<sup>49</sup> The studies have shown that the selection of an appropriate solvent has an impact on the morphology of the fibers and their diameter.

## 3D printing methods

Three-dimensional printing includes a group of computer-assisted techniques to enable the production of 3D models. The starting material is applied to the work area in a layer-by-layer manner and solidified using various physical factors.

The literature presents a handful of approaches to 3D printing of PGS-based materials. Singh et al. used the stereolithography method to manufacture the Nerve Guidance Conduits, taking into account the ability to cross-link PGS with UV radiation.<sup>13</sup> A similar approach was used by Wang et al., who utilized digital-light-processing-based 3D printing for the production of nature-inspired double network (DN) from poly(glycerol sebacate) acrylate (PGSA).<sup>29</sup> A completely different method was proposed by Yeh et al., who used extrusion-based 3D printing of acrylated poly(glycerol sebacate) (Acr-PGS) to manufacture the scaffold with elastic properties.<sup>51</sup>

## Others

In addition to the methods described above, several other methods of fabrication and processing of PGS-based materials have been developed. These include, i.a., gyrosinning<sup>52</sup> and micromoulding<sup>53</sup> techniques. Such broad processing possibilities allow for a more complete use of the PGS application potential.

## Degradation and biodegradation

The degradation behavior of PGS is a desirable characteristic for tissue engineering applications which aim for stimulating cell proliferation with the goal of eliminating the scaffold from the organism. The time needed for the complete dissolution of the PGS implant in the *in vivo* conditions is small and was determined to be 60 days.<sup>6</sup> Its exact length depends on many factors. It was clearly shown by Pomerantseva et al. that curing time, which greatly affects cross-linking PGS degree, affects *in vivo* degradation time.<sup>4</sup> Bulk materials need more time for decomposition in comparison to porous structures utilized as the cellular scaffolds. It naturally indicates the latter as potential candidates for bone tissue engineering applications in terms of biodegradation time.<sup>40</sup> However, the degradation of the material caused by environmental factors such as oxygen or moisture applies to the biological

systems as well. Therefore, *in vitro* and *in vivo* biodegradation studies of the PGS-based scaffolds are of vital importance on the field of tissue engineering applications.

## Biocompatibility and cytotoxicity assessment

To consider any material for biomedical applications, its biocompatibility has to be proven and supported by relevant studies. Within the International Union of Pure and Applied Chemistry (IUPAC) definition, biocompatibility is an ability to be in contact with a living system without producing an adverse effect.<sup>54</sup> Wang et al., while first reporting on biomedical applications of PGS, clearly took that property into consideration. Moreover, they noticed that the ideal scaffold for tissue implantation should be biodegradable and resemble properties of the extracellular matrix (ECM) in its physicochemical aspects.<sup>6</sup> Bone defects after injuries, bone tumor resections or infections need to be supplemented by implants. The problem often faced in modern medicine and tissue engineering is to find a proper material that does not provoke rejection, is not limited in quantity and shape, and has specific mechanical properties similar to natural bone or even replaceable by one. If it is biodegradable and promotes bone

development (i.e., material is osteoinductive), it can be replaced by a natural bone after application in humans. Often to fulfil those restrictive criteria, the implant material needs to be complex and modified.

Following this line of reasoning, many materials based on PGS with an admixture of other compounds (polymers, mineral apatites or others) are manufactured. For example, a study on the PGS/PCL blend of porous scaffolds for cartilage tissue engineering was conducted and showed successful results in terms of biocompatibility.<sup>55</sup> The *in vitro* degradation time, adhesion and proliferation abilities were investigated on bone marrow-derived mesenchymal stem cells (BMSCs) and articular chondrocytes (ACCs). The weight loss rate of PGS/PCL scaffolds was significantly slower than that of pure PGS stent, which shows that PCL was responsible for prolongation of the degradation time. Moreover, PCL helped increase stiffness (evaluated with uniaxial mechanical test). Synthesized PGS/PCL material was analyzed using scanning electron microscope (SEM), as well as BMSC and ACC cell distribution. Cell morphology detection was observed using confocal microscope. As a result, authors obtained a biocompatible, composite material with favorable mechanical strength and appropriate biodegradability. Materials combining poly(glycerol sebacate) with polycaprolactone have also been studied by other scientists, showing a great potential for soft tissue

**Table 1.** Brief literature review of biological evaluations on poly(glycerol sebacate) (PBS)-based materials for tissue engineering

PGS-based material composition	Potential application	Biological material	Results summary	Reference
Biomimetic poly(glycerol sebacate)/polycaprolactone blend scaffolds	cartilage tissue engineering	bone marrow-derived mesenchymal stem cells (BMSCs) and articular chondrocytes (ACCs)	Promising scaffold, biocompatible, prolonged degradation time and increased stiffness, cytocompatibility with both BMSCs and ACCs <i>in vitro</i> . BMSCs successfully underwent chondrogenesis on the PGS/PCL scaffolds.	55
Porous hyaluronic acid (HA)/PGS-M composite scaffold	bone tissue engineering	human adipose-derived stem cells (hADSCs)	Acceptable biocompatibility and mechanical properties, material stimulated hADSC cell proliferation and differentiation.	18
PGS	neural reconstruction	Schwann cells	PGS had no deleterious effect on Schwann cell metabolic activity, attachment, or proliferation, and did not induce apoptosis <i>in vivo</i> . PGS demonstrated a favorable tissue response profile compared with PLGA, with significantly less inflammation and fibrosis and without detectable swelling during degradation.	5
Poly( $\epsilon$ -caprolactone)/poly(glycerol sebacate) electrospun scaffolds	cardiac tissue engineering	bone marrow-derived stroma, ST2 cells	Homogenous and defect-free fiber mats from PCL and PGSP or PGSMXL were successfully electrospun. The mechanical properties of the fiber mats were higher compared to native human myocardial tissue.	56
Microfibrous core-shell mats made of polycaprolactone (PCL)-PGS with heparin immobilized on the surface of the scaffold	tissue engineering	human umbilical vein endothelial cells	Controlled degradation of the scaffold, structural integrity and mechanical support, increased elasticity, maintaining the mechanical properties of the tissue-engineered construct.	57
PGS macroporous scaffolds with extensive micropores	soft tissue engineering	NIH 3T3 mouse embryonic fibroblast cells	Surface supports cell adhesion and proliferation. Mechanical properties are suitable for soft tissue engineering.	8
Shape-memory ternary scaffolds based on PGS and poly(1,3-propylene sebacate) and immobilized kartogenin	cell-free cartilage repair	bone marrow-derived mesenchymal stem cell (BMSC)-specific	Scaffolds exhibited shape-memory properties good potential for minimally invasive implantation.	9

engineering.<sup>56,57</sup> This brief review of the biological evaluation conducted on PGS-based materials is presented in the Table 1.

The PGS-based systems for tissue engineering constitute a diverse range of potential applications supported by biological evaluation. It positions PGS as a candidate for future-generation biomaterial suitable for a variety of biomedical purposes.

## Conclusions

Poly(glycerol sebacate) is an emerging polymeric material for biomedical applications. With plenty of synthetic pathways followed by multiple cross-linking possibilities, the material proves to be a contestant for contemporarily utilized polymers for biomedical applications like PCL or PLA. The wide spectrum of applicable forming techniques broadens the possibilities of implementing this particularly interesting polyester in regenerative medicine. One has to take into consideration its drawbacks including low molecular weight distribution of prepolymer or its high rate of biodegradability. However, PGS displays the properties that modern regenerative medicine is currently searching for.

### ORCID iDs

Paweł Piszko  <https://orcid.org/0000-0002-7577-8509>  
 Bartłomiej Kryszak  <https://orcid.org/0000-0001-9807-964X>  
 Aleksandra Piszko  <https://orcid.org/0000-0003-0386-216X>  
 Konrad Szustakiewicz  <https://orcid.org/0000-0002-2855-852X>

### References

- Ulery BD, Nair LS, Laurencin CT. Biomedical applications of biodegradable polymers. *J Polym Sci B Polym Phys*. 2011;49(12):832–864. doi:10.1002/polb.22259
- Gaharwar AK, Patel A, Dolatshahi-Pirouz A, et al. Elastomeric nanocomposite scaffolds made from poly(glycerol sebacate) chemically crosslinked with carbon nanotubes. *Biomater Sci*. 2015;3(1):46–58. doi:10.1039/c4bm00222a
- Lau CC, Al Qaysi M, Owji N, et al. Advanced biocomposites of poly(glycerol sebacate) and  $\beta$ -tricalcium phosphate by in situ microwave synthesis for bioapplication. *Mater Today Adv*. 2020;5:100023. doi:10.1016/j.mtdadv.2019.100023
- Pomerantseva I, Krebs N, Hart A, Neville CM, Huang AY, Sundback CA. Degradation behavior of poly(glycerol sebacate). *J Biomed Mater Res A*. 2009;91(4):1038–1047. doi:10.1002/jbm.a.32327
- Sundback CA, Shyu JY, Wang Y, et al. Biocompatibility analysis of poly(glycerol sebacate) as a nerve guide material. *Biomaterials*. 2005;26(27):5454–5464. doi:10.1016/j.biomaterials.2005.02.004
- Wang Y, Ameer GA, Sheppard BJ, Langer R. A tough biodegradable elastomer. *Nat Biotechnol*. 2002;20(6):602–606. doi:10.1038/nbt0602-602
- Nagata M, Machida T, Sakai W, Tsutsumi N. Synthesis, characterization, and enzymatic degradation of network aliphatic copolyesters. *J Polym Sci A Polym Chem*. 1999;37(13):2005–2011. doi:10.1002/(SICI)1099-0518(19990701)37:13<2005::AID-POLA14>3.0.CO;2-H
- Gao J, Crapo PM, Wang Y. Macroporous elastomeric scaffolds with extensive micropores for soft tissue engineering. *Tissue Eng*. 2006;12(4):917–925. doi:10.1089/ten.2006.12.917
- Xuan H, Hu H, Geng C, et al. Biofunctionalized chondrogenic shape-memory ternary scaffolds for efficient cell-free cartilage regeneration. *Acta Biomater*. 2020;105:97–110. doi:10.1016/j.actbio.2020.01.015
- Pashneh-Tala S, Moorehead R, Claeysens F. Hybrid manufacturing strategies for tissue engineering scaffolds using methacrylate functionalised poly(glycerol sebacate). *J Biomater Appl*. 2020;34(8):1114–1130. doi:10.1177/0885328219898385
- Pashneh-Tala S, Owen R, Bahmaee H, Rekštyte S, Malinauskas M, Claeysens F. Synthesis, characterization and 3D micro-structuring via 2-photon polymerization of poly(glycerol sebacate)-methacrylate: An elastomeric degradable polymer. *Front Phys*. 2018;6(5):41. doi:10.3389/fphy.2018.00041
- Wang Z, Ma Y, Wang YX, et al. Urethane-based low-temperature curing, highly-customized and multifunctional poly(glycerol sebacate)-co-poly(ethylene glycol) copolymers. *Acta Biomater*. 2018;71:279–292. doi:10.1016/j.actbio.2018.03.011
- Singh D, Harding AJ, Albadawi E, Boissonade FM, Haycock JW, Claeysens F. Additive manufactured biodegradable poly(glycerol sebacate methacrylate) nerve guidance conduits. *Acta Biomater*. 2018;78:48–63. doi:10.1016/j.actbio.2018.07.055
- Lee KW, Gade PS, Dong L, et al. A biodegradable synthetic graft for small arteries matches the performance of autologous vein in rat carotid arteries. *Biomaterials*. 2018;181:67–80. doi:10.1016/j.biomaterials.2018.07.037
- Silva JC, Udangawa RN, Chen J, et al. Kartogenin-loaded coaxial PGS/PCL aligned nanofibers for cartilage tissue engineering. *Mater Sci Eng C Mater Biol Appl*. 2020;2:107. doi:10.1016/j.msec.2019.110291
- Wang CC, Shih TY, Hsieh YT, Huang JL, Wang J. L-arginine grafted poly(glycerol sebacate) materials: An antimicrobial material for wound dressing. *Polymers (Basel)*. 2020;12(7):1–12. doi:10.3390/polym12071457
- Li X, Hong ATL, Naskar N, Chung HJ. Criteria for quick and consistent synthesis of poly(glycerol sebacate) for tailored mechanical properties. *Biomacromolecules*. 2015;16(5):1525–1533. doi:10.1021/acs.biomac.5b00018
- Wang Y, Sun N, Zhang Y, et al. Enhanced osteogenic proliferation and differentiation of human adipose-derived stem cells on a porous n-HA/PGS-M composite scaffold. *Sci Rep*. 2019;9(1):1–10. doi:10.1038/s41598-019-44478-8
- Patel A, Gaharwar AK, Iviglia G, et al. Highly elastomeric poly(glycerol sebacate)-co-poly(ethylene glycol) amphiphilic block copolymers. *Biomaterials*. 2013;34(16):3970–3983. doi:10.1016/j.biomaterials.2013.01.045
- Rostamian M, Kalaei MR, Dehkordi SR, Panahi-Sarmad M, Tirgar M, Goodarzi V. Design and characterization of poly(glycerol-sebacate)-co-poly(caprolactone) (PGS-co-PCL) and its nanocomposites as novel biomaterials: The promising candidate for soft tissue engineering. *Eur Polym J*. 2020;138:109985. doi:10.1016/j.eurpolymj.2020.109985
- Godinho B, Gama N, Barros-Timmons A, Ferreira A. Enzymatic synthesis of poly(glycerol sebacate) pre-polymer with crude glycerol, by-product from biodiesel production. In: AIP Conference Proceedings. Vol 1981. American Institute of Physics Inc.; 2018. doi:10.1063/1.5045893
- Perin GB, Felisberti MI. Enzymatic synthesis of poly(glycerol sebacate): Kinetics, chain growth, and branching behavior. *Macromolecules*. 2020;53(18):7925–7935. doi:10.1021/acs.macromol.0c01709
- Aydin HM, Salimi K, Rzaev ZMO, Pişkin E. Microwave-assisted rapid synthesis of poly(glycerol-sebacate) elastomers. *Biomater Sci*. 2013;1(5):503–509. doi:10.1039/c3bm00157a
- Deniz P, Guler S, Çelik E, Hosseinian P, Aydin HM. Use of cyclic strain bioreactor for the upregulation of key tenocyte gene expression on poly(glycerol-sebacate) (PGS) sheets. *Mater Sci Eng C Mater Biol Appl*. 2020;106. doi:10.1016/j.msec.2019.110293
- Lau CC, Bayazit MK, Knowles JC, Tang J. Tailoring degree of esterification and branching of poly(glycerol sebacate) by energy efficient microwave irradiation. *Polym Chem*. 2017;8(26):3937–3947. doi:10.1039/c7py00862g
- Nijst CLE, Bruggeman JP, Karp JM, et al. Synthesis and characterization of photocurable elastomers from poly(glycerol-co-sebacate). *Biomacromolecules*. 2007;8(10):3067–3073. doi:10.1021/bm070423u
- Conejero-García Á, Gimeno HR, Sáez YM, Vilariño-Feltrer G, Ortuño-Lizarán I, Vallés-Lluch A. Correlating synthesis parameters with physicochemical properties of poly(glycerol sebacate). *Eur Polym J*. 2017;87:406–419. doi:10.1016/j.eurpolymj.2017.01.001

28. Cai W, Liu L. Shape-memory effect of poly (glycerol-sebacate) elastomer. *Mater Lett*. 2008;62(14):2171–2173. doi:10.1016/j.matlet.2007.11.042
29. Wang P, Berry DB, Song Z, et al. 3D printing of a biocompatible double network elastomer with digital control of mechanical properties. *Adv Funct Mater*. 2020;30(14):1910391. doi:10.1002/adfm.201910391
30. Wang Y, Kim YM, Langer R. In vivo degradation characteristics of poly(glycerol sebacate). *J Biomed Mater Res A*. 2003;66(1):192–197. doi:10.1002/jbm.a.10534
31. Tallá Ferrer C, Vilariño-Feltrer G, Rizk M, Sydow HG, Vallés-Lluch A. Nanocomposites based on poly(glycerol sebacate) with silica nanoparticles with potential application in dental tissue engineering. *Int J Polym Mater Polym Biomater*. 2020;69(12):761–772. doi:10.1080/00914037.2019.1616197
32. Kim MJ, Hwang MY, Kim J, Chung DJ. Biodegradable and elastomeric poly(glycerol sebacate) as a coating material for nitinol bare stent. *Biomed Res Int*. 2014;2014:956952. doi:10.1155/2014/956952
33. Aghajani MH, Panahi-Sarmad M, Alikarami N, et al. Using solvent-free approach for preparing innovative biopolymer nanocomposites based on PGS/gelatin. *Eur Polym J*. 2020;131:109720. doi:10.1016/j.eurpolymj.2020.109720
34. Nagata M, Machida T, Sakai W, Tsutsumi N. Synthesis, characterization and enzymatic degradation of novel regular network aliphatic polyesters based on pentaerythritol. *Macromolecules*. 1997;30:6525–6530. doi:10.1021/ma9706860
35. Tadayyon G, Krukiewicz K, Britton J, et al. In vitro analysis of a physiological strain sensor formulated from a PEDOT:PSS functionalized carbon nanotube-poly(glycerol sebacate urethane) composite. *Mater Sci Eng C*. 2021;121:111857. doi:10.1016/j.msec.2020.111857
36. Rai R, Tallawi M, Barbani N, et al. Biomimetic poly(glycerol sebacate) (PGS) membranes for cardiac patch application. *Mater Sci Eng C*. 2013;33(7):3677–3687. doi:10.1016/j.msec.2013.04.058
37. Crapo PM, Gao J, Wang Y. Seamless tubular poly(glycerol sebacate) scaffolds: High-yield fabrication and potential applications. *J Biomed Mater Res A*. 2008;86(2):354–363. doi:10.1002/jbm.a.31598
38. Crapo PM, Wang Y. Physiologic compliance in engineered small-diameter arterial constructs based on an elastomeric substrate. *Biomaterials*. 2010;31(7):1626–1635. doi:10.1016/j.biomaterials.2009.11.035
39. Szustakiewicz K, Gazińska M, Kryszak B, et al. The influence of hydroxyapatite content on properties of poly(L-lactide)/hydroxyapatite porous scaffolds obtained using thermal induced phase separation technique. *Eur Polym J*. 2019;113:313–320. doi:10.1016/j.eurpolymj.2019.01.073
40. Samourides A, Browning L, Hearnden V, Chen B. The effect of porous structure on the cell proliferation, tissue ingrowth and angiogenic properties of poly(glycerol sebacate urethane) scaffolds. *Mater Sci Eng C*. 2020;108:110384. doi:10.1016/j.msec.2019.110384
41. Frydrych M, Chen B. Fabrication, structure and properties of three-dimensional biodegradable poly(glycerol sebacate urethane) scaffolds. *Polymer (Guildf)*. 2017;122:159–168. doi:10.1016/j.polymer.2017.06.064
42. Xiao B, Yang W, Lei D, et al. PGS scaffolds promote the in vivo survival and directional differentiation of bone marrow mesenchymal stem cells restoring the morphology and function of wounded rat uterus. *Adv Healthc Mater*. 2019;8(5):1801455. doi:10.1002/adhm.201801455
43. Sencadas V, Sadat S, Silva DM. Mechanical performance of elastomeric PGS scaffolds under dynamic conditions. *J Mech Behav Biomed Mater*. 2020;102:103474. doi:10.1016/j.jmbbm.2019.103474
44. Lin D, Cai B, Wang L, et al. A viscoelastic PEGylated poly(glycerol sebacate)-based bilayer scaffold for cartilage regeneration in full-thickness osteochondral defect. *Biomaterials*. 2020;253:120095. doi:10.1016/j.biomaterials.2020.120095
45. Brown TD, Dalton PD, Hutmacher DW. Melt electrospinning today: An opportune time for an emerging polymer process. *Prog Polym Sci*. 2016;56:116–166. doi:10.1016/j.progpolymsci.2016.01.001
46. Flaig F, Ragot H, Simon A, et al. Design of functional electrospun scaffolds based on poly(glycerol sebacate) elastomer and poly(lactic acid) for cardiac tissue engineering. *ACS Biomater Sci Eng*. 2020;6(4):2388–2400. doi:10.1021/acsbmaterials.0c00243
47. Denis P, Wrzecieć M, Gadomska-Gajadur A, Sajkiewicz P. Poly (glycerol sebacate)-poly(l-lactide) nonwovens: Towards attractive electrospun material for tissue engineering. *Polymers (Basel)*. 2019;11(12):2113. doi:10.3390/polym11122113
48. Jeffries EM, Allen RA, Gao J, Pesce M, Wang Y. Highly elastic and suturable electrospun poly(glycerol sebacate) fibrous scaffolds. *Acta Biomater*. 2015;18:30–39. doi:10.1016/j.actbio.2015.02.005
49. Fakhrali A, Semnani D, Salehi H, Ghane M. Electrospun PGS/PCL nanofibers: From straight to sponge and spring-like morphology. *Polym Adv Technol*. 2020;31(12):3134–3149. doi:10.1002/pat.5038
50. Hu J, Kai D, Ye H, et al. Electrospinning of poly(glycerol sebacate)-based nanofibers for nerve tissue engineering. *Mater Sci Eng C*. 2017;70:1089–1094. doi:10.1016/j.msec.2016.03.035
51. Yeh YC, Highley CB, Ouyang L, Burdick JA. 3D printing of photocurable poly(glycerol sebacate) elastomers. *Biofabrication*. 2016;8(4):045004. doi:10.1088/1758-5090/8/4/045004
52. Gultekinoglu M, Öztürk Ş, Chen B, Edirisinghe M, Ulubayram K. Preparation of poly(glycerol sebacate) fibers for tissue engineering applications. *Eur Polym J*. 2019;121:109297. doi:10.1016/j.eurpolymj.2019.109297
53. Lee IK, Ludwig AL, Phillips JM, et al. Ultrathin micromolded 3D scaffolds for high-density photoreceptor layer reconstruction. *Sci Adv*. 2021;7(17):1–12. doi:10.1126/sciadv.abf0344
54. Vert M, Doi Y, Hellwich KH, et al. Terminology for biorelated polymers and applications (IUPAC Recommendations 2012). *Pure Appl Chem*. 2012;84(2):377–410.
55. Liu Y, Tian K, Hao J, Yang T, Geng X, Zhang W. Biomimetic poly(glycerol sebacate)/polycaprolactone blend scaffolds for cartilage tissue engineering. *J Mater Sci Mater Med*. 2019;30(5):53. doi:10.1007/s10856-019-6257-3
56. Vogt L, Rivera LR, Liverani L, Piegat A, El Fray M, Boccaccini AR. Poly( $\epsilon$ -caprolactone)/poly(glycerol sebacate) electrospun scaffolds for cardiac tissue engineering using benign solvents. *Mater Sci Eng C Mater Biol Appl*. 2019;103:109712. doi:10.1016/j.msec.2019.04.091
57. Hou L, Zhang X, Mikael PE, et al. Biodegradable and bioactive PCL-PGS core-shell fibers for tissue engineering. *ACS Omega*. 2017;2(10):6321–6328. doi:10.1021/acsomega.7b00460